PARTICLE SHAPE EFFECTS ON GAS-SOLID REACTIONS

Thesis by

Moon Kyu Choi

In Partial Fulfillment of the Requirements

for the Degree of

Doctor of Philosophy

California Institute of Technology

Pasadena, California 91125

1992

(Submitted December 30,1991)

Dedicated to God

Acknowledgments

I would like to express my sincere appreciation to my advisor Professor George R. Gavalas for suggesting this research topic and for his patient guidance and encouragement throughout the course of this investigation. I am also very thankful to Prof. Brady for helping me use the Sun computer of his group. I wish to thank many friends for stimulating discussions and moral support during my stay at Caltech. My special thanks are sent to Dr. In-Seok Kang, Dr. Suk Woo Nam and Dr. Seong Hee Lee. I would like to express my sincere gratitude to all members of my family for their never-ending support and encouragement. Last, but certainly most, special thanks should be given to my friend, Bok, without whom my student life would have been miserable.

Abstract

A theoretical study of the reaction of nonspherical particles is carried out in the shrinking core regime to determine the effect of particle shape on total reaction rate, particle temperature, and to characterize the evolution of shape with consumption of particle. This problem involves the solution of the external diffusion and heat conduction equations with the reaction entering as a boundary condition over the particle surface. Firstly, the problem is treated isothermally by a domain perturbation technique to give analytical results for a slightly nonspherical particle and by the boundary integral technique for spheroids of arbitrary aspect ratio. Secondly, the nonisothermal problem is solved to give the pseudosteady and dynamic behaviors of nonspherical particles taking char combustion as an example. For the dynamic problem the diffusion and heat conduction in the gas phase are assumed to be at pseudosteady state with respect to the evolving particle temperature and particle size and shape. Lastly, the effect of surface roughness on the gas-solid reaction is similarly examined by representing the particle surface as a series in Legendre polynomials superimposed on an underlying spherical surface.

For nonspherical particles of equal volume but varying shape reacting under isothermal or nonisothermal conditions, the total reaction rate increases with the aspect ratio and is approximately equal to that of the sphere of equal surface area, and the local reaction rate increases with the distance from the particle center. The pseudosteady particle temperature under nonisothermal conditions is essentially the same for various spheroidal particles of equal volume. The particle temperature approaches quickly and remains close to its pseudosteady trajectory with conversion. During reaction a particle becomes more and more nonspherical. As for the effect of

roughness, from the method of domain perturbation the nth mode decreases if the Damköhler number $Q > Q_{\rm cr} = \frac{n+1}{n-2}$, and vice versa. For highly irregular particles, too, this criterion applies overall, but they do not have sharp critical values of Q showing mixed behavior in a certain range around $Q_{\rm cr}$.

Table of Contents

List of Figures

Chapter 2

Chapter 3

Chapter 4

Appendices

Chapter 1

Introduction

Reactions between a gas and a solid particle are of great industrial importance. In such reactions frequently encountered in the process industry, a gas contacts a solid to react with it, forming gas or solid products. Particles may shrink or remain unchanged in size, depending on the formation and on the physical structure of a solid product. Several examples of shrinking particle are the manufacture of carbon disulfide from the elements, the formation of metal carbonyls, the water-gas reaction and coal char combustion (Levenspiel, 1972; Szekely *et al.*, 1976). Among the examples where ash remains are the oxidation of sulfide ores to yield metal oxides, the preparation of metals from their oxides by reduction, the nitrogenation of calcium carbide to produce cyanamide, and the regeneration of deactivated catalysts (Levenspiel, 1972). Knowledge of the conversion behavior of gas-solid reactions is a prerequisite to the analysis of many existing processes and to the design of new installations.

For gas-solid reactions, internal and external transport and reaction kinetics have to be considered simultaneously. The rate of the overall process depends on the relative magnitudes of the rate parameters for reaction and transport, both internal and external. Furthermore, since the solid is involved in the reaction, the conditions inside the particle such as the effective pore diffusion coeffeicients can change as a result of changes in the internal pore structure.

Analytical or numerical descriptions of gas-solid reactions are generally based on solutions of linearized or otherwise simplified representations of the general equations. In the shrinking core model, the core is assumed to be impervious to gaseous

reactant, with reaction only occurring on the external surface of the shrinking core (Field *et al.*, 1967; Field, 1969). This analysis was later extended to include a detailed account of external heat and mass transfer while retaining shrinking core oxidation (Ubhayakar, 1976 ; Libby and Blake, 1979 ; Annamalai and Durbetaki, 1979). In the progressive conversion model, the reactant gas is allowed to penetrate into the particle assuming a static internal solid structure, i.e., constant effective diffusivity and constant reaction surface area (Wen, 1968; Ishida and Wen, 1971; Froment and Bischoff, 1979). More sophisticated models dealing with pore branching and pore enlargement are presented by Simons (1979), Gavalas (1981), and Sotirchos and Burganos (1986). Regardless of the treatment afforded to internal and external diffusion, all previous investigations treated the reacting particles as spherical, thus avoiding the mathematical and computational complications entailed by nonspherical geometry.

If the initial particle shape is perfectly spherical and the spherical shape is also stable, this assumption is obviously correct. Since in practice the solid particles cannot be perfectly spherical, it is important to check if they react with sphere-like shape even though the initial shape is not completely spherical. Even if the initial particle shape is perfectly spherical, it may not be stable to small disturbances of surface concentrations of reactants. Therefore, we need to find out whether it is appropriate to assume a spherical shape in the shrinking core model of a gas-solid reaction. Moreover, we would like to explore the effect of nonspherical shape on the reaction rate, particle temperature and other reaction characteristics.

A few experimental results may be indirectly related to the analytical investigations contained in this thesis. Waters *et al.* (1988) obtained overall kinetic parameters describing the combustion of an irregularly shaped carbon char based

on optical measurements of the temperature, size and velocity of individual particles observed in an entrained-flow reactor. According to these authors, the kinetic parameters are not much affected by the simplifying assumption of a spherical particle. Weisz and Goodwin (1963) presented a photograph showing the nearly spherical core shape at 50% decrease of core radius, originated from an initially spherical shape of carbon-deposited catalyst. A picture displayed by Wen and Wang (1970) depicts a geometrical instability for a small core size.

In this thesis we are investigating how the shape of a nonspherical particle evolves with reaction in the shrinking core regime using two different methods. These methods are the method of domain perturbation (DP) and the boundary integral method (BI), both of which are frequently used to study various free boundary problems in fluid mechanics (Brenner, 1964; Youngren and Acrivos; 1975). The DP technique can only be applied to particles slightly different from spherical. The BI technique can be used for smooth particle shapes and has the advantage that the numerical computations are confined to the boundaries only (Liggett and Liu, 1983). This method is particularly suitable for problems where the values of some function or its derivatives are needed only at boundaries like the problem we will be discussing hitherto. We will be restricted to rotationally symmetric particles such as prolate and oblate spheroids of high aspect ratio.

In Chapter 2 the pseudosteady state analysis of the catalytic and noncatalytic reactions on an isothermal particle surface will be carried out using the domain perturbation technique and the boundary integral technique to yield the total reaction rate, the surface averaged reaction rate and the rate of change of the aspect ratio. The results from Chapter 2 are also applicable to steady state gas reactions occurring on a nonspherical catalyst surface. The sublimation of prolate and oblate

spheroids, albeit not directly related to the subject of this thesis, is also analyzed to compare the effects from two different surface boundary conditions.

Chapter 2 treating the isothermal gas-solid reactions can give us some insight on the shape change accompanying conversion. But since the reaction depends exponentially on the temperature, the temperature effect should be included in a more realistic analysis. The inclusion of temperature makes the problem highly nonlinear; therefore, the problem could not be solved without certain additional assumptions. These assumptions may be justified since we focus attention on the shape change of the particle rather than on the issue of reaction rate, etc. Although the rate of change of the aspect ratio for a noncatalytic gas-solid reaction may provide an estimate of how fast the particle shrinks and deforms, it is desirable to follow the particle with time in order to find various properties as functions of time. Chapter 3 will treat the noncatalytic burnout of a nonspherical particle with time, employing a real set of data on a bituminous char combustion.

Another phase of nonsphericity encountered by real particles is the roughness of the particle surface. Chapter 4 is concerned with the evolution of a rough surface using the isothermal linear problem formulation developed in Chapter 2. As in Chapter 2, the analysis is based on the domain perturbation and the boundary integral methods.

The problem of a shrinking particle (Case I) is divided further, according to the diffusion model used, into a linear diffusion problem and a nonlinear diffusion problem. As is well known the nonlinear diffusion equation reduces asymptotically to its linear counterpart as the mole fraction of all the diffusing species becomes very small or in the case of equimolar counterdiffusion. In the special case of binary diffusion the nonlinear diffusion equation can be transformed by a change of

variables to the linear Laplace equation with a nonlinear boundary condition. The latter problem can be treated by the DP technique under the diffusion control and generally by the BI method. When the overall particle shape remains the same with conversion (Case II), we can only use the BI method provided diffusion through the ash layer can be treated as linear. Since most aspects of Case II can be obtained by straightforward modifications of the results of Case I, Case II will be treated briefly in Appendix B.

REFERENCES

Annamalai, K. and Durbetaki, P., 1979, Combustion Behavior of Char/Carbon Particles, *Seventeenth Symposium(International) on Combustion*, 169-178.

Brenner, H., 1964, The Stokes Resistance of a Slightly Deformed Sphere. *Ind. Engng Chem. Fundam.* **16**, 171-181.

Field, M.A., Gill, D.W., Morgan, B.B. and Hawksley, D.W.G., 1967, *Combustion of Pulverized Coal*, BCURA, Leatherhead, pp. 189-208.

Field, M.A., 1969, Rate of Combustion of Size-Graded Fractions of Char from a Low-Rank Coal between 1200 K and 2000 K. *Combustion & Flame* **13**, 237-252.

Froment, G.F. and Bischoff, K.B., 1979, *Chemical Reactor Analysis and Design*, John Wiley, New York, pp. 239-266.

Gavalas, G.R., 1981, Analysis of Char Combustion Including the Effect of Pore Enlargement. *Combust. Sci. Technol.* **24**, 197-213.

Ishida, M. and Wen, C.Y., 1971, Comparison of Zone-Reaction Model and Unreacted-Core Model in Solid-Gas Reactions. *Chem. Engng Sci.* **26**, 1031-1048.

Levenspiel, O., 1972, *Chemical Reaction Engineering*, Wiley, New York, pp. 357-400.

Libby, P.A. and Blake, T.R., 1979, Theoretical Study of Burning Carbon Particles. *Combustion & Flame* **36**, 139-169.

Liggett, J.A. and Liu, P.L-F., 1983, *The Boundary Integral Equation Method for Porous Media Flow*, George Allen & Unwin Ltd, London, pp. 86-110.

Simons, G.A., 1979, Char Gasification: Part I, Transport Model. *Combust. Sci. Technol.* **20**, 107-116.

Sotirchos, S.V. and Burganos, V.N., 1986, Intraparticle Diffusion and Char Combustion. *Chem. Engng Sci.* **41**, 1599-1609.

Szekely, J., Evans, J.W. and Shon, H.Y., 1976, *Gas-Solid Reactions*, Academic Press, New York, pp. 67-107.

Ubahyakar, S.K., 1976, Burning Charateristics of a Spherical Particle Reacting with Ambient Oxidizing Gas at its Surface. *Combustion & Flame* **26**, 23-34.

Waters, B.J., Mitchell, R.E., Squires, R.G. and Laurendeau, N.M., 1988, Overall Kinetic Parameters for Combustion of a Highly Nonspherical Carbon Char. *Twenty-Second Symposium (International) on Combustion*, 17-27.

Weisz, P.B. and Goodwin, R.D., 1963, Combustion of Carbonaceous Deposits within Porous Catalyst Particles. I. Diffusion-Controlled Kinetics. *J. Cat.* **2**, 397-404.

Wen, C.Y., 1968, Noncatalytic Heterogeneous Solid Fluid Reaction Models. *Ind. Engng. Chem. Fundam.* **60**, 34-54.

Wen, C.Y. and Wang, S.C., 1970, Thermal and Diffusional Effects in Noncatalytic Solid Gas Reactions. *Ind. Eng. Chem.* **62**(8), 30-51.

Youngren, G.K. and Acrivos, A., 1975, Stokes Flow Past a Particle of Arbitrary Shape: A Numerical Method of Solution. *J. Fluid Mech.* **69**, 377-403.

Chapter 2

Isothermal Gas-Solid Reaction on Nonspherical Particles

ABSTRACT

Reaction or sublimation of a nonspherical nonporous particle is analyzed to determine the effect of shape on total reaction rate and to characterize the change of shape with conversion. Diffusion is formulated using the Stefan-Maxwell equations at constant temperature and pressure while reaction or sublimation enters as a boundary condition. The problem is treated by a domain perturbation technique to obtain analytical results for slightly nonspherical particles and by the boundary integral technique to obtain numerical solutions for spheroids of arbitrary aspect ratio.

The total reaction rate increases with the aspect ratio at constant particle volume, and is approximately equal to that of a spherical particle of equal surface area. The local reaction rate increases with the distance from the particle center. The resulting change of the aspect ratio is sensitive to the Damköhler number $Q = \frac{k\tilde{R}_s}{D_A}$ and is positive regardless of Q and the aspect ratio. Thus the deviation from the nonspherical shape increases with time. For subliming particles the shape change is negligible.

INTRODUCTION

In the analysis of fluid-solid catalytic and noncatalytic reactions, it is customary to treat the reacting particles as spherical in order to simplify the solution of the relevant reaction-transport equations. The analysis of the spherically symmetric problem is generally assumed to provide the correct trends about the effect of various parameters, even when the reacting particles are nonspherical. In the present paper we analyze reaction and external diffusion for nonspherical but axially symmetric particles to determine (i) the total rate of a catalytic or noncatalytic reaction concentrated on the external surface of the particle and (ii) the change in the shape of a particle due to consumption of the solid material. The shape change can be pronounced over extended conversion even when the initial particle shape is only slightly nonspherical.

We would like from the outset to delimit the scope of the analysis. The reaction is assumed to be concentrated on the external particle surface, and the external mass transfer to be determined by diffusion, with no convective flow other than the Stefan flow. Those restrictions eliminate consideration of most problems pertinent to heterogeneous catalytic reactions where internal rather than external diffusion is rate limiting. With respect to noncatalytic reactions, the assumption that the reaction is concentrated on or very near the external surface is valid for nonporous particles, or porous particles under conditions of high Thiele modulus.

The most important noncatalytic gas-solid reaction which often satisfies the above restrictions is coal or char combustion. However, under conditions of high Thiele modulus, i.e., shrinking core combustion, external heat transfer as well as mass transfer needs to be considered. In the present paper we assume isother-

mal conditions and consider the external mass transfer problem only. However the methodology presented is applicable, with suitable extensions, to simultaneous heat and mass transfer. This latter problem will be treated in a subsequent paper focusing on coal combustion. We have also treated and will briefly discuss the problem of particle sublimation which differs only in the boundary conditions from the reaction problem.

Two techniques are used to treat the problem of reacting nonspherical particles. The first is domain perturbation (DP) (Brenner, 1964; Acrivos and Taylor, 1964), the second is the boundary integral technique (BI) (Brebbia and Walker, 1980; Liggett and Liu, 1972). DP is an analytical technique limited to slightly nonspherical particles. The BI technique is numerical and is applicable to arbitrary particle shapes. The main advantage of the BI technique over the more customary finite element or difference techniques is the much smaller number of unknowns involved in the problem setup. Both techniques can handle multicomponent diffusion with the nonlinearities inherent in the Stefan-Maxwell equations. Both techniques have been used to study more complicated fluid flow problems involving free boundaries (Brenner, 1964; Acrivos and Talyor,1964; Youngren and Acrivos, 1975).

PROBLEM FORMULATION

The gas-solid reactions considered in this paper can be denoted by

$$b_1 P(s) + A(g) \rightarrow b_2 B(g)$$

where $P(s), A(g)$ and $B(g)$ are the solid reactant, the gaseous reactant and the gaseous product and b_1 and b_2 are stoichiometric coefficients. The analysis can be easily extended to the formation of a solid product if the product layer does not offer diffusional resistance.

Linear Diffusion Equation

In this section we consider the linear diffusion problem which provides the simplest setup for investigating the effects of particle shape. The problem is approximately linear under the restrictions:

i) low mole fraction of A in the free stream, or equimolar counterdiffusion, such that the Stefan flow term can be neglected

ii) low heat effect due to reaction, therefore nearly isothermal system

iii) first order reaction in A.

Under the above assumptions the concentration of A in the gas phase, c_A, satisfies Laplace's equation

$$\nabla_{\tilde{x}}^2 c_A = 0. \tag{1}$$

The boundary condition at infinity is

$$c_A \rightarrow c_{Ab} \qquad \text{as } |\tilde{\mathbf{x}}| \rightarrow \infty. \tag{2}$$

At the particle surface we shall consider the "reaction" boundary condition

$$-D_{AB} \nabla_{\tilde{x}} c_A \cdot \tilde{\mathbf{n}} = k c_A \tag{3}$$

or the "sublimation" (or "condensation") boundary condition

$$c_A = c_{As}. \tag{4}$$

After Eq.(1) with boundary conditions (2) and (3) or (2) and (4) has been solved, one can calculate the rate of change of the particle shape locally on the particle surface according to the kinematic equation

$$\frac{1}{|\nabla_{\tilde{x}} \tilde{F}|} \frac{\partial \tilde{F}}{\partial t} - \mathbf{v_s} \cdot \tilde{\mathbf{n}} = 0 \tag{5}$$

where

$$\tilde{F} \equiv \tilde{\rho} - \tilde{R}(\theta, t). \tag{6}$$

Here $\tilde{\mathbf{n}}$ is the unit normal vector pointing towards the particle and $\mathbf{v}_s \cdot \tilde{\mathbf{n}}$ is the surface velocity. The tilde denotes dimensional quantities.

Equation (1) is based on the assumption that the diffusion problem is at quasi-steady state with respect to the slowly changing particle shape. The quasi-steady state assumption is not strictly valid for a semi-infinite medium, but has been shown by Kirkaldy (1958) to be valid for problems of sublimation and crystal growth. It was also found by Bischoff (1963) and Luss (1968) that the quasi-steady state assumption is valid for gas-solid reactions with moving boundary.

Both the domain perturbation and the boundary integral techniques will be applied to axisymmetric particles when Eqs.(1)-(5) are conveniently written in spherical coordinates as shown in Figure 1.

$$\frac{1}{\tilde{\rho}^2}\frac{\partial}{\partial\tilde{\rho}}\left(\tilde{\rho}^2\frac{\partial c_A}{\partial\tilde{\rho}}\right) + \frac{1}{\tilde{\rho}^2\sin\theta}\frac{\partial}{\partial\theta}\left(\sin\theta\frac{\partial c_A}{\partial\theta}\right) = 0 \quad \text{outside the particle}, \tag{7a}$$

$$D_{AB}\left(\alpha\frac{\partial c_A}{\partial\tilde{\rho}} - \frac{\beta}{\tilde{\rho}}\frac{\partial c_A}{\partial\theta}\right) = kc_A \quad \text{at} \quad \tilde{\rho} = \tilde{R}(\theta, t), \tag{7b}$$

$$c_A \to c_{Ab} \qquad \text{as} \quad \tilde{\rho} \to \infty, \tag{7c}$$

$$-\frac{\partial\tilde{R}}{\partial t} = \frac{b_1 k}{\rho_s \alpha}c_A \quad \text{at} \quad \tilde{\rho} = \tilde{R}(\theta, t). \tag{7d}$$

Here, $\tilde{\mathbf{n}}$ is defined as

$$\tilde{\mathbf{n}} = -\alpha\mathbf{i}_{\tilde{\rho}} + \beta\mathbf{i}_\theta, \tag{8a}$$

where

$$\alpha = \frac{1}{\sqrt{1 + \left(\frac{1}{\tilde{R}}\frac{\partial\tilde{R}}{\partial\theta}\right)^2}} \quad \text{and} \quad \beta = \frac{\frac{1}{\tilde{R}}\frac{\partial\tilde{R}}{\partial\theta}}{\sqrt{1 + \left(\frac{1}{\tilde{R}}\frac{\partial\tilde{R}}{\partial\theta}\right)^2}}. \tag{8b}$$

Equations (7d) - (8b) are derived in Appendix A.

We can use dimensionless variables to simplify the appearance of the governing equation and the boundary conditions. For this purpose we define

$$\mathbf{x} = \frac{\tilde{\mathbf{x}}}{\tilde{R}_s(t)}, u_A = \frac{c_A}{c_{Ab}} = \frac{y_A}{y_{Ab}}, R(\theta,t) = \frac{\tilde{R}(\theta,t)}{\tilde{R}_s(t)} \tag{9a}$$

and

$$Q(\tilde{R}_s(t)) = \frac{k\tilde{R}_s(t)}{D_{AB}}, \tau = \frac{b_1 k^2 c_{Ab}}{\rho_s D_{AB}} t, \tag{9b}$$

where $\tilde{R}_s(t)$ is the radius of a sphere of equal volume as the particle. The resulting dimensionless equation and boundary conditions are

$$\nabla_x^2 u_A = 0, \tag{10a}$$

$$R^2 \frac{\partial u_A}{\partial \rho} - \frac{\partial R}{\partial \theta}\frac{\partial u_A}{\partial \theta} = QR^2\sqrt{1+\left(\frac{1}{R}\frac{\partial R}{\partial \theta}\right)^2}\, u_A \quad \text{at} \quad \rho = R(\theta,\tau), \tag{10b}$$

$$u_A \to 1 \quad \text{as} \quad \rho \to \infty, \tag{10c}$$

$$-\left(\frac{dQ(\tau)}{d\tau}R + Q(\tau)\frac{\partial R}{\partial \tau}\right) = \sqrt{1+\left(\frac{1}{R}\frac{\partial R}{\partial \theta}\right)^2}\, u_A \quad \text{at} \quad \rho = R(\theta,\tau). \tag{10d}$$

Nonlinear Diffusion Equations.

In this section we remove assumptions (i) and (iii) implied in the previous subsection but retain assumption (ii) of isothermality. To introduce the essential ideas we first consider the case of binary diffusion and then treat the more general multicomponent diffusion.

1. Binary diffusion

The starting point is the species conservation equations

$$\nabla \cdot \mathbf{N}_A = 0, \tag{11a}$$

$$\nabla \cdot \mathbf{N}_B = 0. \tag{11b}$$

At the particle surface we have the "reaction" boundary conditions

$$\mathbf{N}_A \cdot \mathbf{n} = kr(c_A, c_B), \tag{12a}$$

$$\mathbf{N}_B \cdot \mathbf{n} = -b_2 kr(c_A, c_B), \tag{12b}$$

or the "sublimation" boundary condition

$$c_A = c_{As}, \tag{13a}$$

$$\mathbf{N}_B \cdot \mathbf{n} = 0. \tag{13b}$$

Equations (11a) and (11b) must be supplemented by the binary diffusion relations

$$\mathbf{N}_A = y_A(\mathbf{N}_A + \mathbf{N}_B) - cD_{AB} \nabla y_A, \tag{14a}$$

$$\mathbf{N}_B = y_B(\mathbf{N}_A + \mathbf{N}_B) - cD_{AB} \nabla y_B. \tag{14b}$$

Equations (14a) and (14b) are linearly dependent; therefore, only Eq.(14a) need be considered. The system (11)-(12), (14a) does not have a unique solution but rather an infinite family of solutions, although a mathematical proof of this fact is a nontrivial technical problem outside the scope of this paper. The physical reason for the lack of uniqueness seems to be related to assuming constant pressure rather than including the momentum equation along with Eqs.(11)-(12), (14a). In the spherically symmetric geometry, Eqs.(11)-(12), (14a) have a unique solution despite the approximation of constant pressure. In that geometry Eqs.(11)-(12) yield the relations

$$\mathbf{N}_B = -b_2 \mathbf{N}_A, \tag{15a}$$

$$\mathbf{N}_A = (\text{constant}/\rho^2)\ \mathbf{i}_\rho. \tag{15b}$$

For the nonspherical geometry of interest here we shall use Eq.(15a) as an additional condition to generate a unique solution of Eqs.(11)-(12), (14a) or (11), (13)-(14a). At this time there is no mathematical justification for *a priori* introducing Eq.(15a). It is intuitively appealing, however, to single out the solution which satisfies Eq.(15a) as the physically meaningful among the infinite family of solutions. From Eqs.(14a) and (14b) we obtain

$$\mathbf{N}_A = -\frac{cD_{AB}\ \nabla y_A}{1+(b_2-1)y_A}. \tag{16}$$

Thus the equation satisfied by y_A is nonlinear but can be transformed to Laplace's equation by the simple change of the dependent variable

$$\psi \equiv \begin{cases} \ln(y_A + \frac{1}{b_2-1}), & \text{if } b_2 > 1 \\ \ln(\frac{1}{1-b_2} - y_A), & \text{if } b_2 < 1 \end{cases}. \tag{17}$$

When $b_2 = 1$ no change of variables is needed. The equation and boundary conditions for ψ are

$$\nabla^2\psi = 0, \tag{18a}$$

$$-\nabla\psi\cdot\mathbf{n} = Q|b_2-1|\left(e^{\psi} - \frac{1}{|b_2-1|}\right) \quad \text{at} \quad \rho = R, \tag{18b}$$

$$\psi \to \psi_b \qquad \text{as } |\mathbf{x}| \to \infty, \tag{18c}$$

where the dimensionless variables are defined as in subsection *Linear Diffusion Equation.*

2. Multicomponent Diffusion

The treatment of multicomponent diffusion starts from the Stefan-Maxwell equations and utilizes an assumption analogous to Eq.(15a). The somewhat lengthy manipulations involved are presented in an appendix (Appendix B).

Auxiliary Relations

Before proceeding with the solution of systems (10) and (18) we would like to list for later use certain constraints satisfied by $R(\theta,\tau)$, as well as a general relation for the rate of change of particle shape. The dimensionless variable $R(\theta,\tau)$ describing the particle surface [Eq.(9a)] is subject to two constraints. The first is volume conservation which gives

$$\int_{-1}^{1} R^3(\theta,\tau)d\eta = 2, \tag{19a}$$

where

$$\eta = \cos\theta. \tag{19b}$$

The second constraint is that the center of mass of the particle remains at the origin, which is expressed as

$$\int_{-1}^{1} R^4(\theta,\tau)\eta d\eta = 0. \tag{20}$$

Although the analysis below is applicable to any rotationally symmetric particle, we have chosen to restrict the actual calculations to particles whose initial shape is a prolate or oblate spheroid. A prolate spheroid is obtained from the revolution of an ellipse around its major axis. Revolution around the minor axis yields an oblate spheroid. Both shapes may be characterized either by their eccentricity, e, or by their aspect ratio, A_p. For both spheroids these two parameters are related by $A_p = (1-e^2)^{-1/2}$. Both parameters will be used below, the eccentricity as more basic in the definition of the shape, the aspect ratio as a more intuitive measure of deviation from the spherical shape.

From the defining relationship

$$A_p = \frac{R(0)}{R(\frac{\pi}{2})}, \tag{21}$$

the time derivative of the aspect ratio is obtained as

$$\frac{dA_p}{d\tau} = \frac{1}{R^2(\frac{\pi}{2})}\left[\frac{\partial R}{\partial \tau}(0)R(\frac{\pi}{2}) - R(0)\frac{\partial R}{\partial \tau}(\frac{\pi}{2})\right]. \tag{22}$$

Using the kinematic boundary condition Eq.(10d) in the form

$$\frac{\partial R}{\partial \tau} = -\frac{1}{Q(\tau)}\frac{dQ(\tau)}{d\tau}R - \frac{1}{Q(\tau)}\sqrt{1+\left(\frac{1}{R}\frac{\partial R}{\partial \theta}\right)}\,u_A \tag{23}$$

and noting that $\frac{\partial R}{\partial \theta} = 0$ at $\theta = 0, \frac{\pi}{2}$, we can rewrite Eq.(22) as

$$\frac{dA_p}{d\tau} = \frac{1}{R^2(\frac{\pi}{2})Q(\tau)}\left[R(0)u_A(\frac{\pi}{2}) - R(\frac{\pi}{2})u_A(0)\right]. \tag{24}$$

This last equation may be divided by $R(0) - R(\frac{\pi}{2})$ to give

$$\frac{d\ln(A_p-1)}{d\tau}R(\frac{\pi}{2})Q(\tau) = \frac{A_p u_A(\frac{\pi}{2}) - u_A(0)}{A_p - 1}. \tag{25}$$

For a prolate spheroid, $R(\frac{\pi}{2}) = A_p^{-1/3}$ and

$$\frac{dA_p}{d\tau} = \frac{A_p^{1/3}}{Q(\tau)}\left[A_p u_A(\frac{\pi}{2}) - u_A(0)\right]. \tag{26}$$

In the sections following below the rate of change of the aspect ratio will be calculated from Eq.(25) or Eq.(26) once the surface concentrations are found using either the domain perturbation or boundary integral technique. For easy reference the right hand side of Eq.(25) is denoted by W in the following sections:

$$W \equiv \frac{A_p u_A(\frac{\pi}{2}) - u_A(0)}{A_p - 1}. \tag{27}$$

Certain simple conclusions may be immediately drawn about the asymptotic behavior of W or $\frac{dA_p}{d\tau}$. As the Damköhler number Q approaches 0, the dimensionless concentration u_A approaches 1 over the entire surface of the particle so that W

also approaches 1. Conversely, since u_A becomes very small uniformly on the entire surface as Q becomes very large, within the range of the validity of the quasi-steady state assumption, W also becomes very small.

DOMAIN PERTURBATION FOR THE LINEAR DIFFUSION PROBLEM

This section is pertinent to the limiting case of a particle which is only slightly different from spherical. $R(\theta,\tau)$ and $u_A(\rho,\theta,\tau)$ can then be expanded in the series

$$R(\theta,\tau) = R_0(\theta,\tau) + \epsilon R_1(\theta,\tau) + \epsilon^2 R_2(\theta,\tau) + \cdots \tag{28a}$$

$$u_A(\rho,\theta,\tau) = u_0(\rho,\theta,\tau) + \epsilon u_1(\rho,\theta,\tau) + \epsilon^2 u_2(\rho,\theta,\tau) + \cdots, \tag{28b}$$

where $\epsilon << 1$ is a small dimensionless parameter and R_i's are of $O(1)$ with respect to the parameter ϵ. The parameter ϵ is introduced as usual to indicate the order of approximation of the results finally obtained. We first derive conditions on the coefficients R_i by introducing the expansion (28a) into Eq.(19a). These are

$$\int_{-1}^{1} R_0^3 d\eta = 2, \tag{29a}$$

$$\int_{-1}^{1} R_0^2 R_1 d\eta = 0, \tag{29b}$$

$$\int_{-1}^{1} (R_0^2 R_2 + R_0 R_1^2) d\eta = 0. \tag{29c}$$

$$\vdots$$

Similarly, introducing Eq.(28a) into Eq.(20) yields

$$\int_{-1}^{1} R_0^4 \eta d\eta = 0, \tag{30a}$$

$$\int_{-1}^{1} R_0^3 R_1 \eta d\eta = 0, \tag{30b}$$

$$\int_{-1}^{1} (4R_0^3 R_2 + 6R_0 R_1^3)\eta d\eta = 0. \tag{30c}$$

$$\vdots$$

By definition $\epsilon = 0$ corresponds to a spherical particle; therefore, R_0 is a constant, which by Eq.(29a) is

$$R_0(\theta, \tau) \equiv 1. \tag{31}$$

Equations (29b)-(30c) are now reduced to

$$\int_{-1}^{1} R_1 d\eta = 0, \tag{32a}$$

$$\int_{-1}^{1} (R_2 + R_1^2) d\eta = 0, \tag{32b}$$

$$\int_{-1}^{1} R_1 \eta d\eta = 0, \tag{32c}$$

$$\int_{-1}^{1} (4R_2 + 6R_1^3)\eta d\eta = 0. \tag{32d}$$

We next expand the term $R_1(\theta, \tau)$ in the series

$$R_1 = \sum_{n=0}^{\infty} \beta_n(\tau) P_n(\cos\theta), \tag{33}$$

where P_n is the nth Legendre polynomial. Introducing Eq.(33) into Eqs.(32a) and (32c), we obtain

$$\beta_0(\tau) = \beta_1(\tau) = 0, \tag{34}$$

while the higher coefficients remain unspecified. The term $R_2(\theta, 0)$ should now be chosen to satisfy

$$\int_{-1}^{1} R_2 d\eta = -\sum_{n=2}^{\infty} \beta_n(0) \frac{2}{2n+1} \tag{35a}$$

$$\int_{-1}^{1} R_2 \eta d\eta = -\frac{3}{2} \int_{-1}^{1} R_1^3 \eta d\eta. \tag{35b}$$

It is not easy to find R_2 satisfying Eqs.(35a) and (35b) to all orders in ϵ, but a solution valid to $O(\epsilon)$, involving $O(\epsilon^2)$-error in the particle volume, can be obtained. To obtain the solution up to $O(\epsilon^n)$, we have to satisfy the volume condition, Eq.(19a), of the initial shape up to $O(\epsilon^n)$.

To calculate the concentrations, u_i, we change the boundary conditions from $\rho = R$ to $\rho = 1$ by expanding Eqs.(10b) and (10d) around $\rho = 1$, and grouping terms of equal order in ϵ. The resulting problems for the terms u_i are derived in Appendix C. They are listed below.

$O(1)$-problem

The first term, u_0, in the expansion (28b) satisfies the equations

$$\nabla^2 u_0 = 0, \tag{36a}$$

$$\frac{\partial u_0}{\partial \rho} = Q u_0 \quad \text{at} \quad \rho = 1, \tag{36b}$$

$$u_0 \to 1 \quad \text{as} \quad \rho \to \infty, \tag{36c}$$

$$-\frac{dQ}{d\tau} = u_0 \quad \text{at} \quad \rho = 1. \tag{36d}$$

These equations have spherical symmetry and can be easily solved to obtain

$$u_0 = 1 - [\frac{Q}{Q+1}] \frac{1}{\rho} \tag{37a}$$

$$Q(\tau) = -1 + \sqrt{(1+Q_0)^2 - 2\tau}, \tag{37b}$$

where Q_0 is the initial value of Q.

$O(\epsilon)$-problem

The first order problem derived in Appendix C is

$$\nabla^2 u_1 = 0, \tag{38a}$$

$$u_1 \to 0 \quad \text{as} \quad \rho \to \infty, \tag{38b}$$

$$\frac{\partial u_1}{\partial \rho} - Q u_1 = \frac{Q(Q+2)}{Q+1} R_1 \quad \text{at} \quad \rho = 1, \tag{38c}$$

$$-\left(\frac{dQ}{d\tau} R_1 + Q \frac{\partial R_1}{\partial \tau}\right) = u_1 + \frac{\partial u_0}{\partial \rho} R_1 \quad \text{at} \quad \rho = 1. \tag{38d}$$

Using spherical harmonics and taking into account Eq.(38b), the function u_1 is expanded in the series

$$u_1 = \sum_0^\infty \alpha_n(\tau) \rho^{-(n+1)} P_n(\eta), \tag{39}$$

where $P_n(\eta)$ is the nth Legendre function. The function R_1 is expressed in a similar series

$$R_1 = \sum_2^\infty \beta_n(\tau) P_n(\eta). \tag{40}$$

Introducing the series (39) and (40) into (38) and equating coefficients of the Legendre polynomials we obtain

$$\alpha_0(\tau) = 0, \tag{41a}$$

$$\alpha_1(\tau) = 0, \tag{41b}$$

$$\alpha_n(\tau) = -\frac{Q(Q+2)}{(Q+1)(Q+n+1)} \beta_n(\tau) \quad \text{for n} \geq 2. \tag{41c}$$

Similarly we obtain from Eq.(38d)

$$\frac{d\beta_n}{d\tau} = \gamma_n(\tau) \beta_n, \quad n = 0, 1, 2, \cdots \tag{42a}$$

where

$$\gamma_n(\tau) = -\frac{(n-2)Q-(n+1)}{Q(Q+1)(Q+n+1)}. \tag{42b}$$

Therefore, the coefficients β_n are given by

$$\beta_n(\tau) = \beta_n(0)\exp[\Gamma_n(\tau)], \tag{43a}$$

where

$$\Gamma_n(\tau) = \int_0^\tau \gamma_n(s)ds. \tag{43b}$$

For a smooth and convex surface we have

$$\beta_2(\tau) \gg \beta_n(\tau). \tag{44}$$

Therefore,

$$R_1(\theta,0) \simeq \beta_2(0)P_2(\eta) \tag{45a}$$

and

$$u_1 \simeq -\frac{Q(Q+2)}{(Q+1)(Q+3)}\beta_2(\tau)P_2(\eta)\rho^{-3}. \tag{45b}$$

Discussion

We have seen that for a convex and smooth particle

$$R(\theta,\tau) = 1 + \epsilon\beta_2(\tau)P_2(\eta) + O(\epsilon^2). \tag{46}$$

Since $Q > 0$, and $\beta_2(\tau)$ is monotonically increasing with time, the shape of the particle becomes increasingly nonspherical.

We are interested in the variation of u_A over the surface and the total reaction rate. From the solution derived above the surface value of u_A is given by

$$u_A|_{\rho=R} = \frac{1}{Q+1} + \epsilon\frac{Q}{(Q+1)(Q+3)}\beta_2(\tau)P_2 + O(\epsilon^2), \tag{47}$$

which can be written as

$$\frac{u_A|_{\rho=R} - u_A|^v_{sphere}}{R_{max} - R_{min}} = \frac{2}{3}\frac{Q}{(Q+1)(Q+3)} + O(\epsilon), \tag{48}$$

where $u_A|^v_{sphere}$ is the surface concentration for a spherical particle of equal volume. Since u_1 and R_1 are expressed in terms of Legendre polynomials, the surface integral of u_1 vanishes due to the orthogonality relationship

$$\int_{-1}^{1} P_n(\eta)P_1(\eta)d\eta = 0, \text{ for } n \neq 1. \tag{49}$$

Thus the surface average of u_A is to zero order in ϵ equal to the concentration on the surface of a sphere of equal volume. From Eq.(47) we also see that the local concentration on the surface increases with the radius R.

We next consider the change in the particle shape for a reaction that consumes the solid. We note that the absolute rate of shrinking, $\frac{\partial \tilde{R}}{\partial t}$, increases with the radius $\tilde{R}$, but the relative rate of shrinking, $-\frac{1}{\tilde{R}}\frac{\partial \tilde{R}}{\partial \tau}$, which characterizes the change of the particle shape and is given by

$$\begin{aligned} -\frac{1}{\tilde{R}}\frac{\partial \tilde{R}}{\partial \tau}|_{\tau=0} &\propto \frac{u_A|_{\rho=R}}{R} \\ &\propto \frac{1}{Q+1}\left(1 - \epsilon\frac{3}{Q+3}\beta_2 P_2\right) + O(\epsilon^2), \end{aligned} \tag{50}$$

decreases with the radius.

The shape change can be characterized by the change of the aspect ratio. Using Eqs.(21), (46) and (27),(47) the aspect ratio and the quantity W may be expressed as

$$A_p = 1 + \frac{3}{2}\epsilon\beta_2(\tau) + O(\epsilon^2) \tag{51a}$$

$$W = \frac{3}{(Q+1)(Q+3)} + O(\epsilon). \tag{51b}$$

The asymptotes of W for the two limiting values of Q agree with the general results discussed in the section "Problem Formulation." Substitution of Eq.(51b) in Eq.(25) gives the initial rate of shape change

$$\frac{d\ln(A_p-1)}{d\tau}R\left(\frac{\pi}{2}\right)=\frac{3}{Q(Q+1)(Q+3)}. \tag{52}$$

Equations (48) and (52) are shown as solid lines in Figures 7 and 8.

The method of domain perturbation can also be used to analyze the behavior of a particle under the "sublimation" boundary condition. The solution of the "sublimation" problem proceeds along similar lines, but the rate of change of the aspect ratio is $O(\epsilon^2)$. The shape change of a subliming particle is, therefore, much less than that of a reacting particle.

Particles lacking rotational symmetry

For particles that do not have rotational symmetry, the terms related to the azimuthal ϕ-variation and which have been neglected so far must be retained. It turns out that to first order in ϵ, all the differential equations and boundary conditions remain the same as in the axisymmetric case. If the reduced particle radius R is expressed in terms of spherical harmonics,

$$R=1+\epsilon\sum_{m,n}\beta_{mn}Y_n^m(\theta,\phi), \tag{53}$$

then by following the same procedure as in the axisymmetric case, we obtain

$$\frac{d\beta_{mn}}{d\tau}=\frac{(n+1)-(n-2)Q}{Q(Q+1)(Q+n+1)}\beta_{mn}. \tag{54}$$

Since the coefficient of β_{mn} at the right side does not contain m, the initial shape variations in the azimuthal direction are preserved as reaction progresses.

DOMAIN PERTURBATION FOR THE NONLINEAR DIFFUSION PROBLEM

Following the method used in the previous section we expand $R(\theta,\tau)$ and $\psi(\rho,\theta,\tau)$ as

$$R(\theta,\tau) = 1 + \epsilon R_1(\theta,\tau) + \epsilon^2 R_2(\theta,\tau) + \cdots \tag{55a}$$

$$\psi(\rho,\theta,\tau) = \psi_0(\rho,\tau) + \epsilon\psi_1(\rho,\theta,\tau) + \epsilon^2\psi_2(\rho,\theta,\tau) + \cdots. \tag{55b}$$

The solution will be worked out for $b_2 > 1$, but it turns out also to apply to the case $0 < b_2 < 1$.

$O(1)$-problem

The $O(1)$ equation and boundary conditions

$$\nabla^2\psi_0 = 0, \tag{56a}$$

$$\frac{d\psi_0}{d\rho} = Q(b_2-1)\left(e^{\psi_0} - \frac{1}{b_2-1}\right) \quad \text{at} \quad \rho = 1, \tag{56b}$$

$$\psi_0 \to \psi_b \quad \text{as} \quad \rho \to \infty, \tag{56c}$$

$$-y_{Ab}\frac{dQ}{d\tau} = e^{\psi_0} - \frac{1}{b_2-1} \quad \text{at} \quad \rho = 1, \tag{56d}$$

admit the solution

$$\psi_0 = \psi_b - \frac{c_1}{\rho}, \tag{57}$$

where the constant c_1 is defined implicitly by

$$c_1 = \ln[1 + (b_2-1)y_{Ab}] - \ln(1 + \frac{c_1}{Q}). \tag{58}$$

When diffusion controls (i.e., $Q >> 1$), c_1 is approximately

$$c_1 \simeq \frac{Q}{1+Q}\ln[1 + (b_2-1)y_{Ab}] + \frac{1}{2}\left(\frac{\ln[1 + (b_2-1)y_{Ab}]}{1+Q}\right)^2 + O(Q^{-3}). \tag{59}$$

At $\rho = 1$ we have

$$\psi_0 = \psi_b - c_1, \tag{60}$$

which when substituted in Eq.(56d) gives

$$Q(\tau) = -1 + \sqrt{(1+Q_0)^2 - 2\frac{\ln[1+(b_2-1)y_{Ab}]}{(b_2-1)y_{Ab}}\tau}. \tag{61}$$

$O(\epsilon)$-problem

The first order equation and boundary conditions are as follows:

$$\nabla^2\psi_1 = 0, \tag{62a}$$

$$\psi_1 \to 0 \quad \text{as} \quad \rho \to \infty, \tag{62b}$$

$$\frac{\partial\psi_1}{\partial\rho} = Q(b_2-1)\left[2R_1(e^{\psi_0} - \frac{1}{b_2-1}) + e^{\psi_0}(\psi_1 + c_1R_1)\right] \quad \text{at} \quad \rho = 1, \tag{62c}$$

$$\left(e^{\psi_0} - \frac{1}{b_2-1}\right)c_1 - y_{Ab}Q\frac{\partial R_1}{\partial\tau} = e^{\psi_0}(\psi_1 + c_1R_1) \quad \text{at} \quad \rho = 1. \tag{62d}$$

The solution of Eq.(62a) satisfying boundary condition (62b) is easily derived as a series in spherical harmonics:

$$\psi_1 = \sum_0^\infty \alpha_n(\tau)\rho^{-(n+1)}P_n(\eta) \tag{63}$$

where $P_n(\eta)$ is the nth Legendre function. By expanding R_1 also in Legendre series,

$$R_1 = \sum_0^\infty \beta_n(\tau)P_n(\eta), \tag{64}$$

and applying Eqs. (32a) and (32c) we obtain

$$\beta_0(\tau) = \beta_1(\tau) = 0. \tag{65}$$

Application of boundary condition (62c) provides the additional relationships

$$\alpha_0(\tau) = 0, \tag{66a}$$

$$\alpha_1(\tau) = 0 \tag{66b}$$

and

$$\alpha_n(\tau) = -Q(b_2-1)\frac{2(e^{\psi_0} - \frac{1}{b_2-1}) + c_1 e^{\psi_0}}{n+1+Q(b_2-1)e^{\psi_0}}\beta_n \quad \text{for n} \geq 2. \tag{66c}$$

Introducing the foregoing expressions for ψ_1 and R_1 in Eq.(62d) we obtain

$$\frac{d\beta_n}{d\tau} = \gamma_n(\tau)\beta_n, \tag{67a}$$

where

$$\gamma_n(\tau) = \frac{-\frac{\ln[1+(b_2-1)y_{Ab}]}{(b_2-1)y_{Ab}}\left[(n-2)(Q+\ln[1+(b_2-1)y_{Ab}]) - (n+1)\right]}{Q(1+Q)\left(3+Q+\frac{Q}{1+Q}\ln[1+(b_2-1)y_{Ab}]\right)} + O(Q^{-4}) + O(\epsilon). \tag{67b}$$

When the surface is smooth and convex,

$$\beta_2(\tau) \gg \beta_n(\tau) \tag{68}$$

so that

$$R_1(\theta,\tau) \simeq \beta_2(\tau)P_2(\eta) \tag{69a}$$

$$\psi_1 \simeq -Q(b_2-1)\frac{2(e^{\psi_0} - \frac{1}{b_2-1}) + c_1 e^{\psi_0}}{3+Q(b_2-1)e^{\psi_0}}\beta_2(\tau)P_2(\eta)\rho^{-3}. \tag{69b}$$

Discussion

From the expression for the transformed concentration variable

$$\begin{aligned} y_A\big|_{\rho=R} &= e^{\psi|_{\rho=R}} - \frac{1}{b_2-1} \\ &= \exp(\psi_0|_{\rho=1})\left[1+\epsilon\left(\psi_1|_{\rho=1} + \frac{\partial\psi_0}{\partial\rho}|_{\rho=1}R_1\right) + O(\epsilon^2)\right] - \frac{1}{b_2-1}, \end{aligned} \tag{70}$$

we obtain the following expression for the surface concentration

$$u_A|_{\rho=R} = \frac{\ln[1+(b_2-1)y_{Ab}]}{(b_2-1)y_{Ab}} \frac{1}{1+Q} \times$$

$$\left(1+\epsilon \frac{Q+\frac{Q}{1+Q}\ln[1+(b_2-1)y_{Ab}]}{3+Q+\frac{Q}{1+Q}\ln[1+(b_2-1)y_{Ab}]}\beta_2(\tau)P_2\right) + O(Q^{-3}) + O(\epsilon Q^{-3}) + O(\epsilon^2). \tag{71}$$

Using the orthogonality of P_1 and P_2 we find that the surface average of u_A is to zero order in ϵ equal to that of a spherical particle of equal volume.

Retaining the terms

$$R(\theta,\tau) \simeq 1 + \epsilon\beta_2(\tau)P_2(\eta) \tag{72}$$

and noting that $\beta_2(\tau)$ is monotonically increasing with respect to time we find that the particle shape becomes increasingly nonspherical with time. We also find that the longer the radius of a point on the surface, the higher the concentration; therefore, the absolute rate of shrinking also increases with radius. The shape change is determined by the relative rate of shrinking, $-\frac{1}{\tilde{R}}\frac{\partial \tilde{R}}{\partial \tau}$, which is given by

$$-\frac{1}{\tilde{R}}\frac{\partial \tilde{R}}{\partial \tau}|_{\tau=0} \propto \frac{u_A|_{\rho=R}}{R}$$

$$\propto \frac{\ln[1+(b_2-1)y_{Ab}]}{(b_2-1)y_{Ab}(1+Q)}\left[1-\epsilon\frac{3}{Q+3+\frac{Q}{1+Q}\ln[1+(b_2-1)y_{Ab}]}\beta_2 P_2\right]$$

$$+ O(Q^{-3}) + O(\epsilon Q^{-3}) + O(\epsilon^2). \tag{73}$$

The relative rate of shrinking then also increases with the radius.

The shape of a particle is characterized by its aspect ratio which can be expressed with the help of Eqs.(21) and (72) as

$$A_p = 1 + \frac{3}{2}\epsilon\beta_2(\tau) + O(\epsilon^2). \tag{74}$$

Using Eqs.(27) and (71) to calculate W,

$$W = \frac{3\frac{\ln[1+(b_2-1)y_{Ab}]}{(b_2-1)y_{Ab}}}{(1+Q)\left(3+Q+\frac{Q}{1+Q}\ln[1+(b_2-1)y_{Ab}]\right)} + O(Q^{-3}) + O(\epsilon) \qquad (75)$$

the rate of change of the aspect ratio is obtained as

$$\frac{dA_p}{d\tau} = \frac{A_p - 1}{R(\frac{\pi}{2})} \frac{3\frac{\ln[1+(b_2-1)y_{Ab}]}{(b_2-1)y_{Ab}}}{Q(1+Q)\left(3+Q+\frac{Q}{1+Q}\ln[1+(b_2-1)y_{Ab}]\right)} + O(\epsilon Q^{-4}) + O(\epsilon^2). \qquad (76)$$

Equation (75) possesses the asymptotic behavior indicated at the end of section "Problem Formulation." The foregoing results concerning the change in the particle shape are illustrated in Figure 9 in terms of W vs. Q for several values of the parameter $(b_2 - 1)y_{Ab}$. When the reactant mole fraction in the free stream, y_{Ab}, is very small, the nonlinear binary diffusion equation reduces to the linear equation. Reduction to linear diffusion also obtains in the case of equimolar counterdiffusion, i.e., when the stoichiometric coefficient b_2 is equal to one.

BOUNDARY INTEGRAL SOLUTION

The boundary integral method is applicable to Laplace's equation in a region with a smooth boundary for which Green's second identity yields

$$-2\pi u_{Ai} = \int_\Omega (u_A \frac{\partial g}{\partial n} - g\frac{\partial u_A}{\partial n})\, dS, \qquad (77)$$

where g, Green's function for Laplace's equation, is given by (Stakgold, 1972):

$$g = \frac{1}{|\mathbf{x} - \xi|}. \qquad (78)$$

The subscript i and the position vector ξ denote the position of the singularity and Ω is the boundary of the region. In the present problem Ω consists of two pieces, the surface of the particle and the surface at infinity ($|\mathbf{x}| \to \infty$).

Linear diffusion equation

With the use of the boundary condition

$$u_A \to 1 \qquad \text{as} \quad |\mathbf{x}| \to \infty,$$

Eq.(77) reduces to

$$4\pi - 2\pi u_{Ai} = \int_{\Omega_1} [u_A \frac{\partial g}{\partial n} - g \frac{\partial u_A}{\partial n}] \, dS \tag{79}$$

as shown in Appendix D. Here Ω_1 is the smooth surface of the particle. For axisymmetric particles it is convenient to use cylindrical coordinates and rewrite Eq.(79) as

$$4\pi - 2\pi u_{Ai} = \int_{\Gamma_1} \int_0^{2\pi} [u_A \frac{\partial g}{\partial n} - g \frac{\partial u_A}{\partial n}] \, r d\phi dl, \tag{80}$$

where r is the radius of a surface element from the axis of symmetry and dl is a line element at fixed ϕ. Applying the reaction boundary condition on the particle surface

$$\frac{\partial u_A}{\partial n} = -Q u_A, \tag{81}$$

we finally obtain

$$4\pi - 2\pi u_{Ai} = \int_{\Gamma_1} u_A (\frac{\partial G}{\partial n} + QG) r dl, \tag{82}$$

where

$$G = \int_0^{2\pi} g d\phi. \tag{83}$$

Nonlinear diffusion equation

This has already been reduced to Laplace's equation with nonlinear boundary conditions. The boundary integral method can be applied in the same fashion to obtain

$$4\pi\psi_b - 2\pi\psi_i = \int_{\Omega_1} \left(\psi \frac{\partial g}{\partial n} + gQ[(b_2 - 1)e^{\psi} - 1] \right) dS \tag{84}$$

where Ω_1 is the smooth surface of the particle. This nonlinear integral equation can be solved by an iteration scheme akin to Newton's method. This is implemented by linearizing Eq.(84) by

$$e^{\psi} \simeq e^{\psi_0} + e^{\psi_0}(\psi - \psi_0), \tag{85}$$

to obtain

$$4\pi\psi_b - Z(\psi_0) - 2\pi\psi_i \simeq \int_{\Omega_1} \psi[\frac{\partial g}{\partial n} + gQ(b_2 - 1)e^{\psi_0}]\, dS, \tag{86a}$$

where

$$Z(\psi_0) = \int_{\Omega_1} gQ[(b_2 - 1)e^{\psi_0}(1 - \psi_0) - 1]\, dS. \tag{86b}$$

The solution is then obtained by iteration on the linear equation (84).

Sublimation boundary condition

Using the boundary condition at infinity, Eq.(77) reduces to

$$-2\pi u_{Ai} = \int_{\Omega_1} \left(u_A \frac{\partial g}{\partial n} - g\frac{\partial u_A}{\partial n} \right) dS. \tag{87}$$

Using the condition at the particle surface, $u_A = 1$, and the general identity

$$\int_{\Omega_1} \frac{\partial g}{\partial n} dS = 2\pi, \tag{88}$$

Eq.(87) is further reduced to

$$4\pi = \int_{\Omega_1} g\frac{\partial u_A}{\partial n} dS. \tag{89}$$

In the axisymmetric geometry that we consider here this integral equation takes the form

$$4\pi = \int_{\Gamma_1} G\frac{\partial u_A}{\partial n} r dl, \tag{90}$$

where Γ_1 is the boundary of the two dimensional domain after ϕ-integration and where G has been already defined in Eq.(83).

Method of solution

We first evaluate G and $\frac{\partial G}{\partial n}$ by integration of Green's function and its normal derivative in the azimuthal direction. This integration results in complete elliptic integrals as follows:

$$\frac{\partial G}{\partial n} = \frac{2n_r}{r(a+b)^2}[E_{3/2}(m) - E_{1/2}(m)] - 4\frac{n_r(r+r_i) + n_z(z-z_i)}{(a-b)(a+b)^{1/2}}E_{-1/2}(m) \quad (91a)$$

$$G = \frac{4}{(a+b)^{1/2}}E_{1/2}(m), \quad (91b)$$

where E_k's are elliptic integrals, m is defined as

$$m = \frac{(r-r_i)^2 + (z-z_i)^2}{(r+r_i)^2 + (z-z_i)^2}. \quad (92)$$

r is the distance of a point on the surface from axis of symmetry, and the E_k's, a and b, are defined by

$$E_k = \int_0^{\pi/2} [1 - (1-m)\sin^2\phi]^{-k} d\phi, \quad (93a)$$

$$a = r_i^2 + r^2 + (z-z_i)^2, \quad (93b)$$

$$b = 2rr_i. \quad (93c)$$

The integral equations (82), (84) and (90) were solved by approximating the particle boundary by a piecewise linear surface. The three elliptic integrals were evaluated by approximating polynomials (Liggett and Liu, 1983; Abromowitz and Stegun, 1972) and the integral in the θ-direction was evaluated by 8-point Gaussian quadrature. This numerical procedure gave 0.05% maximum error in the test case of a spherical particle with linear diffusion for which we have a closed form solution.

DISCUSSION

Chemical reaction

Figures 2-4, 7, and 8 show results for linear diffusion and Figures 5, 6, and 9 for binary nonlinear diffusion. Figures 2, 3, 5, and 7-10 show results for several prolate spheroids, and Figures 4, 6, and 11 show similar results for oblate spheroids. The calculations in all these figures were made by the BI technique. Figure 2 shows dimensionless concentrations for $Q = 1$ and three values of eccentricity. In each case the dimensionless surface concentration increases with the radial distance from the origin. Furthermore, the deviation of the concentration from that of a spherical particle increases with the eccentricity.

Figures 3 and 4 show the surface areas and total reaction rates relative to a sphere of equal volume for the linear diffusion problem. The relative reaction rate increases with the aspect ratio and decreases with the Damköhler number Q. For small values of Q, the rate ratio is equal to the surface area ratio but as Q increases, the rate ratio lags behind the surface area ratio. In the range of aspect ratios examined the rate for a prolate spheroid was no more than 20% higher than for a sphere of equal volume. The surface averaged concentration relative to that of a sphere of equal volume decreases with the aspect ratio, and the decrease becomes more pronounced as Q increases. Figure 4 for oblate spheroids looks like Figure 3, but shows more pronounced differences. For both prolate and oblate spheroids, the total reaction rate is nearly equal to that of a sphere of equal surface area. From the standpoint of total reaction rate, therefore, a nonspherical particle can be accurately represented by a spherical particle of equal surface area.

Similar calculations were performed for the nonlinear binary diffusion problem

with the results shown in Figures 5 and 6. The total reaction rate and the surface averaged concentration were normalized by the counterparts of a sphere of equal volume. The difference between the total rate of an ablate spheroid and that of a sphere of equal surface area is somewhat larger than in the linear diffusion problem but still very small.

Figure 7 shows the surface concentrations normalized as suggested by Eq.(48). The two solid lines were calculated with the method of domain perturbation using the initial shape $R(\theta,0) = 1 + (0.01)P_2(\eta)$. The upper line shows the maximum concentration, at $\theta = 0$, and the lower line shows the minimum concentration, at $\theta = \frac{\pi}{2}$. For very large and very small values of Q the concentration approaches the value corresponding to a sphere of equal volume, as expected from the fact that concentration tends to zero or to one repectively at these two limits. The maximum deviation between the two concentrations is attained a little above $Q = 1$.

Figure 8 shows the dimensionless rate of change of the aspect ratio as a function of the Damköhler number Q, with the solid line describing results obtained by domain perturbation and the markers specifying the numerical results obtained by the boundary integral method. The numerical results essentially fall on the analytical curve, showing that the quantity W[Eq.(27)] is not a function of A_p. Going back to Eq.(25) we conclude that the rate of change of the aspect ratio increases with increasing aspect ratio for all values of Q.

Further insight about the shape change of a reacting particle can be obtained from the following expressions for W obtained by domain perturbation. For linear diffusion W is given by

$$W \simeq \frac{3}{(Q+1)(Q+3)} \tag{94a}$$

and for nonlinear binary diffusion by

$$W \simeq \frac{3\frac{\ln[1+(b_2-1)y_{Ab}]}{(b_2-1)y_{Ab}}}{(1+Q)\left(3+Q+\frac{Q}{1+Q}\ln[1+(b_2-1)y_{Ab}]\right)}, \tag{94b}$$

the latter being restricted to large values of the Damköhler number Q. These two expressions are represented by the solid line segments in Figure 9. Equation (84) was solved with all combinations of $b_2 = 1$, $y_{Ab} = 0.1, 0.21, 0.5$, and e=0.6, 0.8, 0.9, 0.95 to calculate the surface concentration distributions which were subsequently used to find W. The results are very close to those obtained with the DP technique. To make Figure 9 legible we show only the BI results for the prolate spheroids of e=0.9 for b_2=2 and y_{Ab}=0.5. As was seen in the linear diffusion problem, W is nearly independent of the degree of particle nonsphericity. In most cases $(b_2 - 1)y_{Ab}$ is between 0.5 and -0.5 when the rate of shape change does not differ much between linear and nonlinear diffusion.

For both linear and nonlinear diffusion W has the asymptotic behavior

$$W \sim \frac{3}{Q^2}\frac{\ln[1+(b_2-1)y_{Ab}]}{(b_2-1)y_{Ab}} \text{ as } Q \to \infty \tag{95a}$$

$$W \sim 1 \text{ as } Q \to 0 \tag{95b}$$

which can be introduced in Eq.(25) to obtain the following asymptotic relations for the rate of change of the aspect ratio:

$$\frac{dA_p}{d\tau} \sim \frac{3}{Q^3}\frac{A_p-1}{R(\frac{\pi}{2})}\frac{\ln[1+(b_2-1)y_{Ab}]}{(b_2-1)y_{Ab}} \text{ as } Q \to \infty \tag{96a}$$

$$\frac{dA_p}{d\tau} \sim \frac{1}{Q}\frac{A_p-1}{R(\frac{\pi}{2})} \text{ as } Q \to 0. \tag{96b}$$

The rate of change of the aspect ratio becomes very large under conditions of reaction control and nearly negligible under diffusion control.

Sublimation

The DP technique applied to the sublimation problem with initial shape $R = 1 + \epsilon\beta_2 P_2$ yields

$$\frac{\partial u_A}{\partial n} = R + O(\epsilon^2) \tag{97}$$

where $u_A = c_A/c_{As}$ and the normal n is based on the dimensionless variable $\mathrm{x} = \tilde{\mathbf{x}}/\tilde{R}_s(t)$. The normal derivative $\frac{\partial u_A}{\partial n}$ on the particle surface was also computed by the BI technique for various prolate and oblate spheroids. The value of $\frac{\partial u_A}{\partial n}$ at $\theta = 0$ and $\theta = \frac{\pi}{2}$ coincides with the values of R at these points. Figures 10 and 11 show the particle surface area, the total sublimation rate and the surface averaged sublimation rate, relative to a sphere of equal volume and the total sublimation rate relative to a sphere of equal surface area, for prolate and oblate spheroids of several eccentricities. The total sublimation rate obtained by integration of the normal derivative, $\frac{\partial u_A}{\partial n}$, given in Eq.(97) yields to zero order in ϵ the value obtained with the sphere of equal volume. Both the surface area ratio and the total sublimation rate ratio increase with the aspect ratio. As in the reaction problem, the sublimation ratio lags the surface area ratio. In the range of aspect ratios examined, the total sublimation rate was no more than 13% higher than that of a sphere of equal volume. On the other hand the surface averaged sublimation rate decreases slightly with the aspect ratio. It is also seen that the total sublimation rate is very close to that of a sphere of equal surface area.

Starting from the kinematic equation (5) and following the procedure explained in Appendix A, one obtains for the sublimation problem

$$\frac{\partial R}{\partial \tau'} = -\frac{R}{\tilde{R}_s}\frac{d\tilde{R}_s}{d\tau'} - \frac{M}{\alpha}\frac{\partial u_A}{\partial n} \tag{98a}$$

where

$$M = \frac{\tilde{R}_s^2(0)}{\tilde{R}_s^2} \tag{98b}$$

$$\tau' = t\frac{D_{AB}c_{As}}{\rho_s \tilde{R}_s^2(0)}. \tag{98c}$$

Substitution of Eq.(98a) in Eq.(22) yields

$$\frac{R^2\left(\frac{\pi}{2}\right)}{M}\frac{dA_p}{d\tau'} = R(0)\frac{\partial u_A}{\partial n}\left(\frac{\pi}{2}\right) - R\left(\frac{\pi}{2}\right)\frac{\partial u_A}{\partial n}(0). \tag{99}$$

Equation (97) and numerical calculations show that $\frac{\partial u_A}{\partial n}$ at $\theta = 0$ and $\theta = \frac{\pi}{2}$ are nearly equal to the respective values of the surface radius, R. Therefore, the rate of change of the aspect ratio given by Eq.(99) is very small.

In its pseudo-steady state formulation, the sublimation problem considered here is identical to the problem of conduction or diffusion around a nonspherical particle. Brenner (1963) treated the more general problem of convective heat and mass transfer in the limit of low Reynolds and Prandtl numbers. Using matched asymptotic expansions he obtained the series solution

$$\frac{\mathrm{Nu}}{\mathrm{Nu_0}} = 1 + \frac{1}{8}\mathrm{Nu_0 Pe} + \cdots, \tag{100}$$

where $\mathrm{Nu_0}$ is the average Nusselt number for the nonspherical particle in the absence of forced convection. The number $\mathrm{Nu_0}$ is the same within a proportionality constant as the total sublimation rate shown in Figures 10 and 11, yielding the relationship

$$\frac{\mathrm{Nu_0}}{2} = \frac{S < \frac{\partial u_A}{\partial n} >}{(S\frac{\partial u_A}{\partial n})_{\mathrm{sphere}}}. \tag{101}$$

The results of Figures 10 and 11 for $\mathrm{Nu_0}$ can be combined with Eq.(100) to provide the total sublimation rate of various spheroids in the limit of low convection.

CONCLUSIONS

1. DP has been used to obtain analytical results for the surface concentration and the initial shape change of a nonspherical axisymmetric particle undergoing reaction with the surrounding fluid in a shrinking core mode. Both linear and nonlinear diffusion were treated. The BI method was used to obtain numerical solutions for particles of highly nonspherical but axisymmetric shape under the same reaction conditions.
2. The local concentration and flux at the particle surface increase with the distance from the particle center. The total reaction rate is almost equal to that of a sphere of equal surface area. From the standpoint of the total reaction rate, therefore, a nonspherical particle is well approximated by a spherical particle of equal surface area. The total reaction rate relative to a sphere of equal volume increases with the aspect ratio and decreases with the Damköhler number, Q. By contrast the surface averaged concentration decreases, albeit only slightly, both with the aspect ratio and with the Damköhler number, Q.
3. The rate of change of the aspect ratio is given by

$$\frac{dA_p}{d\tau} = \frac{1}{Q(\tau)} W \cdot \frac{A_p - 1}{R(\frac{\pi}{2})},$$

where W is defined by

$$W = \frac{A_p u_A\left(\frac{\pi}{2}\right) - u_A(0)}{A_p - 1}.$$

The quantity W is a function of the Damköhler number, Q, approximately independent of the aspect ratio. This function is

$$W \simeq \frac{3}{(1+Q)(3+Q)}$$

for linear diffusion and

$$W \simeq \begin{cases} 1, & \text{if } Q << 1 \\ \dfrac{3\frac{\ln[1+(b_2-1)y_{Ab}]}{(b_2-1)y_{Ab}}}{(1+Q)\left(3+Q+\frac{Q}{1+Q}\ln[1+(b_2-1)y_{Ab}]\right)}, & \text{if } Q >> 1 \end{cases}$$

for nonlinear binary diffusion.

4. In the sublimation problem the normal derivatives $\frac{\partial u_A}{\partial n}(0)$ and $\frac{\partial u_A}{\partial n}(\frac{\pi}{2})$ are equal to $R(0)$ and $R(\frac{\pi}{2})$, respectively. Consequently, the shape change in that problem is negligible. The total sublimation rate relative to a sphere of equal volume increases with the aspect ratio while the surface averaged sublimation rate shows the opposite behavior. The total rate is again very close to that of a sphere of equal area.

NOTATION

$A(g)$	gaseous reactant
A_p	aspect ratio
$B(g)$	gaseous product
b_1, b_2	stoichiometric coefficients
c	total concentration of gas phase
c_A	concentration of A in gas
c_1	integration constant
D_{AB}	binary diffusion coefficient
E_k	elliptic integrals
e	eccentricity
$\tilde{F}$	function defining particle shape
G	Green's function integrated in azimuthal angle [Eq.(83)]
g	Green's function for 3-dimensional Laplace's equation
k	reaction constant
l	surface line of axisymmetric particle
M	defined by Eq.(98b)
$\mathbf{n}$	outward normal unit vector from domain
$P(s)$	solid reactant
P_n	nth Legendre polynomial
Q	Damköhler number [Eq.(9b)]
$R(\theta,\tau)$	dimensionless radial distance from particle center, $\frac{\tilde{R}(\theta,\tau)}{\tilde{R}_s(\tau)}$
R_1	magnitude of 1st mode of surface initially specified
$\tilde{R}(\theta,\tau)$	dimensional radius of a surface point

$\tilde{R}_s(\tau)$	dimensional radius of the fictitious sphere of equal volume
r	cylindrical radius of a surface point
r_A	reaction or sublimation rate of A
S	surface area of particle
t	time
u_A	dimensionless concentration of A $(= \frac{c_A}{c_{Ab}}$ or $\frac{c_A}{c_{As}})$
u_n	nth order perturbation of u_A
$\mathbf{v_s} \cdot \tilde{\mathbf{n}}$	surface velocity
W	defined by Eq.(27)
$\mathbf{x}$	dimensionless position vector $(=\frac{\tilde{\mathbf{x}}}{\tilde{R}_s(\tau)})$
$\tilde{\mathbf{x}}$	dimensional position vector
Y_n^m	spherical harmonics
y_A	mole fraction of A

Greek letters

α_n	coefficients used in expanding u_A
β_n	coefficients used in expanding $R(\theta, \tau)$
Γ_n	defined by Eq.(43b)
Γ_1	line boundary of axisymmetric domain
γ_n	defined by Eq.(42b)
ϵ	small perturbation parameter
ϕ	azimuthal angle
η	$\cos\theta$
θ	spherical angle

ξ	position vector of singular point
ρ	radial variable
ρ_s	molar density of solid
τ	dimensionless time variable defined by Eq.(9b)
τ'	dimensionless time variable defined by Eq.(98c)
ψ	transformed dependent variable defined by Eq.(17)
$\Omega, \Omega_1, \Omega_2$	surface boundaries of domain

Subscripts

A	gaseous reactant A
b	bulk position at ∞
i	singular point
0	initial value
t	total rate all over particle surface

Superscripts

v	sphere of equal volume
s	sphere of equal surface area

REFERENCES

Abramowitz, M. and Stegun, I.A., 1972, *Handbook of Mathematical Functions*, 8th ed., pp. 590-591, Dover, New York.

Acrivos, A. and Taylor, T.D., 1964, The Stokes flow past an arbitrary particle: The slightly deformed sphere. *Chem. Engng Sci.* **19**, 445-451.

Bird, R.B., Stewart, W.E. and Lightfoot, E.N., 1960, *Transport Phenomena*, pp. 569-572, Wiley, New York.

Bischoff, K.B., 1963, Accuracy of the pseudo steady state approximation for moving boundary diffusion problems. *Chem. Engng Sci.* **18**, 711-713.

Brebbia, C.A. and Walker, S., 1980, *Boundary Element Techniques in Engineering*, pp. 25-53, Newnes-Butterworths, London.

Brenner, H., 1963, Forced convection heat and mass transfer at small Peclet numbers from a particle of arbitrary shape. *Chem. Engng Sci.* **18**, 109-122.

Brenner, H., 1964, The Stokes resistance of a slightly deformed sphere. *Chem. Engng Sci.* **19**, 519-539.

Kirkaldy, J.S., 1958, The time-dependent diffusion theory for condensation on spherical and plane surfaces. *Can. J. Phys.* **36**, 446-455.

Krishna, R. and Standart, G.L., 1976, A multicomponent film model incorporating a general matrix method of solution to the Maxwell-Stefan equations. *AIChE J.* **22**, 383-389.

Liggett, J.A. and Liu, P.L-F., 1983, *The Boundary Integral Equation Method for Porous Media Flow*, pp. 86-110, George Allen & Unwin Ltd, London.

Luss, D., 1968, On the pseudo steady state approximation gas solid reactions. *Can. J. Chem. Eng.* **46**, 154-156.

Stakgold, I., 1972, *Boundary Value Problems of Mathematical Physics*, Vol. II, pp. 88-193, Macmillan, New York.

Stewart, W.E. and Prober, R., 1964, Matrix calculation of multicomponent mass transfer in isothermal system. *I&EC Fund.* **3**, 224-235.

Toor, H.L., 1964, Solution of the linearized equations of multicomponent mass transfer: II. Matrix methods. *AIChE J.* **10**, 460-465.

Youngren, G.K. and Acrivos, A., 1975, Stokes flow past a particle of arbitrary shape: A numerical method of solution. *J. Fluid Mech.* **69**, 377-403.

APPENDIX A: DERIVATION OF EQS.(7d)-(8b)

In this appendix we derive Eqs.(7d)-(8b). The particle shape is defined by the equation

$$\tilde{F} \equiv \tilde{\rho} - \tilde{R}(\theta, t) \equiv 0, \tag{A.1}$$

which is differentiated with respect to time to give

$$\frac{\partial \tilde{F}}{\partial t} + \mathbf{v_s} \cdot \nabla_{\tilde{x}} \tilde{F} = 0. \tag{A.2}$$

Expressing $\nabla_{\tilde{x}} \tilde{F}$ in spherical coordinates,

$$\nabla_{\tilde{x}} \tilde{F} = \mathbf{i}_\rho - \mathbf{i}_\theta \frac{1}{\tilde{R}} \frac{\partial \tilde{R}}{\partial \theta} \tag{A.3}$$

and noting that

$$\frac{\nabla_{\tilde{x}} \tilde{F}}{|\nabla_{\tilde{x}} \tilde{F}|} = -\tilde{\mathbf{n}}, \tag{A.4}$$

we can derive the unit normal outward vector

$$\tilde{\mathbf{n}} = -\alpha \mathbf{i}_{\tilde{\rho}} + \beta \mathbf{i}_\theta, \tag{8a}$$

where

$$\alpha = \frac{1}{\sqrt{1 + \left(\frac{1}{\tilde{R}} \frac{\partial \tilde{R}}{\partial \theta}\right)^2}} \quad \text{and} \quad \beta = \frac{\frac{1}{\tilde{R}} \frac{\partial \tilde{R}}{\partial \theta}}{\sqrt{1 + \left(\frac{1}{\tilde{R}} \frac{\partial \tilde{R}}{\partial \theta}\right)^2}}. \tag{8b}$$

Substitution of Eq.(A.4) in Eq.(A.2) gives

$$\frac{1}{|\nabla_{\tilde{x}} \tilde{F}|} \frac{\partial \tilde{F}}{\partial t} - \mathbf{v_s} \cdot \tilde{\mathbf{n}} = 0 \quad \text{on the particle surface}. \tag{5}$$

Finally, introducing the mass balance,

$$\rho_s \mathbf{v_s} \cdot \tilde{\mathbf{n}} dS = b_1 k c_A dS \tag{A.5}$$

we obtain

$$-\frac{\partial \tilde{R}}{\partial t} = \frac{b_1 k}{\rho_s \alpha} c_A \quad \text{at} \quad \tilde{\rho} = \tilde{R}(\theta, t). \tag{7d}$$

APPENDIX B: MULTICOMPONENT DIFFUSION

Diffusion in an n-component gas under isothermal and isobaric condition is described by the Stefan-Maxwell equations. For an n-component system there are n-1 independent equations (Bird *et al.*, 1960):

$$\nabla y_i = \sum_{\substack{j=1 \\ j \neq i}}^{n} \frac{1}{cD_{ij}} (y_i \mathbf{N}_j - y_j \mathbf{N}_i) \,, \text{ i=1,} \cdots \text{,n-1.} \tag{B.1}$$

We wish to decouple these equations by a matrix transformation. This problem has been considered previously for special cases. Toor (1960) and Stewart and Prober (1964) linearized the Stefan-Maxwell equations to solve certain flow problems. Krishna and Standart (1976) used the Stefan-Maxwell equations for steady one dimensional multicomponent diffusion. We here extend Krishna and Standart's approach to the three dimensional steady state problem with arbitrary boundary shape. The n independent species balance equations

$$\nabla \cdot \mathbf{N}_i = 0, i = 1, \cdots, n \tag{B.2}$$

and the relation

$$y_1 + y_2 + \cdots + y_n = 1 \tag{B.3}$$

along with Eqs.(B.1) constitute a system in the 2n unknowns $y_1, \cdots, y_n, \mathbf{N}_1, \cdots, \mathbf{N}_n$. We shall consider a "reaction" boundary condition along with the boundary condition at infinity

$$y_i \rightarrow y_{ib} \text{ as } |\mathbf{x}| \rightarrow \infty. \tag{B.4}$$

As in the case of nonlinear binary diffusion, the system (B.1)-(B.4) has an infinite family of solutions. We shall again single out the solution satisfying the relationships

$$\frac{\mathbf{N}_i}{\nu_i} \equiv \text{ independent of } i. \tag{B.5}$$

Using Eq.(B.5) we can eliminate $\mathbf{N}_2, \cdots, \mathbf{N}_n$ and obtain

$$\nabla \mathbf{y} = \frac{\mathbf{N}_1}{c\nu_1} \mathbf{K}\mathbf{y}, \tag{B.6}$$

where

$$\mathbf{y}^T = (y_1, y_2, \cdots, y_n), \tag{B.7}$$

and $\mathbf{K}$ is the matrix

$$\mathbf{K} = \begin{pmatrix} K_{11} & -\frac{\nu_2}{D_{12}} & \cdots & -\frac{\nu_n}{D_{1n}} \\ -\frac{\nu_1}{D_{21}} & K_{22} & \cdots & -\frac{\nu_n}{D_{2n}} \\ \vdots & \vdots & \ddots & \vdots \\ -\frac{\nu_1}{D_{n1}} & -\frac{\nu_2}{D_{n2}} & \cdots & K_{nn} \end{pmatrix} \tag{B.8}$$

with K_{ii} given by

$$K_{ii} = \sum_{\substack{j=1 \\ j \neq i}}^{n} \frac{\nu_j}{D_{ij}}. \tag{B.9}$$

If $\mathbf{K}$ is diagonalized by a matrix $\mathbf{T}$,

$$\mathbf{\Lambda} = \mathbf{T}^{-1}\mathbf{K}\mathbf{T} \tag{B.10}$$

with $\Lambda_{ij} = \delta_{ij}\lambda_i$, then Eq.(B.6) can be decoupled,

$$\nabla \mathbf{z} = \frac{\mathbf{N}_1}{c\nu_1} \mathbf{\Lambda}\mathbf{z}, \tag{B.11}$$

where

$$\mathbf{z} = \mathbf{T}^{-1}\mathbf{y}. \tag{B.12}$$

The basic species conservation $\nabla \cdot \mathbf{N}_i = 0$ now yields

$$\nabla^2 \ln z_i = 0 \text{ (all i)} \tag{B.13}$$

with boundary condition at infinity

$$z_i = z_{ib} = \left(\mathbf{T}^{-1}\mathbf{y}_b\right)_i \text{ as } |\mathbf{x}| \to \infty. \tag{B.14}$$

We set

$$w_i = \ln z_i \tag{B.15}$$

and consider the reaction rate a function of $w_1, \cdots, w_n$ by virtue of Eq.(B.12):

$$r = f(w_1, \cdots, w_n). \tag{B.16}$$

Introducing Eq.(B.15) into Eq.(B.11) we obtain

$$\nabla w_i = \frac{\mathbf{N}_i}{c\nu_i}\lambda_i,\ i = 1, \cdots, n. \tag{B.17}$$

The boundary conditions at the particle surface are

$$\mathbf{N}_i \cdot \mathbf{n} = -\nu_i f(w_1, \cdots, w_n) \tag{B.18}$$

which upon introduction of Eq.(B.17) becomes

$$\mathbf{n} \cdot \nabla w_i = -\frac{\lambda_i}{c} f(w_1, \cdots, w_n). \tag{B.19}$$

The problem has been finally transformed to the form

$$\nabla^2 w_i = 0,\ i = 1, \cdots, n \tag{B.20}$$

with boundary conditions given by Eqs.(B.14) and (B.19), the latter weakly coupling the unknowns $w_1, \cdots, w_n$. Using the boundary integral method, Eqs.(B.20), (B.14) and (B.19) can be converted to a single nonlinear integral equation.

APPENDIX C: DOMAIN PERTURBATION DETAILS

Here we present the derivation of various relationships in the application of domain perturbation for the linear diffusion problem. The derivations are very similar for the problem of nonlinear binary diffusion. Using domain perturbation, Eqs. (10b) and (10d) are expressed as

$$[1+\epsilon(2R_1)+\epsilon^2(2R_2+R_1^2)+\cdots][\frac{\partial u_0}{\partial\rho}+\epsilon(\frac{\partial u_1}{\partial\rho}+\frac{\partial^2 u_0}{\partial\rho^2}R_1)$$

$$+\epsilon^2(\frac{\partial u_2}{\partial\rho}+\frac{\partial^2 u_0}{\partial\rho^2}R_2+\frac{\partial^2 u_1}{\partial\rho^2}R_1+\frac{1}{2}\frac{\partial^3 u_0}{\partial\rho^3}R_1^2)+\cdots]$$

$$-(\epsilon\frac{\partial R_1}{\partial\theta}+\epsilon^2\frac{\partial R_2}{\partial\theta}+\cdots)$$

$$\times[\frac{\partial u_0}{\partial\theta}+\epsilon(\frac{\partial u_1}{\partial\theta}+\frac{\partial^2 u_0}{\partial\rho\partial\theta}R_1)+\epsilon^2(\frac{\partial u_2}{\partial\theta}+\frac{\partial^2 u_0}{\partial\rho\partial\theta}R_2+\frac{\partial^2 u_1}{\partial\rho\partial\theta}R_1+\frac{1}{2}\frac{\partial^3 u_0}{\partial\rho^2\partial\theta}R_1^2)+\cdots]$$

$$=Q[1+\epsilon(2R_1)+\epsilon^2(2R_2+R_1^2+\frac{1}{2}(\frac{\partial R_1}{\partial\theta})^2)+\cdots]$$

$$\times[u_0+\epsilon(u_1+\frac{\partial u_0}{\partial\rho}R_1)+\epsilon^2(u_2+\frac{\partial u_1}{\partial\rho}R_1+\frac{\partial u_0}{\partial\rho}R_2+\frac{1}{2}\frac{\partial^2 u_0}{\partial\rho^2}R_1^2)+\cdots] \qquad \text{(C.1)}$$

and

$$-\frac{dQ}{d\tau}-\epsilon(\frac{dQ}{d\tau}R_1+Q\frac{\partial R_1}{\partial\tau})-\epsilon^2(\frac{dQ}{d\tau}R_2+Q\frac{\partial R_2}{\partial\tau})-\cdots=u_0+\epsilon(u_1+\frac{\partial u_0}{\partial\rho}R_1)$$

$$+\epsilon^2[u_2+\frac{\partial u_1}{\partial\rho}R_1+\frac{\partial u_0}{\partial\rho}R_2+\frac{1}{2}\frac{\partial^2 u_0}{\partial\rho^2}R_1^2+\frac{1}{2}(\frac{\partial R_1}{\partial\theta})^2u_0]+\cdots. \qquad \text{(C.2)}$$

The boundary conditions at $\rho=1$ for the $O(1)$-problem are

$$\frac{\partial u_0}{\partial\rho}=Qu_0, \qquad \text{(C.3)}$$

$$-\frac{dQ}{d\tau}=u_0, \qquad \text{(C.4)}$$

and similar boundary conditions apply to the $O(\epsilon)$-problem

$$\frac{\partial u_0}{\partial \rho}(2R_1) + \frac{\partial u_1}{\partial \rho} + \frac{\partial^2 u_0}{\partial \rho^2} R_1 - \frac{\partial R_1}{\partial \theta}\frac{\partial u_0}{\partial \theta} = Q[u_1 + \frac{\partial u_0}{\partial \rho} R_1 + u_0(2R_1)], \tag{C.5}$$

$$-(\frac{dQ}{d\tau} R_1 + Q\frac{\partial R_1}{\partial \tau}) = u_1 + \frac{\partial u_0}{\partial \rho} R_1. \tag{C.6}$$

The $O(1)$-problem can be solved with Eqs.(C.3) and (C.4) to obtain

$$u_0|_{\rho=1} = \frac{1}{Q+1}, \tag{C.7}$$

$$\frac{\partial u_0}{\partial \rho}|_{\rho=1} = \frac{Q}{Q+1}, \tag{C.8}$$

$$\frac{\partial^2 u_0}{\partial \rho^2}|_{\rho=1} = -\frac{2Q}{Q+1}, \tag{C.9}$$

$$\frac{\partial^3 u_0}{\partial \rho^3}|_{\rho=1} = \frac{6Q}{Q+1} \tag{C.10}$$

$$\frac{\partial u_0}{\partial \theta} = 0. \tag{C.11}$$

With the use of

$$\frac{dQ}{d\tau} = -\frac{1}{Q+1}, \tag{C.12}$$

Eqs. (C.5) and (C.6), B.C.'s for the $O(\epsilon)$-problem, reduce to

$$\frac{\partial u_1}{\partial \rho} - Qu_1 = \frac{Q(Q+2)}{(Q+1)} R_1, \tag{C.13}$$

$$Q\frac{\partial R_1}{\partial \tau} + \frac{Q-1}{Q+1} R_1 + u_1 = 0. \tag{C.14}$$

APPENDIX D: DERIVATION OF BOUNDARY INTEGRAL EQUATIONS

When the singular point ξ lies on the boundary and if the boundary is smooth at the point ξ, the exterior problem of Laplace's equation is equivalent to (Liggett and Liu, 1972)

$$-2\pi u_{Ai} = \int_\Omega (u_A \frac{\partial g}{\partial n} - g\frac{\partial u_A}{\partial n})\, dS. \tag{D.1}$$

We now apply Eq.(D.1) to the problem of a reacting particle. The boundary condition at infinity can be treated by considering a fictitious large sphere surrounding the particle and let the radius of that sphere go to infinity. As shown in Figure 12 the boundary Ω is separated into two pieces, Ω_1 and Ω_2. Ω_1 is the boundary of the particle and Ω_2 is the boundary of the fictitious surrounding sphere centered at the singular point, ξ. Therefore,

$$\int_{\Omega} (u_A \frac{\partial g}{\partial n} - g \frac{\partial u_A}{\partial n}) \, dS = \int_{\Omega_1} + \lim_{R_\infty \to \infty} \int_{\Omega_2} . \tag{D.2}$$

With the use of the boundary condition at infinity

$$u_A \to 1 \quad \text{as } |\mathbf{x}| \to \infty,$$

Eq.(D.2) changes to

$$\begin{aligned} \lim_{R_\infty \to \infty} \int_{\Omega_2} &= \lim_{R_\infty \to \infty} \int_{\Omega_2} [u_A(-\frac{1}{{R_\infty}^2}) - \frac{1}{R_\infty} \frac{\partial u_A}{\partial n}] \, dS \\ &= -4\pi - \lim_{R_\infty \to \infty} \int_{\Omega_2} \frac{1}{R_\infty} \frac{\partial u_A}{\partial n} dS. \end{aligned} \tag{D.3}$$

Any harmonic function which goes to 1 at infinity can be written for sufficiently large ρ in the form

$$1 + \sum_{n=0}^{\infty} \sum_{m=-n}^{n} b_{mn} \rho^{-n-1} Y_n^m(\theta, \phi). \tag{D.4}$$

Therefore,

$$u_A|_{R_\infty} = 1 + O(\frac{1}{R_\infty}) \tag{D.5}$$

and

$$\frac{\partial u_A}{\partial n}|_{R_\infty} = O(\frac{1}{R_\infty^2}). \tag{D.6}$$

Taking the limit

$$\lim_{R_\infty \to \infty} \int_{\Omega_2} \frac{1}{R_\infty} \frac{\partial u_A}{\partial n} dS = 0, \tag{D.7}$$

we finally obtain

$$4\pi - 2\pi u_{Ai} = \int_{\Omega_1} [u_A \frac{\partial g}{\partial n} - g \frac{\partial u_A}{\partial n}] \, dS, \tag{D.8}$$

which was used as Eq.(79).

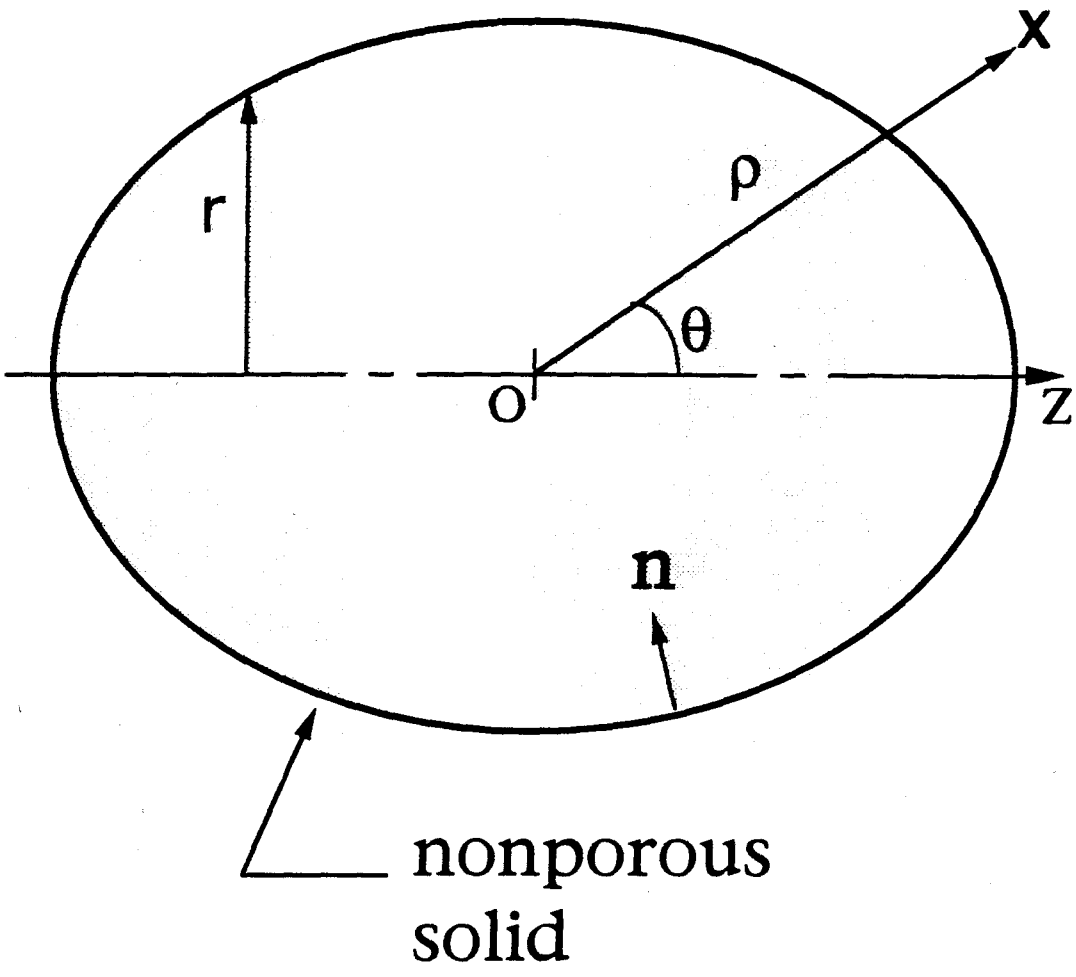

Figure 1. Geometry and notation for a nonspherical particle.

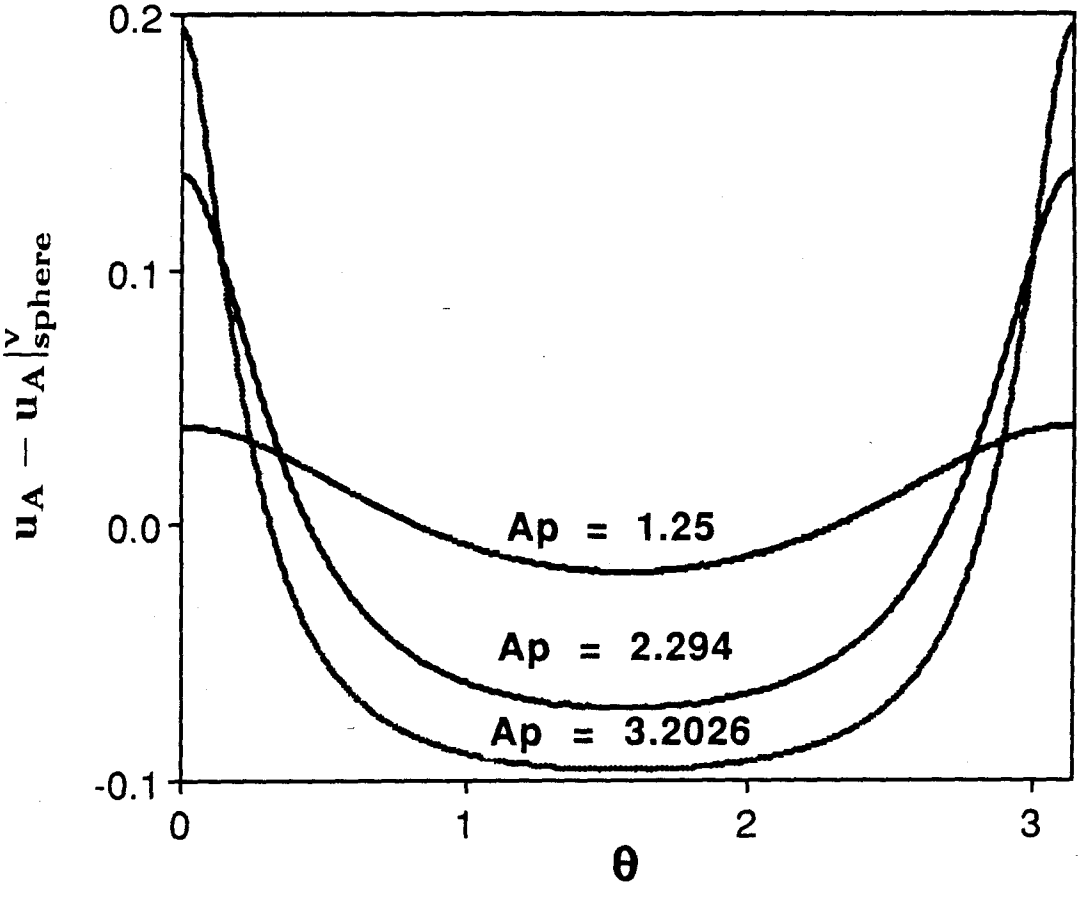

Figure 2. Variation of surface concentration for Q=1.

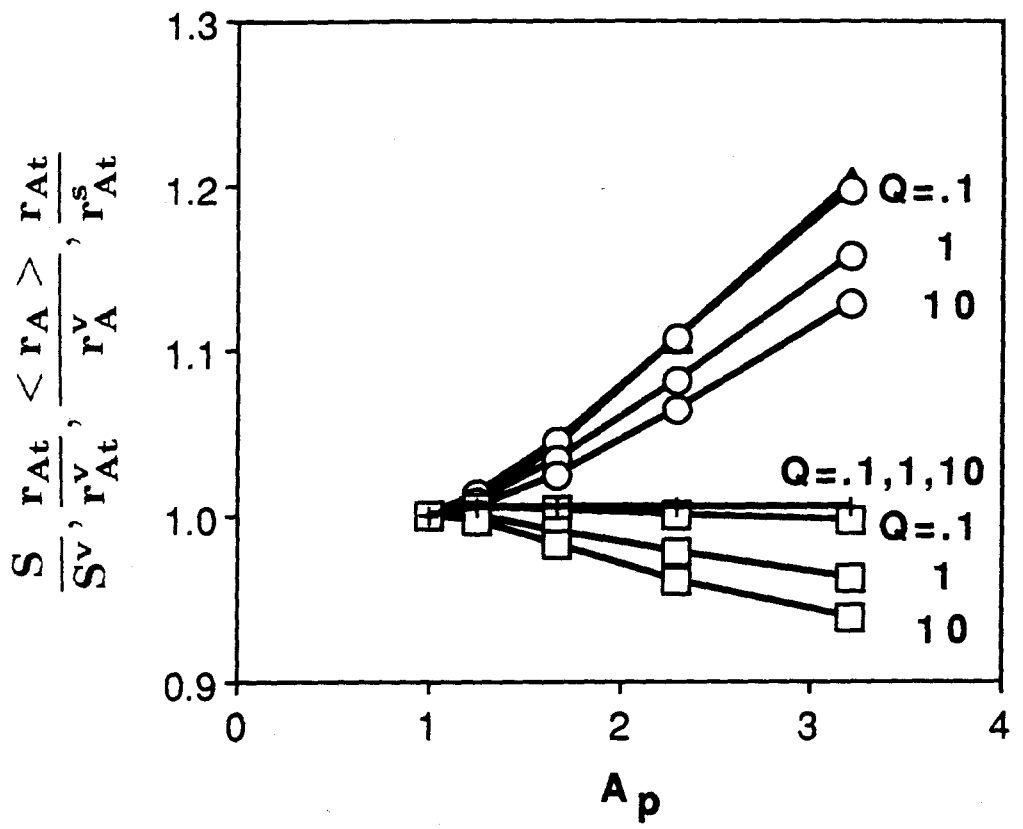

Figure 3. Surface area $S/S^v(\triangle)$, total reaction rate $r_{At}/r^v_{At}(\bigcirc)$, surface averaged reaction rate $< r_A > /r^v_A(\square)$ normalized by those of a sphere of equal volume and total reaction rate $< r_A > /r^s_A(+)$ normalized by that of a sphere of equal surface area vs. the aspect ratio of a reacting prolate spheroid in the linear diffusion regime.

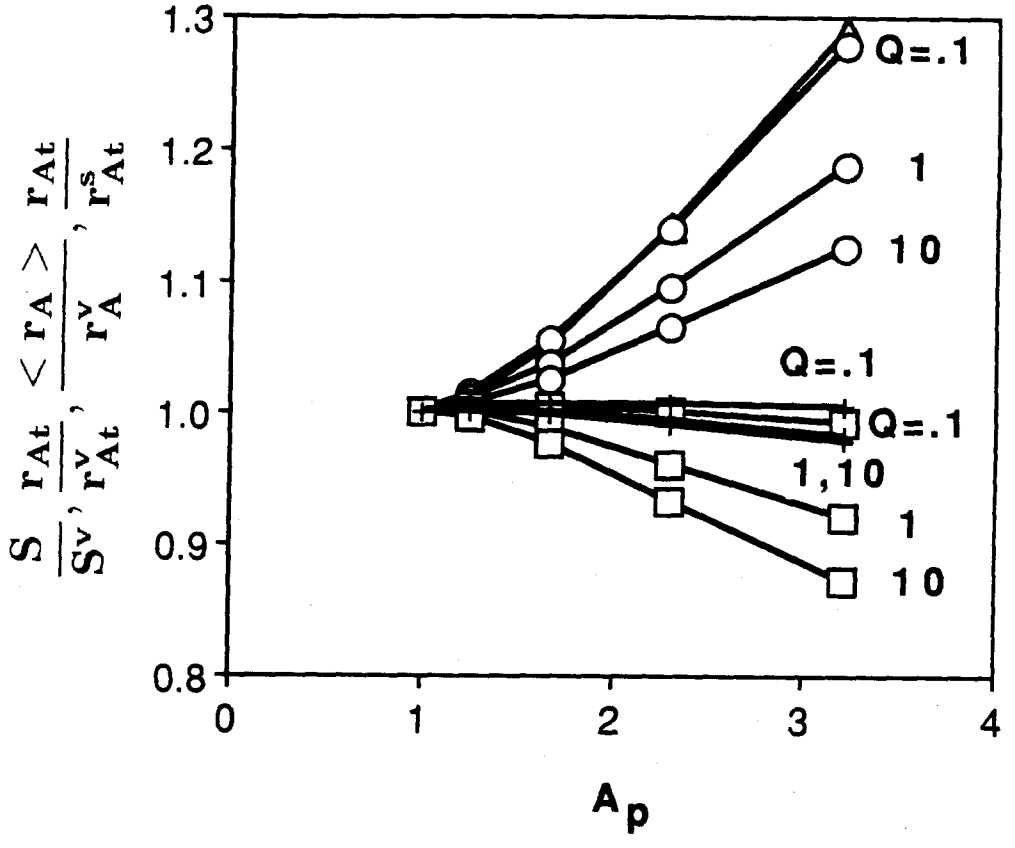

Figure 4. Surface area $S/S^v(\triangle)$, total reaction rate $r_{At}/r^v_{At}(\bigcirc)$, surface averaged reaction rate $< r_A > /r^v_A(\square)$ normalized by those of a sphere of equal volume and total reaction rate $< r_A > /r^s_A(+)$ normalized by that of a sphere of equal surface area vs. the aspect ratio of a reacting oblate spheroid in the linear diffusion regime.

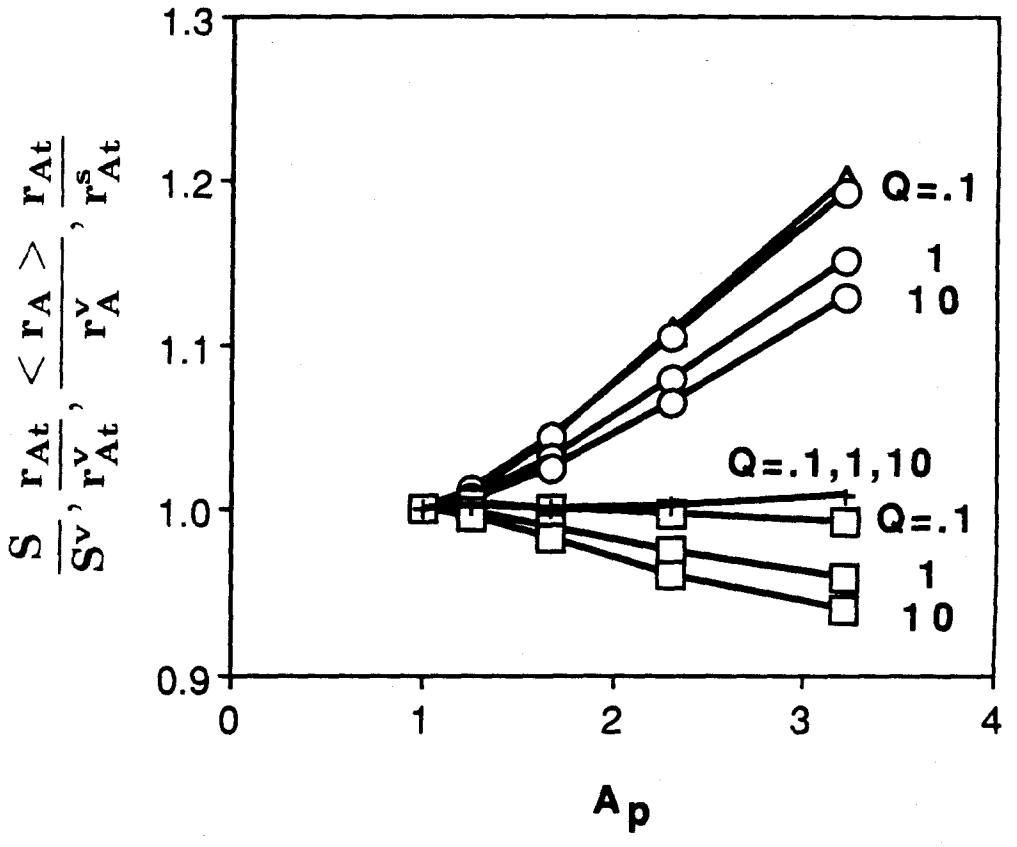

Figure 5. Surface area $S/S^v(\triangle)$, total reaction rate $r_{At}/r^v_{At}(\bigcirc)$, surface averaged reaction rate $< r_A > /r^v_A(\square)$ normalized by those of a sphere of equal volume and total reaction rate $< r_A > /r^s_A(+)$ normalized by that of a sphere of equal surface area vs. the aspect ratio of a reacting prolate spheroid in the nonlinear diffusion regime.

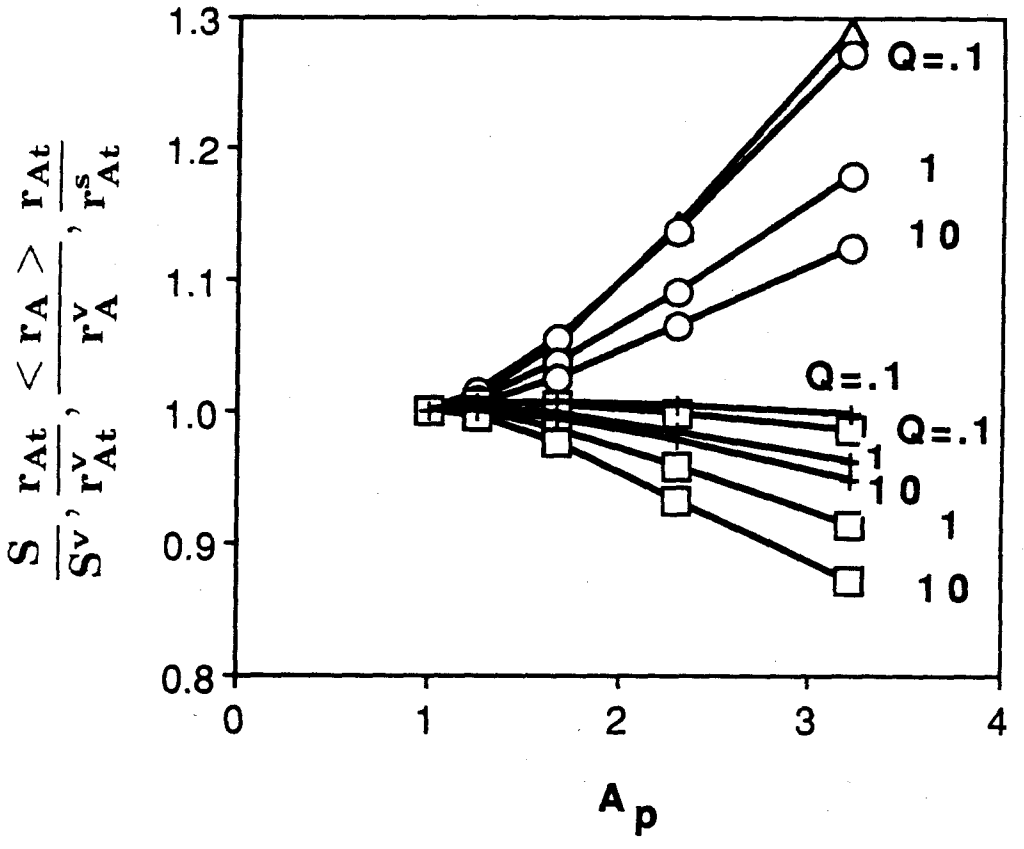

Figure 6. Surface area $S/S^v(\triangle)$, total reaction rate $r_{At}/r^v_{At}(\bigcirc)$, surface averaged reaction rate $< r_A > /r^v_A(\square)$ normalized by those of a sphere of equal volume and total reaction rate $< r_A > /r^s_A(+)$ normalized by that of a sphere of equal surface area vs. the aspect ratio of a reacting oblate spheroid in the nonlinear diffusion regime.

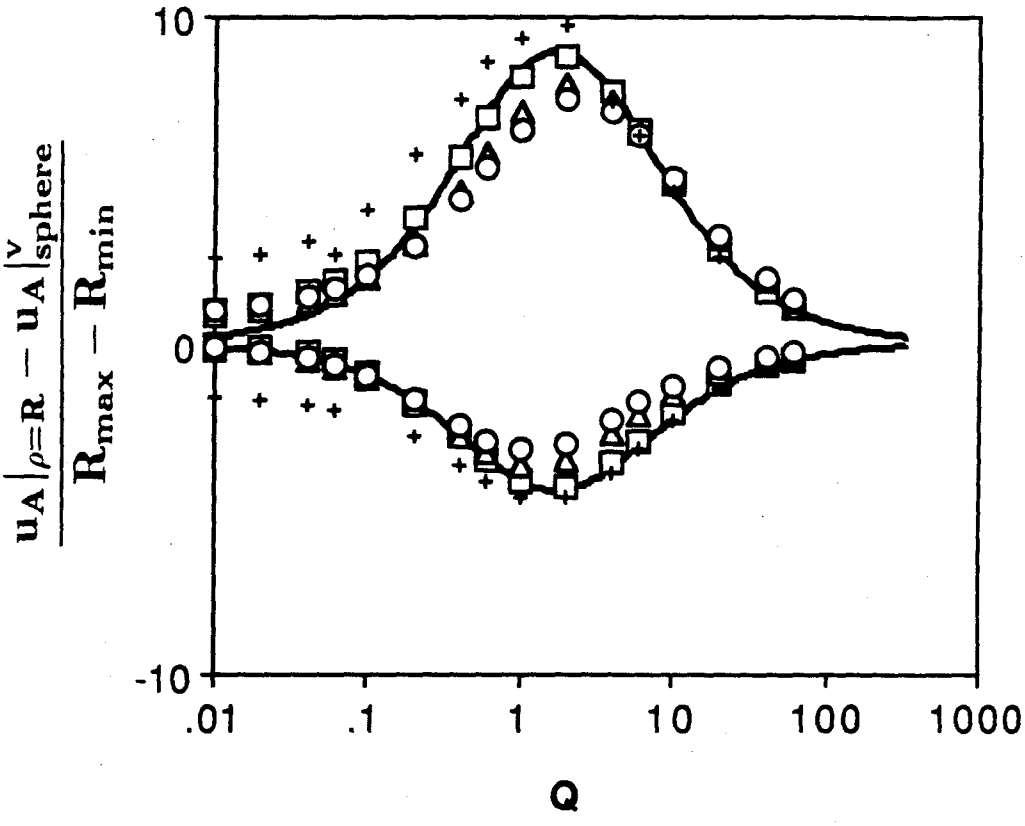

Figure 7. Variation of maximum and minimum surface concentrations with Q.

DP ; solid line

BI ; +(ϵ=0.01), □(e=0.6), △(e=0.9), ○(e=0.95)

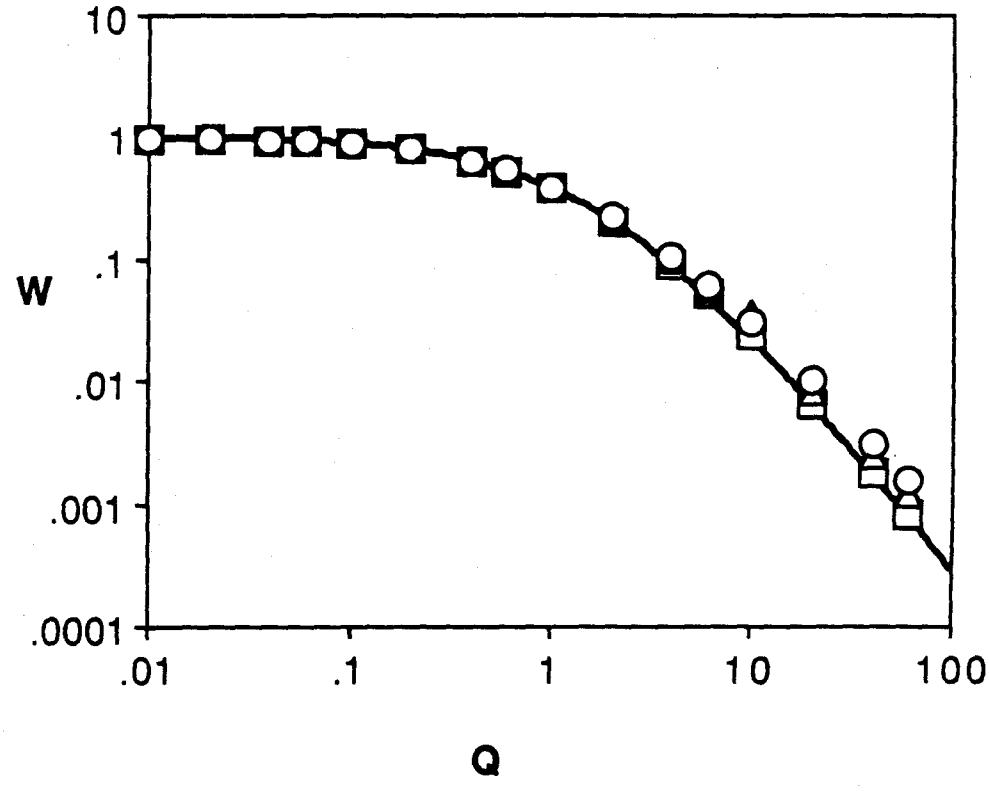

Figure 8. Rate of change of aspect ratio of a reacting particle vs. Q for linear diffusion.

DP ; solid line

BI ; +(ϵ=0.01), □(e=0.6), △(e=0.9), ○(e=0.95)

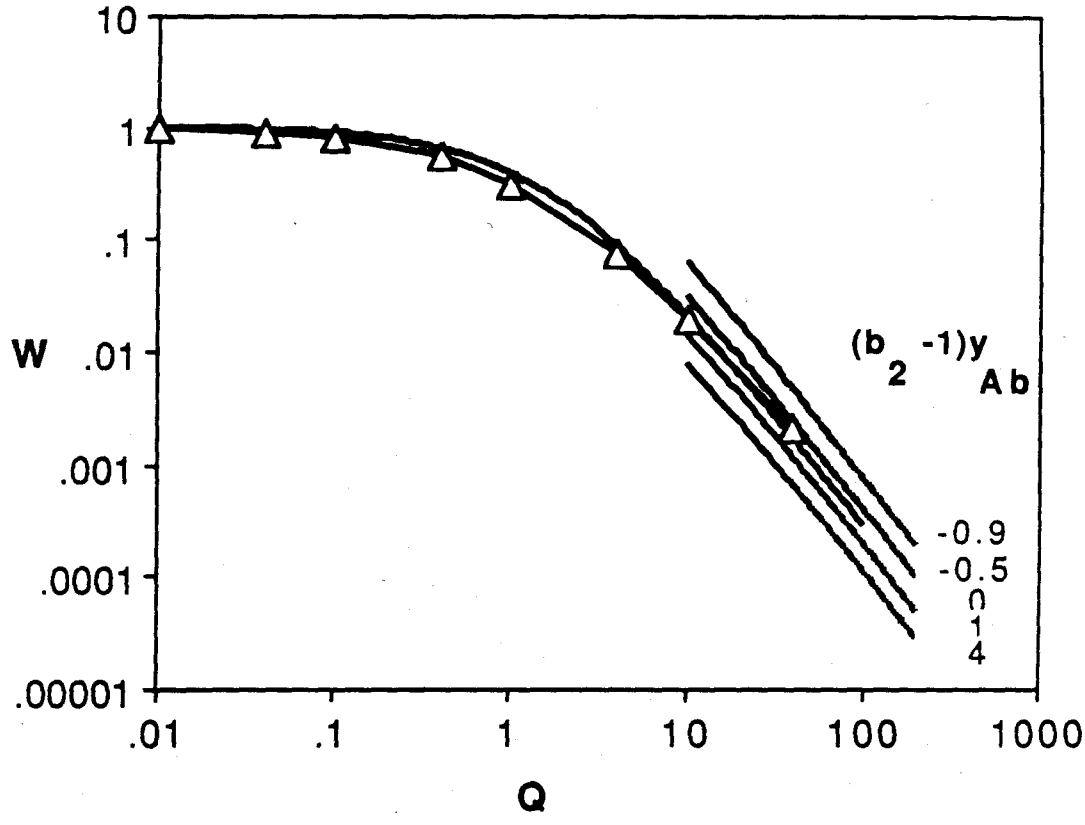

Figure 9. Rate of change of aspect ratio of a reacting particle vs. Q for nonlinear diffusion.

DP ; solid line

BI ; $\triangle$(e=0.9, b_2=2, y_{Ab}=0.5)

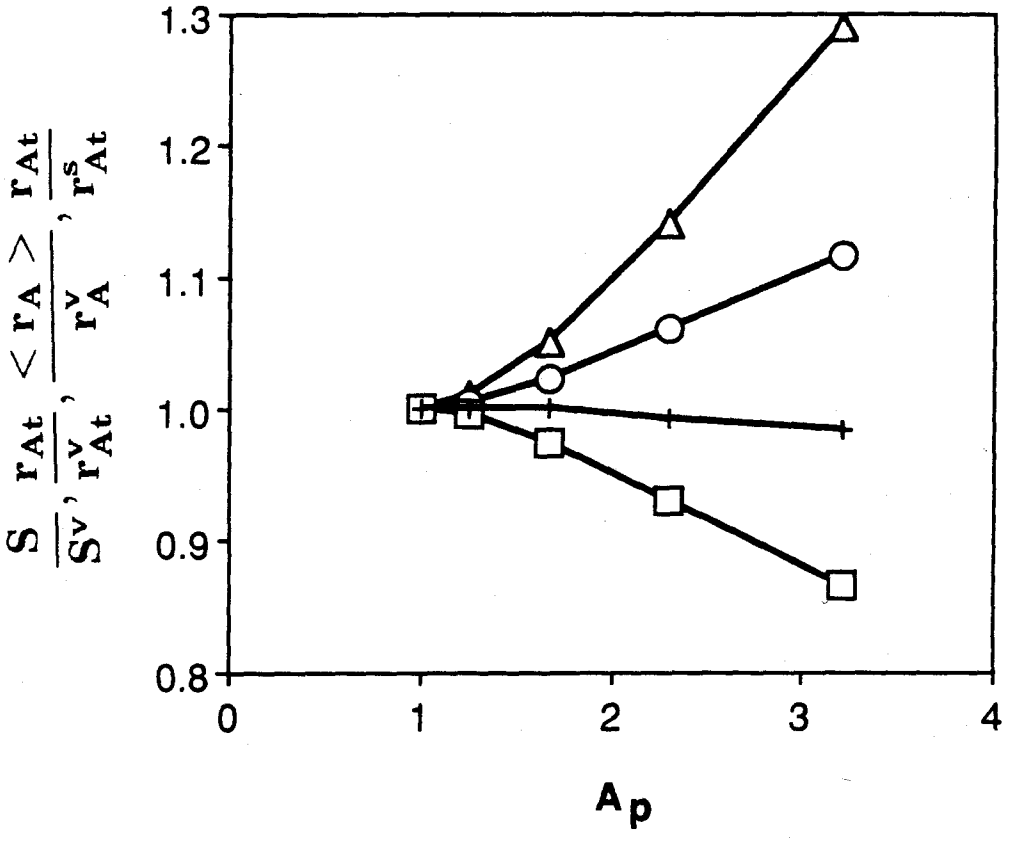

Figure 10. Surface area $S/S^v(\triangle)$, total sublimation rate $r_{At}/r^v_{At}(\bigcirc)$, surface averaged sublimation rate $< r_A > /r^v_A(\square)$ normalized by those of a sphere of equal volume and total reaction rate $< r_A > /r^s_A(+)$ normalized by that of a sphere of equal surface area vs. the aspect ratio of a subliming prolate spheroid.

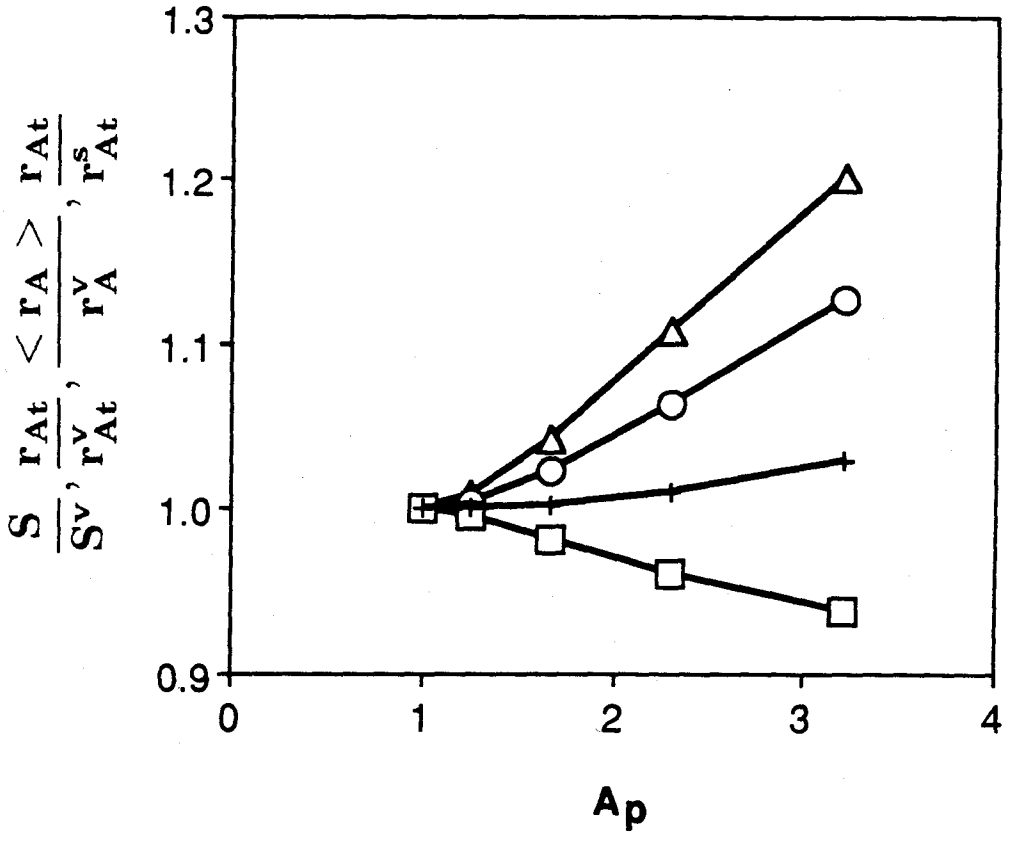

Figure 11. Surface area $S/S^v(\triangle)$, total sublimation rate $r_{At}/r^v_{At}(\bigcirc)$, surface averaged sublimation rate $< r_A > /r^v_A(\square)$ normalized by those of a sphere of equal volume and total reaction rate $< r_A > /r^s_A(+)$ normalized by that of a sphere of equal surface area vs. the aspect ratio of a subliming oblate spheroid.

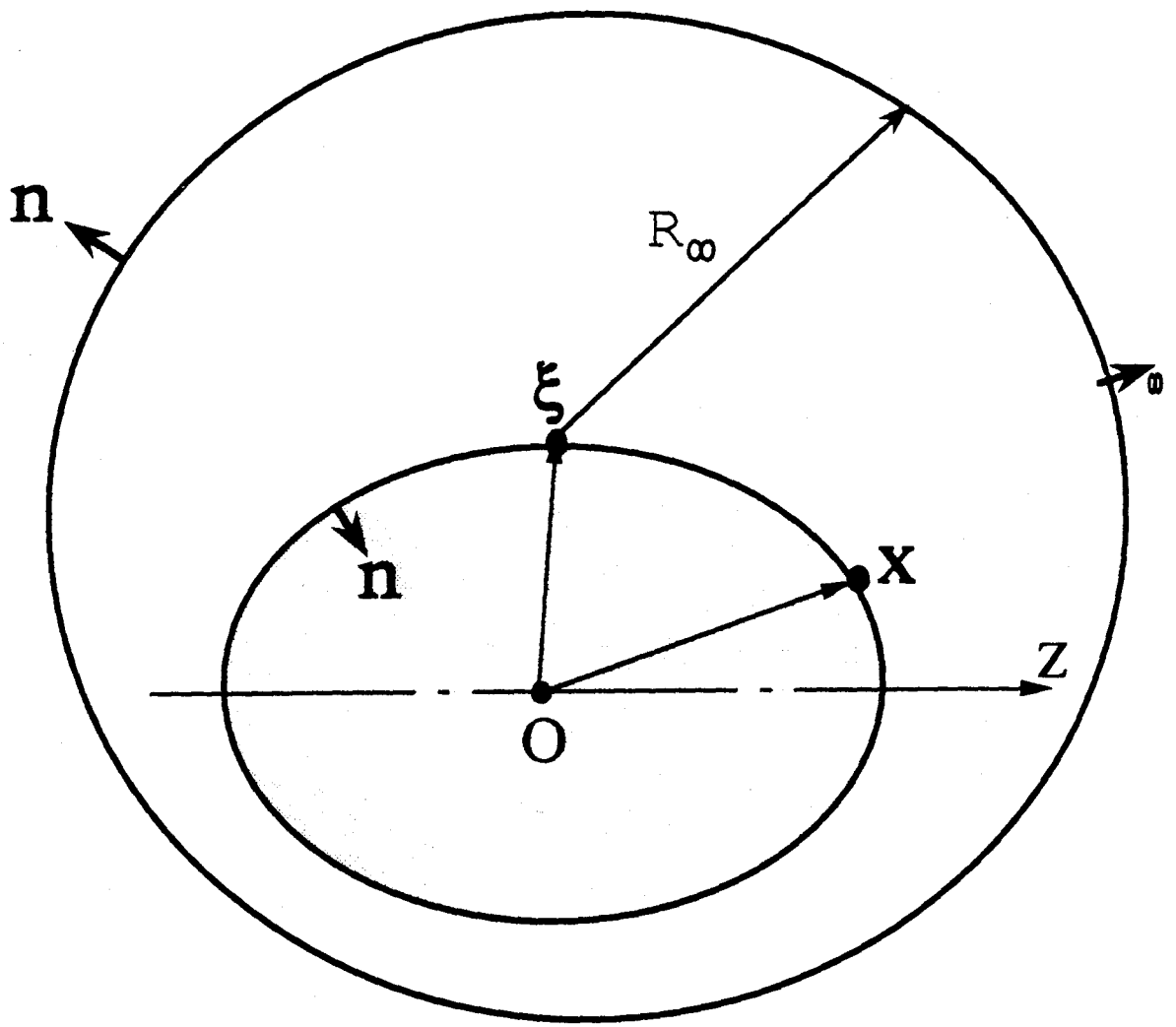

Figure 12. Geometry used in deriving the boundary integral equation.

Chapter 3

A Theoretical Study of Combustion of Nonspherical Particles

Moon Kyu Choi and George R. Gavalas
Chemical Engineering 210-41
California Institute of Technology
Pasadena, CA 91125

Submitted to *Comb. Sci. and Tech.*

Abstract

A theoretical study is carried out of the combustion of nonspherical carbonaceous particles in the regime of shrinking core reaction. The first problem addressed is the calculation of the pseudosteady temperature and oxidation rate for a particle of given shape. This problem involves the solution of the external diffusion and heat conduction equations with the reaction entering as a boundary condition over the particle surface. Using the boundary integral method, the problem is reformulated as a system of two coupled integral equations which are solved numerically by suitable discretization. The complete transient problem addressing the evolution of particle shape and particle temperature during burnout is similarly formulated by the boundary integral method and solved numerically. Over a broad range of parameters, the pseudosteady particle temperature and rate of oxidation are very nearly equal to those of spherical particles of equal volume and surface area respectively. The transient solutions obtained for parameters typical of pulverized combustion show that during burnout the particle becomes increasingly nonspherical. As expected, nonspherical particles burn faster than spherical particles of the same initial volume, but the difference in burnout times is less than 20% for initial aspect ratios between one and three.

NOMENCLATURE

A_p	aspect ratio
b_1	stoichiometric coefficient
c	total concentration of gas phase
c_1	concentration of oxygen
D	diffusion coefficient of oxygen
g	Green's function for 3-dimensional Laplace's equation
k'	reaction constant
$\|\Delta H\|$	heat of reaction
$\mathbf{n}$	outward normal unit vector
P_n	nth Legendre polynomial
Q	defined by Eq.(13)
q_R	heat flux by radiation
$R(\theta,\tau)$	$\frac{\tilde{R}(\theta,\tau)}{\tilde{R}_s(\tau)}$
$\tilde{R}_s(\tau)$	radius of the fictitious sphere of equal volume
r	reaction rate of oxygen
S	surface area of particle
T	temperature
t	time
$\mathbf{x}$	dimensional position vector
y	mole fraction of oxygen

Greek letters

β_n	coefficients used in expanding $R(\theta, \tau)$
ϵ	emissivity of particle
λ	thermal conductivity of gas phase
ρ	radial variable
ρ_p	particle density
τ	dimensionless time variable
Ω	surface boundary of domain

Subscripts

∞	quantity evaluated using the bulk temperature
v	sphere of equal volume
s	sphere of equal surface area

INTRODUCTION

The analysis of particle (coal char, coke, etc.) combustion has undergone significant refinement over the years. Early analyses exemplified by the reports of Field *et al.* (1967) and Field (1969) employed simple heat and mass transfer coefficients and assumed shrinking core reaction. The analysis was later extended to include a detailed account of external heat and mass transfer while retaining shrinking core oxidation (Ubhayakar, 1976; Libby and Blake, 1979; Annamalai and Durbetaki, 1979). Further extensions invoked considerations of intraparticle diffusion, reaction and pore growth. A comprehensive review of work up to 1984 has been published by

Sotirchos *et al.* (1984). Regardless of the treatment afforded to internal and external diffusion, all previous investigations treated the reacting particles as spherical thus avoiding the mathematical and computational complications entailed by nonspherical geometry. In the present paper we explore the effect of nonspherical shape on the reaction rate, particle temperature and other combustion characteristics.

Grinding coal, coke, etc. produces particles of widely varying size and shape. Upon heating and devolatilization, bituminous coal particles tend to become smoother and more spherical, while particles of other coals retain their original shape. The nonuniformity of shape and size arising from grinding and devolitilization can cause a spread in the time for complete burnout, the maximum particle temperature, and the size distribution of flyash, all important properties for coal combustion practice. In this paper we explore the effect of the initial shape on the combustion history of a particle. We consider the instantaneous temperature and oxidation rate for a given particle shape, and the evolution of the particle shape as reaction progresses. We also examine the degree to which the combustion of nonspherical particles can be approximated by that of spherical particles of appropriate size.

As we relax the assumption of spherical shape we are forced to make other simplifications or restrictions in order to contain the mathematical-computaional effort. The analysis is thus restricted to shrinking core combustion, spatially uniform transport coefficients and negligible Stefan flow. Furthermore, we only consider particle shapes which are rotationally symmetric and choose the initial shape to be a prolate or oblate spheroid. With these simplifications and restrictions the problem becomes one of external diffusion and heat conduction with the reaction entering as a boundary condition on the particle surface. We treat this problem numerically using

the boundary integral method which converts the spatial differential equations to integral equations over the particle surface and thereby reduces the computational effort. Although not explicitly considered, the case of negligible pore diffusion resistance, such that the particle size and shape remain constant during burnout, is also subsumed in the analysis developed here.

THE PSEUDOSTEADY PROBLEM

In this section we formulate the pseudosteady problem, i.e., for a given particle shape and free stream conditions, calculate the particle temperature and the reaction rate. In a strict sense, these pseudosteady properties are not exactly realized, because the particle shape evolves with oxidation. However, except for a brief initial transient, the thermal inertia is negligible and the particle temperature approaches and remains close to the pseudosteady temperature corresponding to the instantaneous particle shape. Having established that pseudosteady relation, in the next section we examine the evolution of particle shape due to the reaction.

Figure 1 shows a rotationally symmetric particle with O being the particle center and Oz the axis of symmetry. Although not essential, we shall also assume that the particle has a plane of symmetry perpendicular to Oz. The particle surface Ω is then defined by some equation

$$\rho = F(\theta, t), \quad 0 < \theta < \pi \tag{1}$$

where ρ is the distance from the center O and, because of the plane of symmetry, $F(\pi - \theta, t) = F(\theta, t)$.

Physical parameters such as the thermal conductivity and the diffusivity are functions of temperature with an approximate power dependence (Hirschfelder *et*

al., 1954),

$$\lambda \propto T^{0.5}, \quad D \propto T^{1.5}.$$

Thus the thermal conductivity λ and the product cD are represented as

$$\lambda = \lambda_\infty \left(\frac{T}{T_\infty}\right)^{0.5}, \quad cD = c_\infty D_\infty \left(\frac{T}{T_\infty}\right)^{0.5}$$

with the subscript ∞ denoting free stream properties.

In a further approximation, the product cD_{ij} of total concentration and any diffusion coefficient will be taken as spatially uniform, equal to its value at the particle surface Ω. Moreover, the flux of oxygen will be described by the approximate expression $-Dc \bigtriangledown y$, where y is the oxygen mole fraction and D is the binary diffusion coefficient for the $O_2 - N_2$ pair. This simple flux expression neglects the minor convective contribution due to the relative velocity between particle and free stream, the "Stefan flow" terms induced by multicomponent diffusion, and the direct contributions of pressure and temperature gradients included in the Stefan-Maxwell equations.

The approximation of spatially uniform cD was evaluated for a spherical particle where the exact and approximate problems could be solved in closed form(see Appendix). Even when surface and free stream temperatures differed by 640°C, the error in the reaction rate was less than 8%. The error committed by neglecting the Stefan flow depends mainly on the magnitude of the surface reaction rate. The analytical solution available for a spherical particle suggests that this error is less than 10% for the range of parameters used in the numerical calculations. In view of the modest magnitude of these errors we believe that the two approximations are reasonable for evaluating differences in the combustion rate, burnout time, etc., between a spherical and a nonspherical particle.

With the above approximations, the oxygen mole fraction y and the temperature T satisfy the equations

$$\nabla^2 y = 0 \tag{2}$$

$$\nabla \cdot (\lambda \nabla T) = 0 \tag{3}$$

with boundary conditions at the free stream

$$\rho \to \infty \ : \ y \to y_\infty \ ; \ T \to T_\infty . \tag{4}$$

The boundary conditions on the particle surface will be based on two additional assumptions : uniform particle temperature and shrinking core reaction(high Thiele modulus). The relevance of the latter assumption depends on several factors among which particle temperature, particle size, and porous structure. A particle initially burning in the shrinking core mode(decreasing size, constant density) after a certain reduction in size will switch to a mode of decreasing size and density.

On the basis of the last two assumptions, the boundary condition for the oxygen mole fraction becomes

$$\rho \in \Omega \ : \ cD\frac{\partial y}{\partial n} = r(p_1, T) \tag{5}$$

where $p_1 = yP$ is the partial pressure of oxygen on the surface. There are two boundary conditions for the temperature

$$\rho \in \Omega \ : \ T = T_s \tag{6}$$

where T_s is the unknown particle temperature, and

$$\int_\Omega \left[\lambda \frac{\partial T}{\partial n} - q_R + r|\Delta H| \right] dS = 0 \tag{7}$$

where q_R is the net radiative flux, r is the rate of oxygen consumption per unit external area of the particle. This latter condition is simply a thermal energy

balance for the whole particle between heat generated by the reaction and heat lost by radiation and conduction. It must be noted that whereas T_s is uniform over the surface, $p_1 = yP$ and $\frac{\partial T}{\partial n}$ are variable. The radiative flux q_R will be taken as

$$q_R = \sigma\epsilon(T_s^4 - T_\infty^4) \tag{8}$$

where the temperature of the surrounding surfaces is taken equal to that of the free stream, and a common emisivity is used for all radiating surfaces.

For a spherical particle of radius a, Eqs. (2)-(7) can be reduced easily to the solution of two equations in the unknowns, y_s, T_s,

$$\frac{PD(T_s)}{R_g T_s a}(y_\infty - y_s) = r(Py_s, T_s) \tag{9}$$

$$\frac{\lambda(T_s - T_\infty)}{a} + \sigma\epsilon(T_s^4 - T_\infty^4) = |\Delta H_r| r(Py_s, T_s). \tag{10}$$

If the reaction is first order with Arrhenius temperature dependence,

$$r = k' p_1 = A\exp(-E/R_g T_s) P y_s, \tag{11}$$

Eqs. (9) and (10) can be combined in a single equation for T_s :

$$\frac{\lambda(T_s - T_\infty)}{a} + \sigma\epsilon(T_s^4 - T_\infty^4) = |\Delta H_r| \frac{A\exp(-E/R_g T_s) P y_\infty}{1 + Q(T_s)} \tag{12}$$

where

$$Q(T_s) = \frac{k'(T_s) R_g T_s a}{D(T_s)} = \frac{A R_g T_s a}{D(T_s)} \exp(-E/R_g T_s). \tag{13}$$

Equation (12) exhibits the well-known multiplicity and ignition phenomena.

BOUNDARY INTEGRAL METHOD

For nonspherical particles the problem defined by Eqs.(2)-(7) can be reformulated using single layer and double layer potentials (Stakgold,1972) into two integral

equations for the surface values of y and $\frac{\partial T}{\partial n}$. Once the two integral equations are solved numerically, the particle temperature, the total reaction rate, and the values of T and y outside of the particle can be computed, if desired. This approach, which is known as the "boundary integral method", involves a much smaller number of unknowns than the finite difference method and is, accordingly, much more computationally economical. The boundary integral method has been used extensively in low Reynolds number hydrodynamics.

The integral form of Eq.(2) with boundary conditions (4) and (5) can be derived by standard potential theory, using a double layer potential. For any $\mathbf{x}_s \in \Omega$ we have

$$y(\mathbf{x}_s) = 2y_\infty - \frac{1}{2\pi}\int_\Omega \left[-y(\xi)\frac{\partial g}{\partial n} + g\frac{r(Py(\xi), T_s)}{(cD)_s}\right] dS_\xi \tag{14}$$

where $\frac{\partial}{\partial n}$ is the outward normal derivative and

$$g = \frac{1}{|\mathbf{x}_s - \xi|}. \tag{15}$$

For axially symmetric particles, integration over the azimuthal angle converts the double integral in Eq.(14) to a single integral over the angular variable θ :

$$y(\mathbf{x}_s) = 2y_\infty - \frac{1}{2\pi}\int_0^\pi \left[-y(\theta')\frac{\partial G}{\partial n} + G\frac{r(Py(\theta'), T_s)}{(cD)_s}\right] v(\rho)\sin\theta' d\theta' \tag{16}$$

where

$$\rho = F(\theta, t)$$

and

$$v(\rho) = \rho^2\left[1 + \frac{1}{\rho^2}\left(\frac{dF}{d\rho}\right)^2\right]^{1/2} \tag{17}$$

$$G = \int_0^{2\pi} g d\phi \tag{18}$$

$$\frac{\partial G}{\partial n} = \int_0^{2\pi} \frac{\partial g}{\partial n} d\phi. \tag{19}$$

Equation (16) is an integral equation in the unknown function $y(\theta)$, with T_s appearing as an unknown parameter to be determined in conjunction with the energy equation.

An integral equation equivalent to (3), (4) and (6) can be derived using a single layer potential after introducing a new variable defined by

$$\psi = \frac{(T/T_\infty)^{1+\alpha} - 1}{(T_s/T_\infty)^{1+\alpha} - 1}. \tag{20}$$

It is

$$-\int_\Omega g \frac{\partial \psi}{\partial n} dS_\xi = 4\pi. \tag{21}$$

Integration over the azimuthal angle now yields

$$-\int_0^\pi G \frac{\partial \psi}{\partial n} v(\rho) \sin\theta' d\theta' = 4\pi. \tag{22}$$

This is an integral equation in the unknown function $\frac{\partial \psi}{\partial n}(\theta)$ with the unknown T_s appearing as a parameter. For any given T_s, Eq.(16) can be solved for $y(\theta)$, and Eq.(21) for $\frac{\partial \psi}{\partial n}(\theta)$, or $\frac{\partial T}{\partial n}(\theta)$. The unknown T_s can then be determined from Eq.(7).

THE TRANSIENT PROBLEM

The transient problem is a conceptually simple extension of the pseudo-steady problem. It is still assumed that the oxygen mole fraction y and temperature T satisfy the pseudosteady equations (2) and (3) and boundary conditions (4)-(6). However, boundary condition (7) does not apply any more since the particle temperature is variable ; it is replaced by

$$\rho_p C_p V_p \frac{dT_s}{dt} = \int_\Omega [\lambda \frac{\partial T}{\partial n} - q_R + r|\Delta H|] dS \tag{23}$$

where ρ_p, C_p and V_p are the density, specific heat, and volume of the particle. An additional equation is needed governing the changing particle shape on account of carbon consumption. This is

$$\frac{\partial F(\theta,t)}{\partial t} = -\frac{b_1}{\rho_p} r(p_1, T_s)\sigma(\theta,t) \tag{24}$$

$$t = 0 \; ; \; F = F_0(\theta) \tag{25}$$

where the shape function F was introduced by Eq.(1). F_0 is the initial value of F, b_1 is the stoichiometric coefficient between grams of carbon and moles of oxygen ($b_1 = 24$ if CO is the only product), ρ_p is the particle density and r is the reaction rate in moles of oxygen per unit surface area per unit time. The factor $\sigma(\theta,t)$ converts a displacement of the surface perpendicular to itself due to the reaction to a displacement along OP (see Figure 1). One can easily derive

$$\sigma(\theta,t) = \left[1 + \left(\frac{1}{F}\frac{\partial F}{\partial \theta}\right)^2\right]^{1/2}. \tag{26}$$

As before, Eqs.(2)-(6) are equivalent to the two integral equations (16) and (21), therefore the transient problem is governed by Eqs. (16), (22) supplemented by (23)-(25).

NUMERICAL RESULTS FOR THE PSEUDO-STEADY PROBLEM

As a preliminary to the solution of Eqs. (16) and (22) it is necessary to evaluate the functions G and $\frac{\partial G}{\partial n}$ defined as integrals of the Green's function g and its normal derivative $\frac{\partial g}{\partial n}$(Eqs. (18),(19)). Carrying out these integrations yields G and $\frac{\partial G}{\partial n}$ in terms of three complete elliptic integrals which were evaluated by the approximating polynomials given in Abramowitz and Stegun (1972). Next, equations (16) and (22)

were discretized using the values of the unknowns y, and $\frac{\partial \psi}{\partial n}$ at 2N+1 discrete points over $0 < \theta < \pi$ and evaluating the integrals by an 8-point Gaussian quadrature. By this discretization, Eq.(22) was converted to a system of 2N+1 linear equations for the values of $\frac{\partial \psi}{\partial n}$ at the discrete points in $0 < \theta < \pi$. This linear system was decoupled from the rest of the equations and had to be solved only once.

The other integral equation, Eq.(16), was discretized into a system of 2N+1 nonlinear equations(or linear equations for a first order reaction) in the 2N+1 unknown values of y. This system contained the unknown surface temperature T_s as a parameter and was solved in conjunction with Eq.(7) by successive substitutions. To this end, Eq.(7) was rewritten as

$$\int \left(q_R - \lambda \frac{\partial T}{\partial n} \right) dS = \int r |\Delta H| dS$$

But on the surface

$$r = cD \frac{\partial y}{\partial n} = c_\infty D_\infty \left(\frac{T_s}{T_\infty} \right)^{1.5} \frac{\partial y}{\partial n}$$

so that

$$\left(\frac{T_s}{T_\infty} \right)^{1.5} = \frac{\int \left(q_R - \lambda \frac{\partial T}{\partial n} \right) dS}{c_\infty D_\infty \int \frac{\partial y}{\partial n} |\Delta H| dS} \tag{27}$$

Starting from an initial guess of T_s, Eq.(16) was solved for $\frac{\partial y}{\partial n}$ and Eq.(22) gave $\frac{\partial T}{\partial n}$. The values of $\frac{\partial y}{\partial n}$ and $\frac{\partial T}{\partial n}$ were introduced into the right side of Eq.(27) to yield an improved value for T_s, and the procedure was repeated until successive values of T_s differed by less than one degree. Convergence took 5 to 10 iterations depending on the shape of the particle.

Table I gives the values used in the calculations. With the exception of the oxygen concentration in the free stream, these values were taken from a paper by Sahu *et al.* (1988). These authors had estimated the oxidation rate for shrinking

core combustion of a bituminous coal char as

$$R_a = 107.1 \exp(-17,000/RT) \text{ gcm}^{-2}\text{s}^{-1}\text{atm}^{-1},$$

which yields the value of k'_∞ listed in Table 1.

Numerical results for the pseudosteady problem are presented in Figures 2-4. Figure 2 shows the particle temperature vs. Q_∞. At each value of Q_∞, various prolate and oblate spheroids of equal volume but different aspect ratios are considered. The temperature varies significantly with Q_∞ but is insensitive to the shape, with the curves for both prolate and oblate spheroids of different aspect ratios essentially coinciding. This insensitivity on particle shape seems to be due to the approximate cancellation of two opposite effects. Increasing the aspect ratio decreases the local mass transfer coefficient on the particle surface, thereby decreasing the heat release. The same increase of the aspect ratio decreases the local heat transfer coefficient as well, thereby decreasing the heat loss. The sensitivity of the particle temperature to the particle shape may be higher in other operating regions, e.g., at higher gas temperatures or oxygen contents where the effect of radiative heat transfer would be more pronounced. It should be further noted that for the set of parameters used here(Table I), all particle temperatures shown in Figure 2 correspond to the upper(ignited) branch of the usual ignition diagram.

Figure 2 also shows the normalized reaction rate vs. Q_∞ for particles of different shapes. For any given particle shape, the normalized rate initially decreases with increasing Q_∞, then levels off and remains constant as Q_∞ increases beyond 1. At low values of Q_∞ the normalized rate is equal to the ratio of the surface area of the particle to that of a sphere of equal volume. As Q_∞ increases, the rate ratio falls below the surface area ratio, and eventually reaches a limiting value as the reaction

becomes mass transfer limited. For fixed Q_∞, the rate ratio increases significantly with the aspect ratio, with the oblate spheroids yielding higher reaction rates than the corresponding prolate spheroids. For aspect ratios between 1 and 3.2 the rate for the prolate and oblate spheroids was no more than 20% and 28% higher than that of a sphere of equal volume.

Figure 3 shows the surface area normalized with respect to that of a sphere of equal volume as a function of aspect ratio for prolate and oblate spheroids. Oblate spheroids have a somewhat higher surface area than prolate spheroids of the same aspect ratio. At the highest aspect ratio of 3.2 used in most calculations the prolate and oblate spheroids have surface area 20 and 29% higher than a sphere of the same volume. Figure 4 shows the total rate normalized by the total rate of a sphere of equal surface area vs. A_p for different values of Q_∞. For the whole range of Q_∞ and A_p examined, the rate is within 3% of the rate of a sphere of equal surface area. From the standpoint of the instantaneous total reaction rate, therefore, a nonspherical particle can be closely represented by a spherical particle of equal surface area. The curves for a few of the prolate spheroids show oscillatory behavior, which seems to be due to numerical errors, but in these curves the normalized total rate is very close to unity.

NUMERICAL RESULTS FOR THE TRANSIENT PROBLEM

The transient problem consists of Eqs. (23) and (24) with the respective initial conditions. Eq.(24) was written at M discrete points of $\theta, \theta_1 = 0, \cdots, \theta_M = \pi/2$ which were more densely distributed at the points of higher curvature, i.e., near $\theta = 0$ for prolate spheroids. M was chosen in the range 25 - 50. Each evaluation of the right side of these equations required solving the pseudosteady equations (16),

(22) for y and $\frac{\partial \psi}{\partial n}$(giving $\frac{\partial T}{\partial n}$). Equations (23) and (24) become increasingly stiffer with decreasing Damköhler number Q_∞ because small Q_∞ implies rapid change of shape in terms of the dimensionless time, τ defined by

$$\tau = \frac{b_1 (k'_\infty)^2 y_\infty}{\rho_\infty c_\infty D_\infty}. \tag{28}$$

In view of the lack of explicit expressions for the right sides of the differential equations, we could not conveniently use a stiff equation solver. Instead we used the explicit fourth order Runge-Kutta method with step size control, decreasing the step size as integration progressed to compensate for the gradually increasing aspect ratio. In the calculations reported below, the time increment $\Delta\tau$ varied from 0.1 to 0.01.

Figure 5 shows the fractional conversion vs. dimensionless time for particles of the same initial volume but different initial aspect ratios. The conversion curves for different aspect ratios are quite close to each other. For example, the dimensionless time to 0.95 conversion changes from 3.1 for $A_p(0) = 1$ to 2.7 for $A_p(0) = 3.2$. Figure 6 shows the aspect ratio as a function of dimensionless time for particles of different initial aspect ratios. The aspect ratio increases with time for all particles and this increase accelerates with increasing A_p. Thus, a particle with initially nearly spherical shape will change little during burnout(curve for $A_p(0)$=1.667) while a particle with initial $A_p(0)$=3.2 will become much more elongated($A_p \simeq 4.3$) when the dimensionless time reaches 2.5, i.e., at 0.95 conversion. Figure 7 shows the evolution of particle temperature during burnout. The temperature transients of particles of different initial aspect ratios, but equal volume, nearly coincide. Although not portrayed in Figure 7, the calculations also show that for any given initial particle shape, the transient temperature rapidly approaches and remains

close to the pseudosteady temperature corresponding to the instantaneous particle volume.

CONCLUSIONS

An analysis of nonspherical particle combustion was carried out using the boundary integral method. For particles of equal volume, the pseudosteady temperature is nearly independent of shape, but the combustion rate increases with increasing aspect ratio. The local combustion rate varies moderately over the particle surface increasing with the distance from the particle center. The total combustion rate depends on the particle surface area alone, i.e., particles of equal surface area but different volumes and shapes have the same rate. This dependence on the surface area is less than linear, becoming linear only in the limit of low Damköhler numbers.

The effect of initial particle shape on the burnout transient was explored for a set of parameters typical of a bituminous coal char burning in the shrinking core regime. The calculations show the particle shape to become increasingly nonspherical with the progress of combustion and this change to be more pronounced for particles with larger initial aspect ratios. For particles of equal initial volume, the burnout time decreases slightly with the initial aspect ratio. For example a particle of initial aspect ratio 3.2 requires 12 % less time to reach 80 % burnout compared to a spherical particle of the same initial volume.

APPENDIX

The purpose of this appendix is to estimate the error made by treating the quantity cD as temperature independent in the derivation of Eq.(2) from the equa-

tion

$$\nabla \cdot (cD \nabla y) = 0. \tag{A1}$$

This evaluation is carried out by comparing the approximate solution with the exact solution for a spherical particle. In the case of a spherical particle, Eq.(3) can be easily integrated to obtain

$$\frac{T}{T_\infty} = \left[1 + \frac{(T/T_\infty)_s^{1.5} - 1}{\rho/a}\right]^{\frac{1}{1.5}}. \tag{A2}$$

Equations (A1),(4),(5) can now be solved along with Eq.(A2) to obtain the dimensionless surface concentration as

$$y_s = \frac{y_\infty}{1 + Q(1.5)\frac{(T_s/T_\infty)^{1.5} - (T_s/T_\infty)^{0.5}}{(T_s/T_\infty)^{1.5} - 1}}. \tag{A3}$$

The approximate dimensionless surface concentration obtained from Eqs. (2), (4) and (5) is

$$y_{s,\text{approx}} = \frac{y_\infty}{1+Q}. \tag{A4}$$

Eqs.(A3) and (A4) are the exact and approximate solutions to Eqs. (A1) and (3) for a sphere. The relative error between exact and approximate solutions is

$$\left|\frac{y_s - y_{s,\text{approx}}}{y_s}\right| = \frac{Q}{1+Q}\left|(1.5)\frac{(T_s/T_\infty)^{1.5} - (T_s/T_\infty)^{0.5}}{(T_s/T_\infty)^{1.5} - 1} - 1\right|. \tag{A5}$$

The quantity

$$F(T_s/T_\infty) = \left|(1.5)\frac{(T_s/T_\infty)^{1.5} - (T_s/T_\infty)^{0.5}}{(T_s/T_\infty)^{1.5} - 1} - 1\right|, \tag{A6}$$

is an increasing function of T_s/T_∞ starting from zero at $T_s = T_\infty$ and remaining small. For example at $T_s/T_\infty = 1.4$, $F(T_s/T_\infty) = 0.08$ and the error is less than 8%, in as much as the factor$Q/(Q+1)$is less than one.

REFERENCES

Abramowitz, M. and Stegun, I.A.(1972). *Handbook of Mathematical Functions*, 8th ed., Dover, New York, pp. 590-591.

Annamalai, K. and Durbetaki, P.(1979). Combustion Behavior of Char/Carbon Particles, *Seventeenth Symposium(International) on Combustion*, 169.

Field, M.A., Gill, D.W., Morgan, B.B. and Hawksley, D.W.G.(1967). *Combustion of Pulverized Coal*, BCURA, Leatherhead, pp. 189-208.

Field, M.A.(1969). Rate of Combustion of Size-Graded Fractions of Char from a Low-Rank Coal between 1200 K and 2000 K. *Combustion & Flame*, **13**, 237.

Hirschfelder, J.O., Curtiss, C.F. and Bird, R.B.(1954). *Molecular Theory of Gases and Liquids*, Wiley, New York, pp. 533-591.

Libby, P.A. and Blake, T.R.(1979). Theoretical Study of Burning Carbon Particles. *Combustion & Flame*, **36**, 139.

Mon, E. and Amundson, N.R.(1980). Diffusion and Reaction in a Stagnant Boundary Layer about a Carbon Particle. 4. Dynamic Behavior. *Ind. Eng. Chem. Fund.*, **19**, 243.

Sahu, R., Northrop, P.S., Flagan , R.C., and Gavalas, G.R.(1988). Char Combustion : Measurement and Analysis of Particle Temperature Histories, *Comb. Sci. and Tech.*, **60**, 215.

Sotirchos, S.V., Srinivas, B. and Amundson, N.R.(1984). Modelling of the Combustion of Single Char Particles. In Amundson, N.R. and Luss, D., *Reviews in Chemical Engineering*, D. Reidel Publishing Co., London.

Stakgold, I.(1972). Boundary Value Problems of Mathematical Physics, vol.II, Macmillan, New York, pp. 88-193.

Ubahyakar, S.K.(1976). Burning Charateristics of a Spherical Particle Reacting with Ambient Oxidizing Gas at its Surface. *Combustion & Flame*, **26**, 23.

Table I. The parameter values used in the calculations.

Physical Parameters	Values Used
bulk temperature, T_∞	1600 K
initial radius of equivalent sphere, $\tilde{R}_s(0)$	25 μm
bulk mole fraction of oxygen, y_∞	0.1
heat of reaction, $-\Delta H_r$	2.32 x 10^8 J/kgmol O_2
solid density, ρ_p	800 kg/m^3
solid emisivity, ϵ	1
diffusion coefficient of oxygen at T_∞, D_∞	2.80 x 10^{-4} m^2/s
thermal conductivity of gas at T_∞, λ_∞	5.38 x 10^{-2} J/m-s-K
activation energy, E	17,000 cal
heat capacity of gas, C_p	2.5 x 10^4 J/kgmol-K
total molar concentration at T_∞, c_∞	7.62 x 10^{-3} kgmol/m^3
1st order reaction constant at T_∞, k'_∞	0.2119 kgmol O_2/m^2 – atm
dimensionless time, τ	63.135$sec^{-1}t$

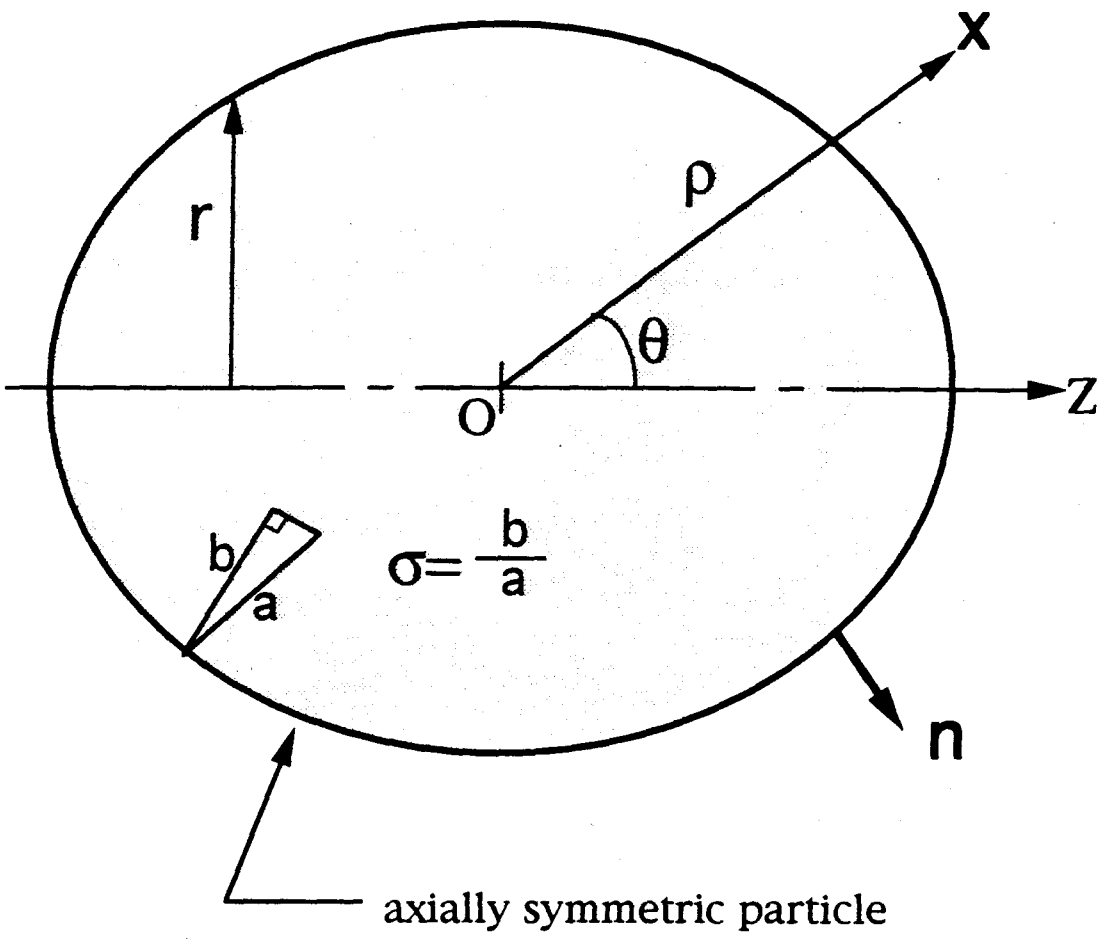

Figure 1. Geometry and notation for a nonspherical particle.

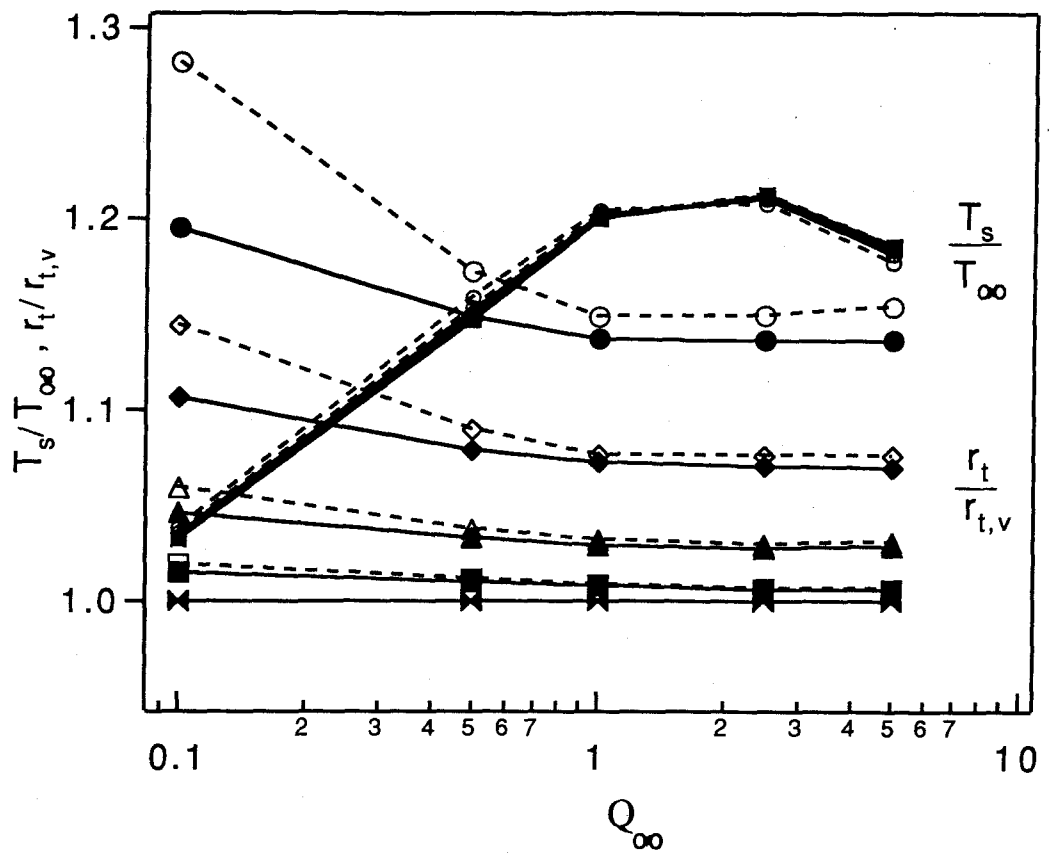

Figure 2. Pseudosteady particle temperature normalized by free stream temperature and reaction rate normalized by that of a sphere of equal volume vs. Damköhler number (⋈: $A_p = 1$, □: $A_p = 1.25$, △: $A_p = 1.667$, ◇: $A_p = 2.294$, ○: $A_p = 3.2026$; solid lines : prolate spheroids, dashed lines : oblate spheroids). The parameters other than the particle volume are fixed at the values given in Table I. A higher value of Q_∞ signifies a larger particle volume.

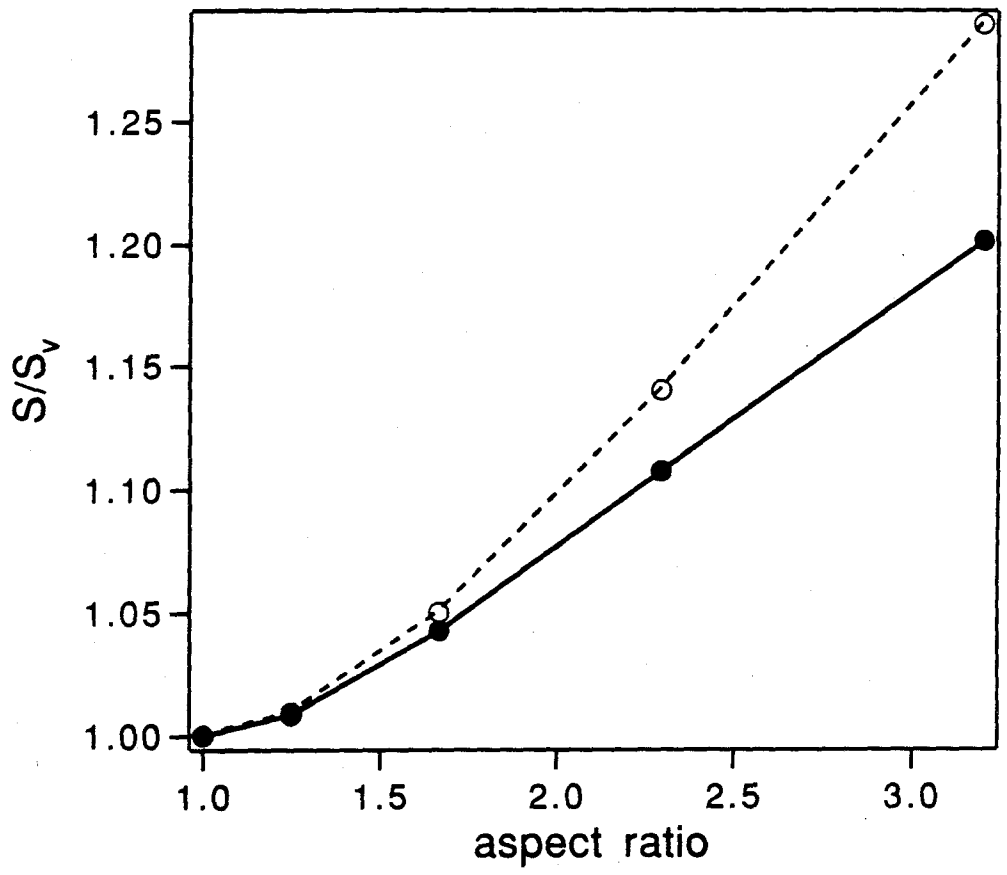

Figure 3. Surface area normalized by that of a sphere of equal volume vs. aspect ratio(solid lines : prolate spheroids, dashed lines : oblate spheroids).

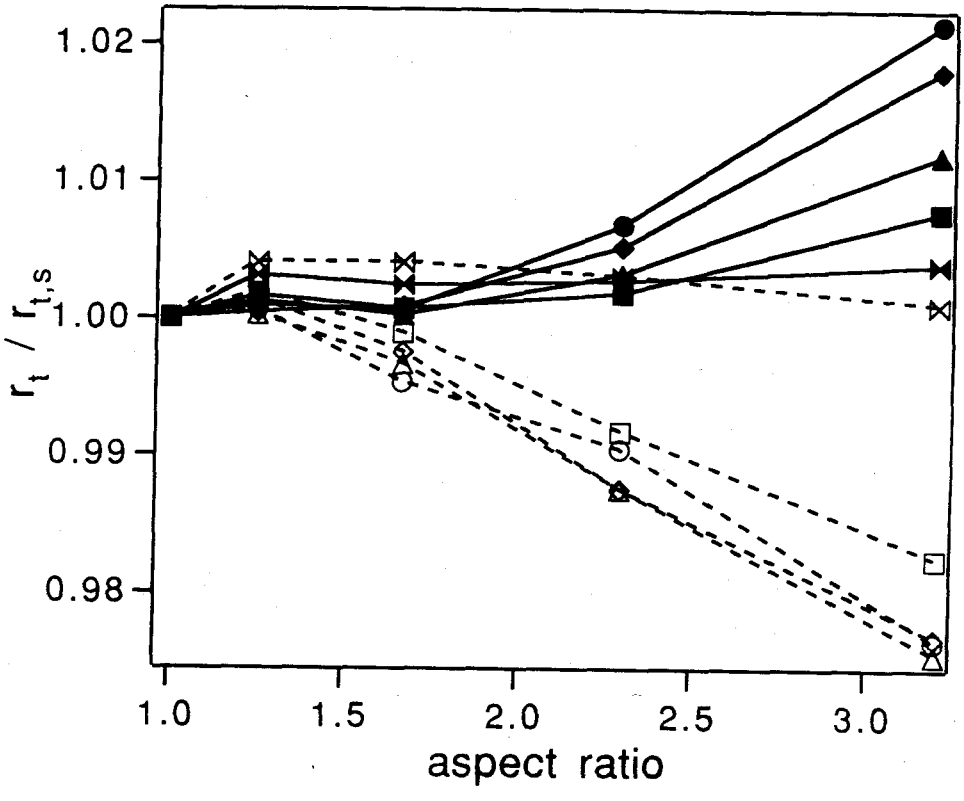

Figure 4. Total reaction rate normalized by that of a sphere of equal surface area vs. aspect ratio($\bowtie$:Q_∞ = 0.1,□: Q_∞ = 0.5,△:Q_∞ = 1,◇:Q_∞ = 2.483, ○:Q_∞ = 5 ; solid lines : prolate spheroids, dashed lines : oblate spheroids).

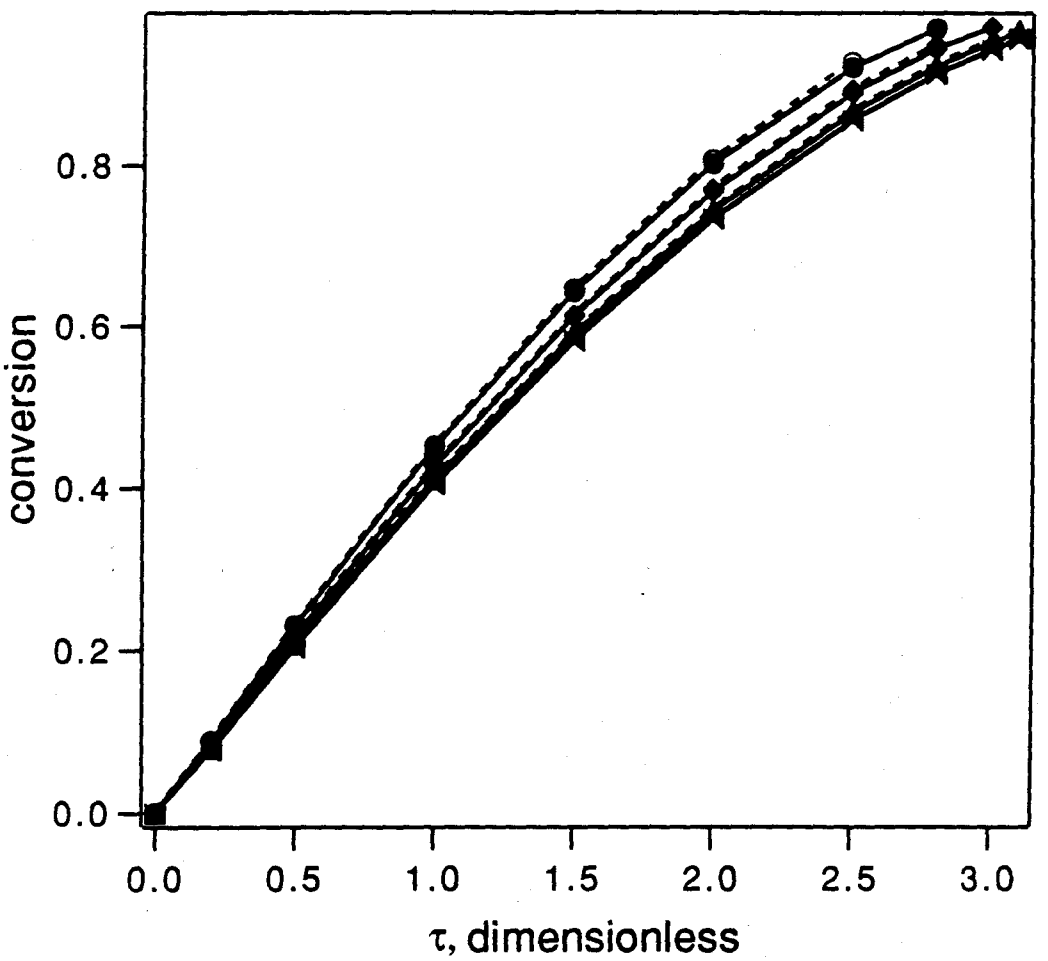

Figure 5. Conversion vs. dimensionless time for prolate and oblate spheroids($\bowtie$:$A_p(0) = 1$,$\triangle$:$A_p(0) = 1.667$,$\circ$:$A_p(0) = 2.294$, $\bigcirc$:$A_p(0) = 3.2026$; solid lines : prolate spheroids, dashed lines : oblate spheroids).

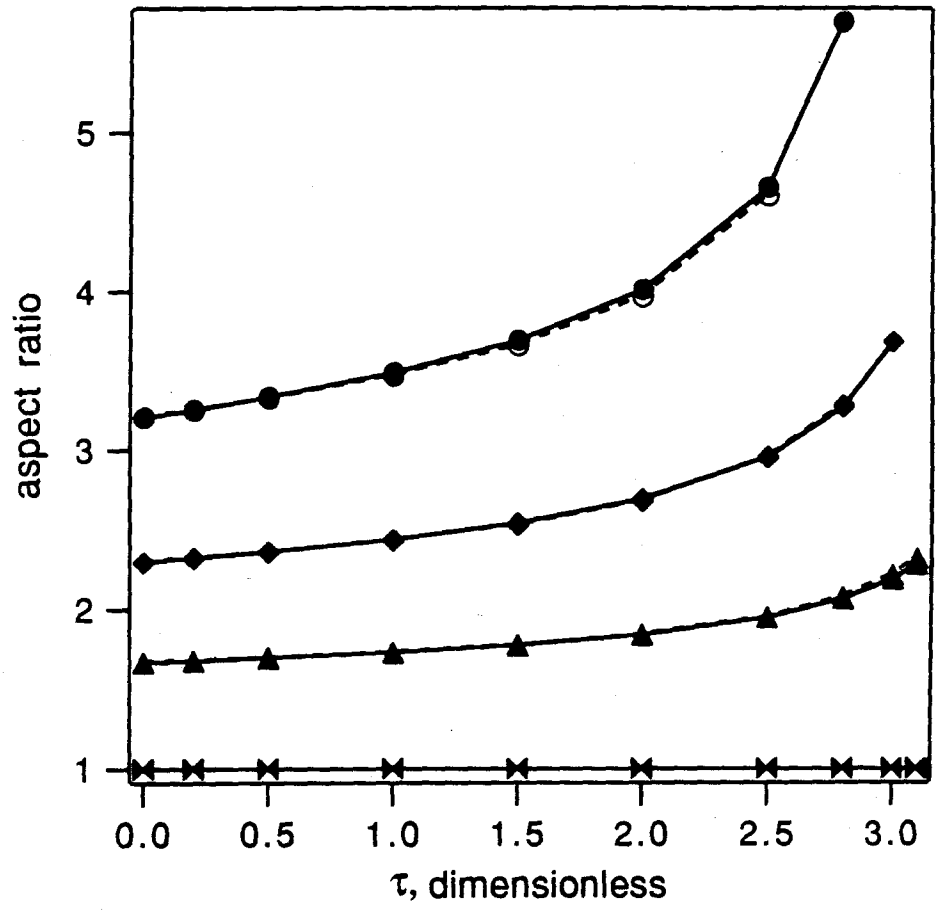

Figure 6. Aspect ratio vs. dimensionless time for prolate and oblate spheroids($\bowtie$:$A_p(0) = 1$,$\triangle$:$A_p(0) = 1.667$, $\diamond$:$A_p(0) = 2.294$, $\bigcirc$:$A_p(0) = 3.2026$; solid lines : prolate spheroids, dashed lines : oblate spheroids).

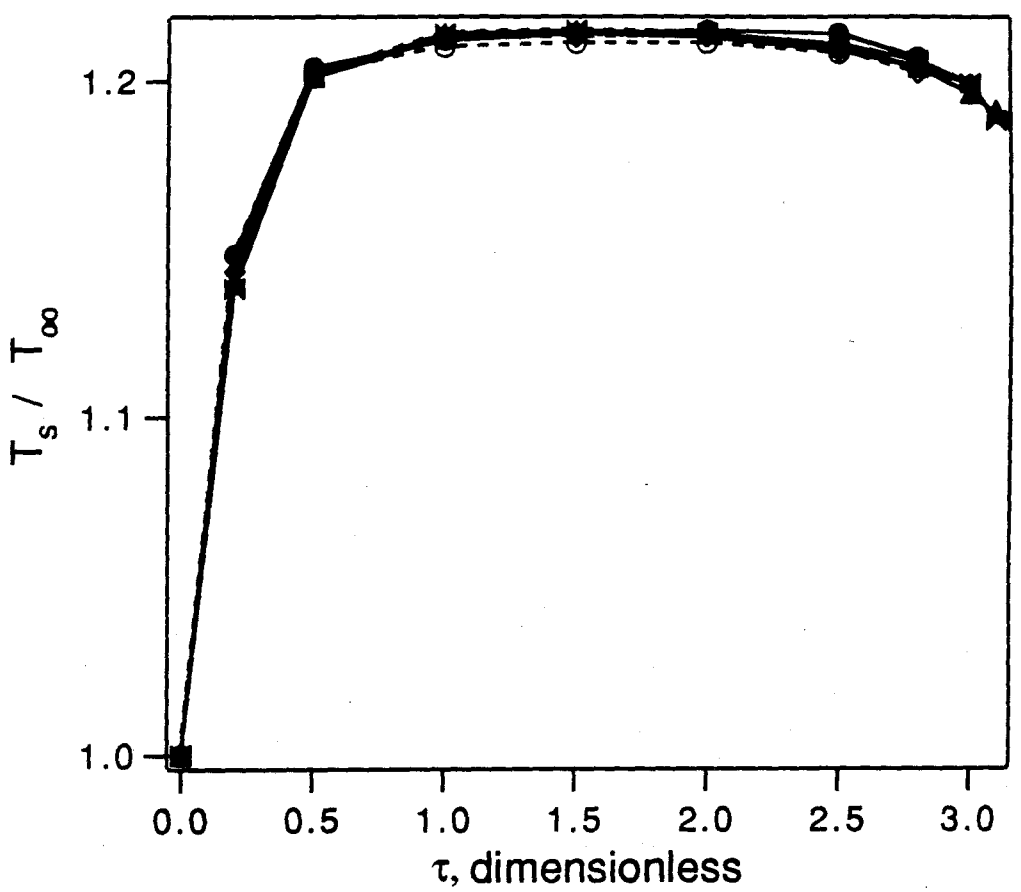

Figure 7. Transient particle temperature vs. dimensionless time for prolate and oblate spheroids($\bowtie$:$A_p(0) = 1$,$\triangle$:$A_p(0) = 1.667$, $\diamond$:$A_p(0) = 2.294$, $\bigcirc$:$A_p(0) = 3.2026$; solid lines : prolate spheroids, dashed lines : oblate spheroids).

Chapter 4

Shape Change of Rough Particles

ABSTRACT

The problem of a rough particle undergoing surface reaction is analyzed to calculate the total reaction rate and to characterize the surface behavior with time. The problem is formulated as one of the external diffusion with the the surface reaction entering as a boundary condition. A slightly rough particle can be treated by domain perturbation in terms of an infinite number of modes. The nth mode decreases if the Damköhler number is larger than $\frac{n+1}{n-2}$ and vice versa. This criterion also applies, approximately, for particles of more pronounced roughness treated by the boundary integral method. If the Damköhler number is well above or below the criterion, the surface mode increases or decreases, but nearby the criterion the particle shows a mixed behavior.

INTRODUCTION

For the shrinking core model of gas-solid reaction, the solid is assumed to be a sphere as an *ad hoc* assumption since the spherical shape is most convenient in the mathematical formulation. In practice particles are neither spherical nor smooth, but their surfaces could be irregular and the shape might be nonspherical. In Chapter 2 an isothermal nonspherical particle was examined to give the local concentration, the total reaction rate and the rate of change of shape, and a similar but nonisothermal analysis was carried out in Chapter 3. The particles treated in the former chapters were spheroidal and smooth. In this chapter particles that are overall spherical, but have a rough surface are examined. First, the method of domain perturbation (DP) will be used for a sphere with a slight roughness and then the boundary integral method (BI) will be applied to particles with larger roughness.

PROBLEM FORMULATION AND DISCUSSION

Since the Stefan flow and the temperature were shown to have small effect quantitatively, especially on the shape change of particle, the analysis will be based on the linear diffusion model. The governing equation and boundary conditions will be those formulated in Chapter 2. We need to represent the surface roughness by some mathematical formula. Since the Legendre polynomials are complete, they can be used to represent any surface shape. As before, the concentration of A in the gas phase, c_A, satisfies Laplace's equation

$$\nabla^2_{\tilde{x}} c_A = 0. \tag{1}$$

The boundary conditions are

$$c_A \rightarrow c_{Ab} \text{ as } |\tilde{\mathbf{x}}| \rightarrow \infty \tag{2a}$$

and

$$-D_A \bigtriangledown_{\tilde{x}} c_A \cdot \tilde{\mathbf{n}} = k c_A \text{ on particle surface.} \tag{2b}$$

After Eqs.(1)-(2) have been solved, the recession rate of each point on the surface can be calculated from the expression

$$\frac{1}{|\bigtriangledown \tilde{F}|}\frac{\partial \tilde{F}}{\partial t} - \mathbf{v_s} \cdot \tilde{\mathbf{n}} = 0 \tag{3a}$$

where

$$\tilde{F} \equiv \tilde{\rho} - \tilde{R}(\theta, t). \tag{3b}$$

Introducing the dimensionless variables and parameters defined by

$$\mathbf{x} = \frac{\tilde{\mathbf{x}}}{\tilde{R}_s(t)}, u_A = \frac{c_A}{c_{Ab}}, R(\theta, t) = \frac{\tilde{R}(\theta, t)}{\tilde{R}_s(t)} \tag{4a}$$

and

$$Q(\tilde{R}_s(t)) = \frac{k\tilde{R}_s(t)}{D_A}, \tau = \frac{b_1 k^2 c_{Ab}}{\rho_s D_A} t, \tag{4b}$$

where $\tilde{R}_s(t)$ is the radius of the sphere having the same volume as the particle, yields the following dimensionless governing equation and boundary conditions:

$$\nabla_x^2 u_A = 0. \tag{5a}$$

$$R^2 \frac{\partial u_A}{\partial \rho} - \frac{\partial R}{\partial \theta}\frac{\partial u_A}{\partial \theta} = QR^2\sqrt{1 + \left(\frac{1}{R}\frac{\partial R}{\partial \theta}\right)^2}\, u_A \quad \text{at} \quad \rho = R(\theta, \tau). \tag{5b}$$

$$u_A \rightarrow 1 \quad \text{as} \quad \rho \rightarrow \infty. \tag{5c}$$

$$-\left(\frac{dQ(\tau)}{d\tau}R + Q(\tau)\frac{\partial R}{\partial \tau}\right) = \sqrt{1 + \left(\frac{1}{R}\frac{\partial R}{\partial \theta}\right)^2}\, u_A \quad \text{at} \quad \rho = R(\theta, \tau). \tag{5d}$$

$$\frac{dQ}{d\tau} = -\frac{1}{2}\int_{-1}^{1} R^2 \sqrt{1+\left(\frac{1}{R}\frac{\partial R}{\partial \theta}\right)^2}\, u_A\, d\eta \tag{5e}$$

A slightly deformed sphere

For a slightly deformed sphere, the method of domain perturbation can be used to obtain an analytical solution and thus gain a qualitative understanding about the change of the surface shape. The solution developed in Chapter 2 can be applied to an arbitrary shape by decomposing this shape into an infinite number of modes. We just recall a few important results from Chapter 2,

$$Q = -1 + \sqrt{[1+Q_0]^2 - 2\tau} + O(\epsilon^2), \tag{6a}$$

$$R = 1 + \epsilon \sum_{n=2}^{\infty} \beta_n P_n(\cos\theta) + O(\epsilon^2), \tag{6b}$$

$$u_A = \frac{1}{Q+1}\frac{1}{\rho} + \epsilon \sum_{n=2}^{\infty} \frac{Q(Q+2)}{(Q+1)(Q+n+1)} \beta_n(\tau) P_n(\cos\theta) \rho^{-(n+1)} + O(\epsilon^2). \tag{6c}$$

The zeroth and the first modes in R vanish by virtue of the condition of volume conservation. The nth mode β_n is governed by the differential equation,

$$\frac{d\beta_n}{d\tau} = \frac{(n+1)+(2-n)Q}{Q(Q+1)(Q+n+1)}\beta_n. \tag{7}$$

Integration of Eq.(7) using Eq.(6a) yields

$$\beta_n(\tau) = \beta_n(0)\frac{Q_0}{Q}\left(\frac{Q+n+1}{Q_0+n+1}\right)^{n-1}. \tag{8}$$

Since the sign of $\frac{d\beta_n}{d\tau}$ is determined by the values of n and Q in Eq.(7), the second mode should increase monotonically while the third and higher modes can increase or decrease depending on the Damköhler number, Q. The third or higher mode has

a critical Q below and above which the mode increases or decreases. The critical value of the nth mode is given by

$$Q_{cr} = \frac{n+1}{n-2}, \tag{9}$$

which is equal to 4 for the mode n=3 and 2.5 for the mode n=4.

We take an example of the evolution of a rough surface using the results from the DP technique. Suppose the particle starts with a large initial value of Q and the initial second mode is zero. Then all the modes decay to zero until Q decreases to the largest critical value, and the particle may become a perfect sphere. As the Damköhler number, Q, becomes smaller and smaller, more modes begin to grow. Even if the particle is perfectly spherical, it will be unstable to small disturbances once the Damköhler number, Q, becomes less than a certain critical value.

Particles with larger irregularities

In the previous subsection the DP technique was applied to treat a slightly deformed sphere. Now by using the BI technique we shall treat the same problem for a surface with larger irregularities which is beyond the scope of domain perturbation. There could be various ways to express the surface roughness mathematically but Legendre polynomials are most convenient because of their completeness property. Using Legendre polynomials will also enable comparison with the results obtained in the previous subsection by the DP technique. We consider two modes of roughness represented by

$$R = a_3 + b_3 P_3(\eta) \text{ and } R = a_4 + b_4 P_4(\eta).$$

These shapes must satisfy volume conservation,

$$\int_0^{\pi} R^3 \sin\theta d\theta = 2, \tag{10}$$

which should be met with the appropriate $a_i's$ and $b_i's$. For sphere-like particle shapes $a_i's$ and $b_i's$ should be chosen to make the ratio, $\frac{b_i}{a_i}$, small.

After u_A is obtained using the BI technique, $\frac{\partial R}{\partial \tau}$ over the particle surface can be calculated from Eqs.(5d) and (5e). The curves of $\frac{\partial R}{\partial \tau}$ are shown in Figure 1 for $R = 0.994 + (0.2)P_3$ and $Q = 0.1, 5, 10$. The critical value obtained by the DP technique is $Q_{\rm cr} = 4$ for $n = 3$. The graph for $Q = 0.1$ in Figure 1 depicts that $\frac{\partial R}{\partial \tau}$ is positive for R larger than unity and vice versa. Thus the particle becomes more and more nonspherical. For $Q = 10$ in the same figure $\frac{\partial R}{\partial \tau}$ is negative for R larger than unity and vice versa. Then the shapes reduce to spherical, as was predicted by the DP technique. The curve for $Q = 5$ shows that the particle surface goes neither away from nor toward spherical with time, giving a mixed behavior, converse to a slightly nonspherical particle which goes towards spherical. Although the analysis using the domain perturbation does not show oscillation of shape for a deformed sphere, it happens to highly irregular shapes. The graphs for $R = 0.977 + (0.4)P_3$ shown in Figure 2 lead to the same discussions as done for $R = 0.994 + (0.2)P_3$.

Figures 3 and 4 displaying the curves of $\frac{\partial R}{\partial \tau}$ obtained for $R = 0.997 + (0.2)P_4$ and $R = 0.983 + (0.4)P_4$, respectively, lead to the discussions similar to those done above except the graphs of $\frac{\partial R}{\partial \tau}$ for $R = a_4 + b_4 P_4$ are symmetric just as R. The graphs for $Q = 0.1$ in Figures 3 and 4 show that $\frac{\partial R}{\partial \tau}$ is positive for R larger than unity and vice versa, and consequently imply the particle shapes become more and more nonspherical. Oppositely it is shown that for $Q = 10$ the particle shapes go toward spherical. At $Q = 5$, which is close to $Q_{\rm cr} = 2.5$ obtained by the DP technique, the behavior seems transient (i.e., the shape shows a mixed behavior).

Figures 5 and 6 show the total reaction rates normalized by a sphere of equal volume (i.e., solid lines) and by that of a sphere of equal surface area (i.e., dashed

lines) versus Q for the shapes, $R = a_3 + b_3 P_3$ and $R = a_4 + b_4 P_4$, respectively. For any given particle shape, the total rate normalized by a sphere of equal volume decreases with increasing Q, then levels off and remains constant as Q increases beyond 5. At low values of Q, it is equal to the ratio of the surface area of the particle to that of a sphere of equal volume. As Q increases, the rate ratio falls below the surface area ratio, and eventually reaches a limiting value as the reaction becomes mass transfer limited. The dashed lines denoting the total rate normalized by a sphere of equal surface area are within 3% deviation from unity. The total rate of a rough particle represented by P_3 or P_4, therefore, can be closely approximated by a sphere of equal surface area.

Figure 7 depicts an example of shape change with conversion. The initial particle shape is $R = 0.990 + (0.3)P_4$ and the initial Damköhler number, $Q(0) = 0.1$. The curves represent the particle shapes at three consecutive conversions, X = 0, 0.582, 0.892. Since the particle is symmetric rotationally and with respect to y-axis, quarters of the particle are drawn. All the surface points are shown to shrink by equal amount. However, since the whole volume reduces, the surface roughness increases relatively. At 58.2% conversion the overall particle shape is very close to the initial shape, but quite different from the initial shape at 89.2% conversion.

Since the Legendre functions are complete, any particle shape can be represented by their infinite series. Although only the effects of P_3 and P_4 modes were treated in the present chapter, one could attack any shape of particle in a similar way. A very irregular surface, having many modes, is expected to show an irregular surface evolution with time.

Particles lacking rotational symmetry

For particles that do not have rotational symmetry, the terms related to the

azimuthal ϕ-variation and which have been neglected so far must be retained. It turns out that to first order in ϵ, all the differential equations and boundary conditions remain the same as in the axisymmetric case. If the reduced particle radius R is expressed in terms of spherical harmonics,

$$R = 1 + \epsilon \sum_{m,n} \beta_{mn} Y_n^m(\theta, \phi), \tag{11}$$

then by following the same procedure as in the axisymmetric case, we obtain

$$\frac{d\beta_{mn}}{d\tau} = \frac{(n+1) - (n-2)Q}{Q(Q+1)(Q+n+1)} \beta_{mn}. \tag{12}$$

Since the coefficient of β_{mn} at the right side does not contain m, the initial shape variations in the azimuthal direction are preserved as reaction progresses.

CONCLUSIONS

1. From the method of domain perturbation the mode of $n = 2$ increases with time but the higher modes increase or decrease depending on Q. The nth mode decreases if $Q > Q_{cr} = \frac{n+1}{n-2}$ and vice versa.
2. The boundary integral method applied to the particle shapes $a_3 + b_3 P_3$ and $a_4 + b_4 P_4$ with small ratios of b_i/a_i shows that the particle becomes more and more nonspherical for $Q = 0.1$ and that the particle shape goes toward spherical for $Q = 10$. The particle shows the transient behavior for $Q = 5$. Highly irregular particles do not have sharp critical values of Q but show mixed behaviors in a certain range around Q_{cr}.

NOTATION

Notation is the same as in Chapter 2.

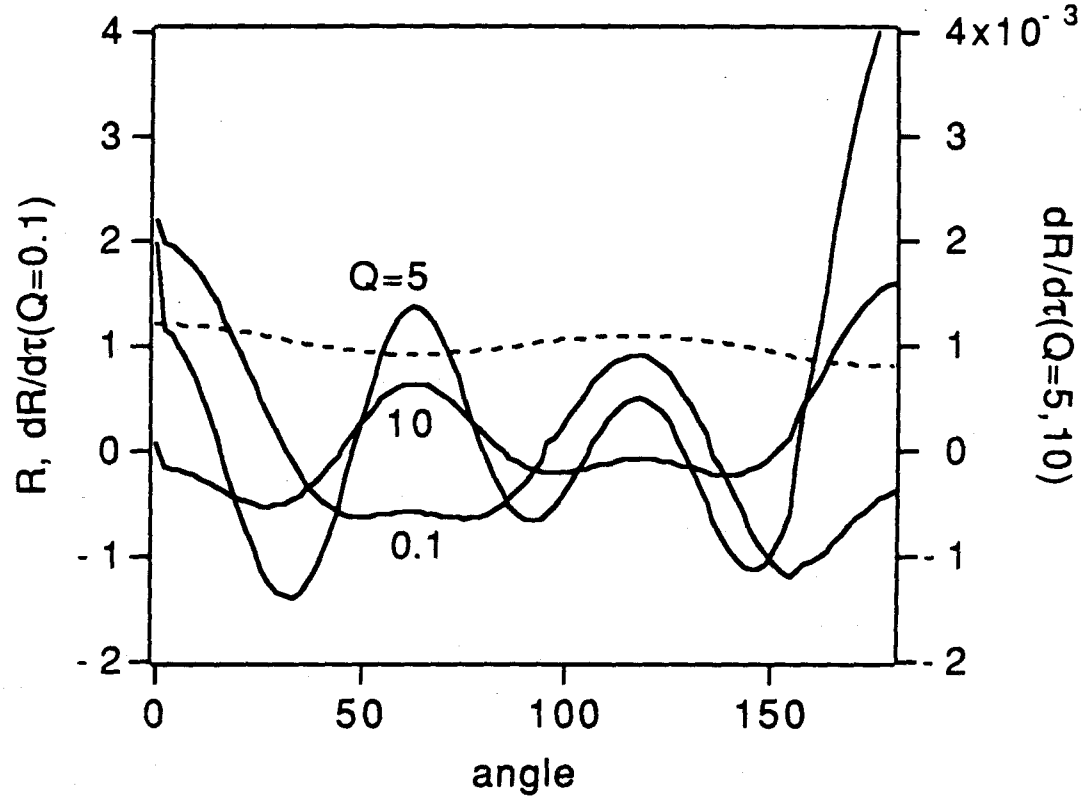

Figure 1. Surface distance from the origin (dashed line), $R = 0.994 + (0.2)P_3$, and moving rate of surface (solid lines), $\frac{\partial R}{\partial \tau}$, for $Q = 0.1, 5, 10$ vs. angle over surface.

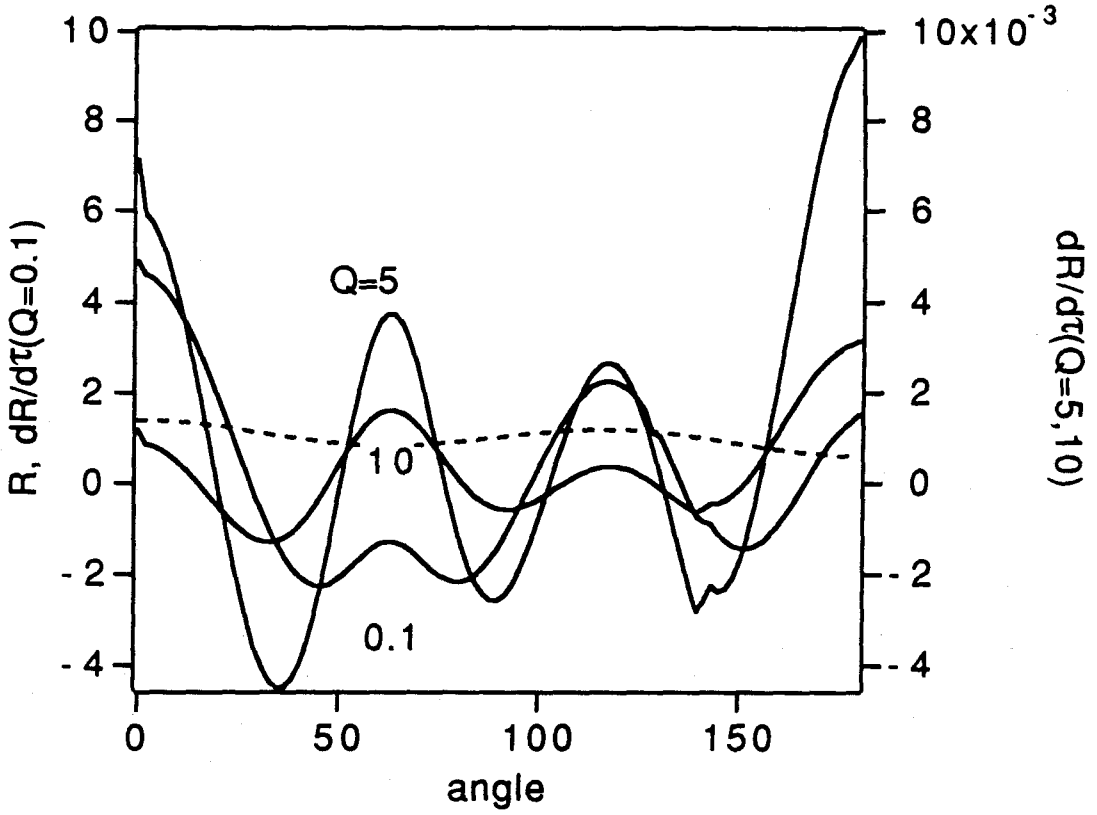

Figure 2. Surface distance from the origin (dashed line), $R = 0.977 + (0.4)P_3$, and moving rate of surface (solid lines), $\frac{\partial R}{\partial \tau}$, for $Q = 0.1, 5, 10$ vs. angle over surface.

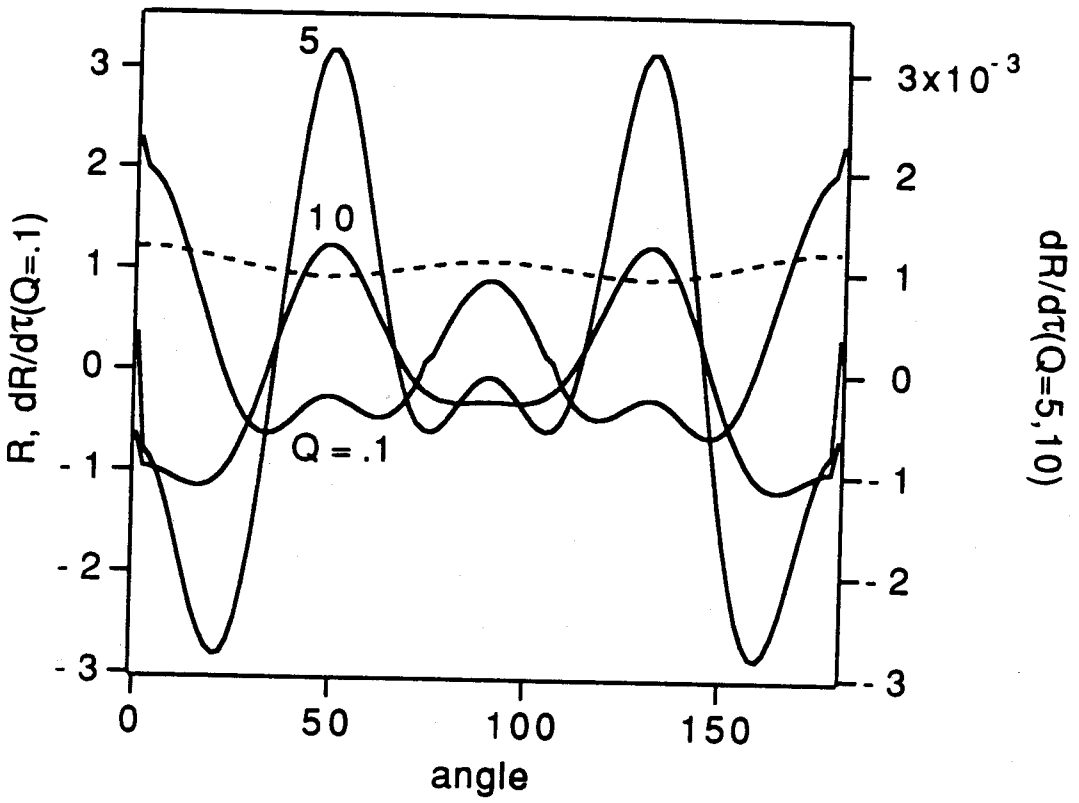

Figure 3. Surface distance from the origin (dashed line), $R = 0.997 + (0.2)P_4$, and moving rate of surface (solid lines), $\frac{\partial R}{\partial \tau}$, for $Q = 0.1, 5, 10$ vs. angle over surface.

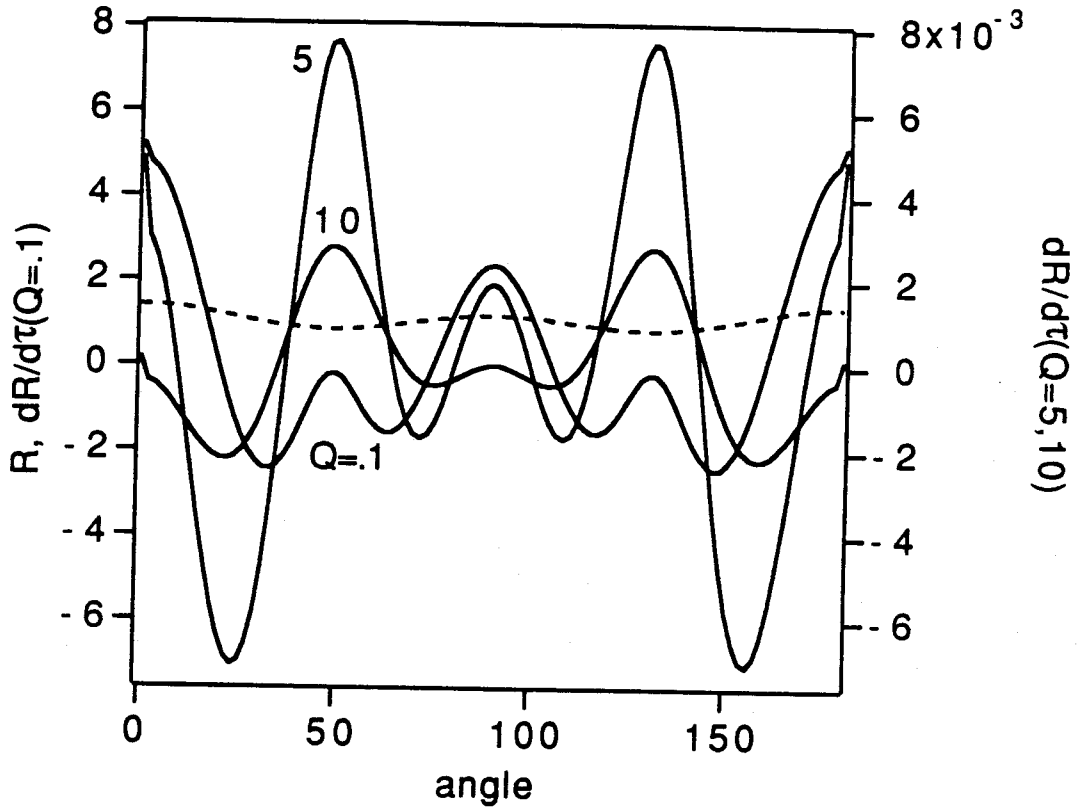

Figure 4. Surface distance from the origin (dashed line), $R = 0.983 + (0.4)P_4$, and moving rate of surface (solid lines), $\frac{\partial R}{\partial \tau}$, for $Q = 0.1, 5, 10$ vs. angle over surface.

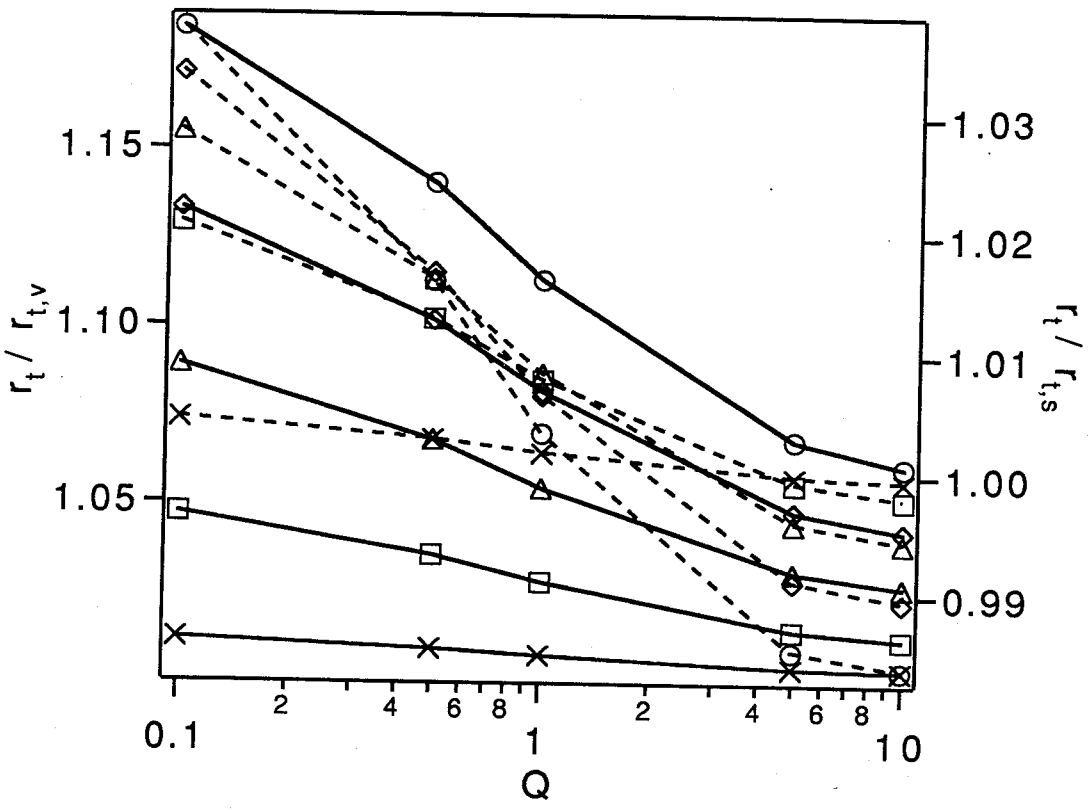

Figure 5. Total reaction rates normalized by that of a sphere of equal volume (solid lines) and by that of a sphere of equal surface area (dashed lines) vs. Q for various shapes, $R = a_3 + b_3 P_3 (b_3 = 0.1 - 0.5)$($x$:$b_3 = 0.1$, □: $b_3 = 0.2$, △: $b_3 = 0.3$, ◇: $b_3 = 0.4$, ◯: $b_3 = 0.5$).

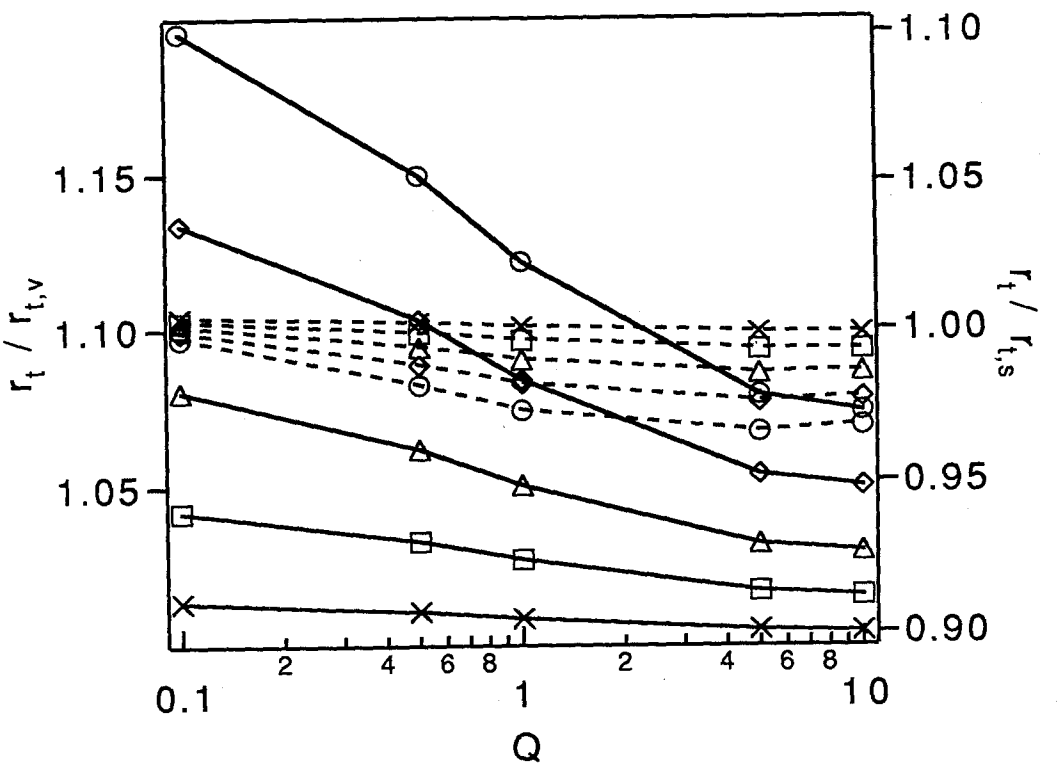

Figure 6. Total reaction rates normalized by that of a sphere of equal volume (solid lines) and by that of a sphere of equal surface area (dashed lines) vs. Q for various shapes, $R = a_4 + b_4 P_4 (b_4 = 0.1 - 0.5)$($x$:$b_4 = 0.1$, □: $b_4 = 0.2$, △: $b_4 = 0.3$, ◇: $b_4 = 0.4$, ◯: $b_4 = 0.5$).

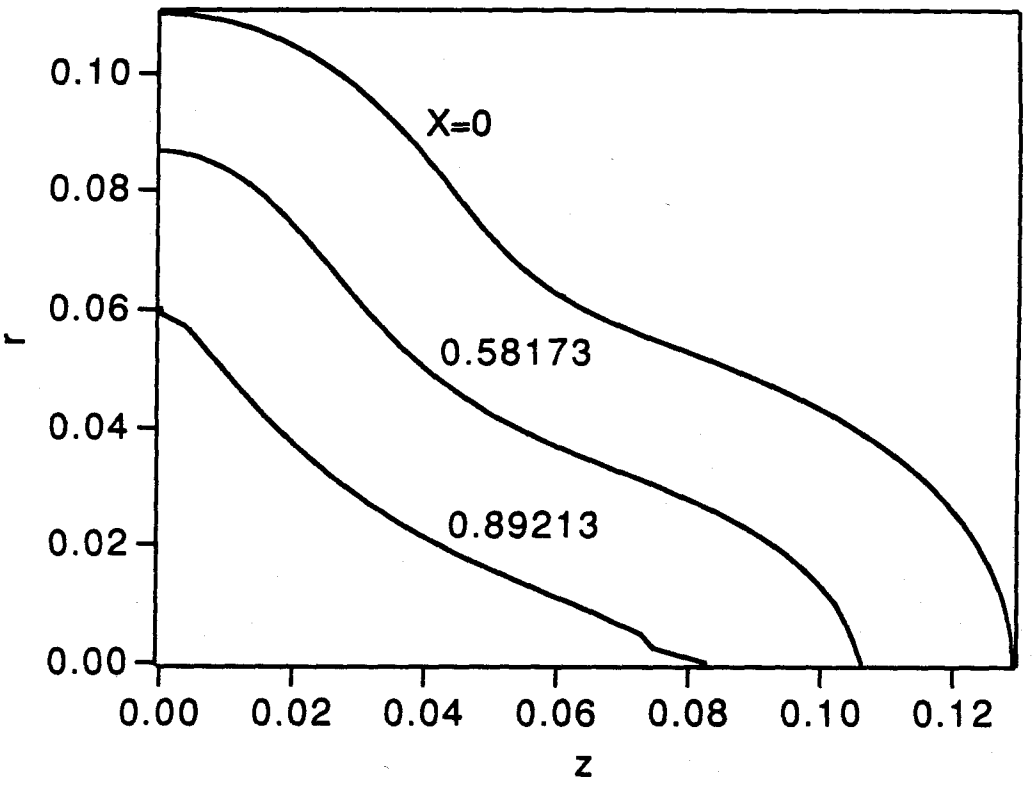

Figure 7. A typical example showing how the surface moves with conversion starting with $Q(0) = 0.1$ and $R = 0.990 + (0.3)P_4$.

Conclusions

The method of domain perturbation and the boundary integral method are employed to see the effect of nonspherical shape of particle on the reaction or the sublimation for the isothermal linear or nonlinear problem. The domain perturbation gave analytical results for the local surface concentration and the initial rate of shape change of a nonspherical axisymmetric particle undergoing surface reaction with the surrounding fluid in a shrinking core mode. Both linear and nonlinear diffusion models were treated. The boundary integral method was used to obtain numerical solutions for particles of highly nonspherical but axisymmetric shape under the same reaction conditions. The local concentration and flux at the particle surface increase with the distance from the particle center. The total reaction rate is almost equal to that of a sphere of equal surface area. From the standpoint of the total reaction rate, therefore, a nonspherical particle is well approximated by a sphere of equal surface area. The total reaction rate relative to a sphere of equal volume increases with the aspect ratio and decreases with the Damköhler number, Q. By contrast the surface averaged concentration decreases, albeit only slightly, both with the aspect ratio and with the Damköhler number, Q. The rate of change of the aspect ratio is given by

$$\frac{dA_p}{d\tau} = \frac{1}{Q(\tau)} W \cdot \frac{A_p - 1}{R(\frac{\pi}{2})},$$

where W is defined by

$$W = \frac{A_p u_A\left(\frac{\pi}{2}\right) - u_A(0)}{A_p - 1}.$$

The quantity W is a function of the Damköhler number, Q, approximately independent of the aspect ratio. This function is

$$W \simeq \frac{3}{(1+Q)(3+Q)}$$

for linear diffusion and

$$W \simeq \begin{cases} 1, & \text{if } Q << 1 \\ \dfrac{3\frac{\ln[1+(b_2-1)y_{Ab}]}{(b_2-1)y_{Ab}}}{(1+Q)\left(3+Q+\frac{Q}{1+Q}\ln[1+(b_2-1)y_{Ab}]\right)}, & \text{if } Q >> 1 \end{cases}$$

for nonlinear binary diffusion.

Since in the sublimation problem the normal derivatives $\frac{\partial u_A}{\partial n}(0)$ and $\frac{\partial u_A}{\partial n}(\frac{\pi}{2})$ are equal to $R(0)$ and $R(\frac{\pi}{2})$, respectively, the shape change is negligible. The total sublimation rate relative to a sphere of equal volume increases with the aspect ratio while the surface averaged sublimation rate shows the opposite behavior. The total rate is again very close to that of a sphere of equal area.

In order to examine the dynamic behavior of nonisothermal nonspherical particles, a nonspherical bituminous char combustion was analyzed using the boundary integral method. Spheroidal particles of equal volume gave nearly coinciding pseudosteady temperature independent of shape, but the total combustion rate increases with increasing aspect ratio. The total combustion rate depends on the particle surface area alone, i.e., particles of equal surface area but different volumes and shapes have the same rate. The local combustion rate on the particle surface increases with the distance from the particle center.

The effect of initial particle shape on the burnout transient was explored for a set of parameters typical of a bituminous coal char. The aspect ratio of spheroids increases with the progress of combustion and this change is more pronounced for particles with larger initial aspect ratios. For particles of equal initial volume, the burnout time decreases slightly with the initial aspect ratio. For example, a particle of initial aspect ratio 3.2 requires 12% less time to reach 80% burnout compared to a spherical particle of the same initial volume.

Another aspect of particle nonsphericity, the rough surface, was also examined

expressing the particle surface in terms of Legendre polynomials. From the method of domain perturbation the second mode increases with time but the higher modes increase or decrease depending on Q. The nth mode decreases if $Q > Q_{cr} = \frac{n+1}{n-2}$ and vice versa. Highly irregular particles, however, do not have sharp critical values of Q but show mixed behaviors in a certain range around Q_{cr}. The boundary integral method applied to the particle shapes $a_3 + b_3 P_3$ and $a_4 + b_4 P_4$ depicts that the particle becomes more and more nonspherical for $Q = 0.1$ and that the particle goes back to a sphere for $Q = 10$. The particle shows a mixed behavior for $Q = 5$.

Appendix A : Linear Isothermal Transient Problem

The important results derived in the present isothermal transient analysis using the linear diffusion analytically by the DP technique for a slightly nonspherical particle, and numerically by the BI technique for spheroids of arbitrary aspect ratio are useful to obtain insight on the evolution of particle with time. The governing equation and boundary conditions are

$$\nabla_x^2 u_A = 0 \text{ outside the particle} \tag{A1a}$$

$$-\frac{\partial u_A}{\partial n} = Q u_A \text{ on particle surface} \tag{A1b}$$

$$u_A \to 1 \text{ as } |\mathbf{x}| \to \infty \tag{A1c}$$

$$\frac{1}{|\nabla_{\tilde{x}} \tilde{F}|}\frac{\partial \tilde{F}}{\partial t} - \mathbf{v_s} \cdot \tilde{\mathbf{n}} = 0 \tag{A1d}$$

where

$$\tilde{F} \equiv \tilde{\rho} - \tilde{R}(\theta, t). \tag{A1e}$$

Slightly deformed sphere

The solution for a slightly deformed sphere is particularly simple and instructive since one can easily obtain intuition about the transient behavior of the particle. Brief explanation is, therefore, presented with no detailed derivation which can be looked up in Chapter 2. The important results about the dynamic behavior of particle are

$$Q = -1 + \sqrt{[1+Q_0]^2 - 2\tau} + O(\epsilon^2), \tag{A2a}$$

$$R = 1 + \epsilon \sum_{n=2}^{\infty} \beta_n P_n(\cos\theta) + O(\epsilon^2), \tag{A2b}$$

$$\beta_n(\tau) = \beta_n(0)\frac{Q_0}{Q}\left(\frac{Q+n+1}{Q_0+n+1}\right)^{n-1}. \tag{A2c}$$

For the spheroid-like particles with $\beta_2 \neq 0$ and $\beta_{n\neq 2} = 0$, in which one is most interested, the relationship between the aspect ratio A_p and the second mode β_2 is represented as

$$A_p = 1 + \frac{3}{2}\epsilon\beta_2(\tau) + O(\epsilon^2). \tag{A3}$$

From Eq.(A2c) the nonsphericity of a spheroid-like particle is expressed as functions of the Damköhler number, Q, by

$$\beta_2(\tau) = \beta_2(0)\left(\frac{Q_0}{3+Q_0}\frac{3+Q}{Q}\right), \tag{A4a}$$

$$A_p - 1 = (A_{p0} - 1)\left[\frac{Q_0}{3+Q_0}\frac{3+Q}{Q}\right]. \tag{A4b}$$

Equation (A2a) is equal to the solution for a sphere to the error of $O(\epsilon^2)$. As shown in Eq.(A3), however, the leading value of the aspect ratio is $1 + O(\epsilon)$, which implies that the nonsphericity of particle has much effect on the aspect ratio of particle. This means A_p grows faster as the shape becomes more nonspherical. Thus it is expected that the rate of shrinking of particle depends on the nonsphericity of particle less than the aspect ratio does. Equation (A4b) suggests that the aspect ratio will grow very rapidly with small Q. Although both of these two expressions derived by the DP technique can be employed, strictly speaking, for a slightly nonspherical particle, they will give us some insight or intuition on the behavior of highly nonspherical particles.

Spheroids with big eccentricities.

Highly nonspherical particles can be treated for the surface concentration of $A(g)$ by the BI technique well developed in Chapter 2. To follow the shape change of

particle with time, one has to integrate the kinematic condition, (A1d), numerically using u_A calculated by the BI technique. The explicit fourth order Runge-Kutta method was used to yield numerical solutions to Eq.(A1d) for various prolate and oblate spheroids. Figure A1 describes the conversion and the aspect ratio with respect to dimensionless time, τ, for various prolate and oblate spheroids. The solid lines are for prolate spheroids while the dashed lines are for oblate spheroids. Since the surface area of an oblate spheroid is somewhat larger than the counterpart of the prolate spheroid of equal aspect ratio, the aspect ratio and the conversion for oblate spheroids increase with time a little faster than for prolate spheroids.

CONCLUSIONS

For a slightly nonspherical particle the particle size (i.e., the Damköhler number Q) derived by the DP technique is the same as that of the sphere of equal volume to $O(\epsilon)$. The Damköhler numbers obtained using the BI technique for several prolate spheroids also show slightly faster decreases than for the sphere of equal volume. But the decrease speed of Q becomes higher and higher as the particle shrinks. The aspect ratio is $1+O(\epsilon)$ by the DP technique, and grows very slowly for large Q and very fast for small Q.

NOTATION

Notation is the same as in Chapter 2.

Appendix B : Nonspherical Particles Leaving Ashes

INTRODUCTION

In many gas-solid reactions encountered in chemical and metallurgical processes, solid products are generated. The overall volume of particle could change with the reaction if the density of product is different from that of reactant, but it remains unchanged in most reactions. Such reactions may be described by the general reaction equation

$$b_1 P(s) + A(g) \rightarrow b_2 B(g) + b_3 D(s).$$

The representative examples of such a system are the kinetic processes of combustions, with oxygen, of carbonaceous matter contained within the pores of granules of a porous solid. In the practice of catalysis, we encounter this circumstance in catalyst regeneration, i.e., in the process of removal by combustion of carbonaceous deposits (coke) accumulated during catalytic operation with hydrocarbon or other organic reactants. Sometimes porous adsorbents are similarly regenerated. Besides the same analysis may be applicable to the reduction of some metal oxides and the roasting of sulfide ores.

Though theoretical researches of gas-solid reactions have been carried out with various models, the shrinking core model is the simplest to work with. Duong D. Do (1982) justified the validity of the shrinking core model and found that to apply this useful model in a proper way the reaction rate should be much faster than the diffusion rate; i.e., the Thiele modulus is high enough. There are two cases where we can apply the unreacted core shrinking model. One is when the effective diffusivity in the core is much smaller than that in the ash layer and the other is

when the whole process is controlled by the diffusion through the ash layer. The former might be too ideal to be true in reality. One can easily realize the latter case, which prevails for sufficiently high temperature or sufficiently large particle size. Then the reaction occurs only on the core surface.

When one wants to analyze the shrinking core model, it is most convenient to use the spherical core as was done by Yagi and Kunii (1955) and explained in detail by Levenspiel (1972). So far the assumption of spherical core has been taken for granted with no justifications. One needs to check whether the core maintains the spherical shape or the particle shape becomes nonspherical during reaction. We considered this problem already in the previous chapters with a shrinking particle. As was the case for gas-solid reactions leaving no ashes, the core may become more nonspherical unless the overall shape is not perfectly spherical. Or, even if the overall shape of particle is perfectly spherical, the spherical core surface could be unstable to a certain small disturbance. Thus we would like to examine the behavior of the core surface in case the initial surface is not spherical. Since the domain is finite, we can only use the boundary integral method (hereafter BI) and can investigate the shape change assuming a form of core shape is given.

PROBLEM FORMULATION

Governing equation and boundary conditions

By introducing the effective diffusion coefficient defined by

$$\mathbf{N}_A = -D_e \nabla c_A, \tag{B1}$$

the diffusion through the ash layer can be formulated under the assumptions :

1. The concentration of A on the particle surface is uniformly equal to that in the bulk gas phase.

2. The whole system is isothermal.
3. Reaction occurs only on the core surface.
4. Reaction is first order and is proportional to the concentration of species A.
5. All the transport coefficients and physical properties are constant.
6. Since the core shrinks very slowly, the concentration profile of species A is in quasi-steady state.

to obtain the governing equation and boundary conditions,

$$\nabla^2_{\tilde{x}} c_A = 0 \qquad \text{in the ash} \tag{B2a}$$

$$-D_e \nabla_{\tilde{x}} c_A \cdot \tilde{\mathbf{n}} = k c_A \qquad \text{on the core surface} \tag{B2b}$$

$$c_A \rightarrow c_{Ab} \qquad \text{on the particle surface} \tag{B2c}$$

$$\frac{1}{|\nabla \tilde{F}|} \frac{\partial \tilde{F}}{\partial t} - \mathbf{v}_s \cdot \tilde{\mathbf{n}} = 0 \quad \text{on the core surface} \tag{B2d}$$

$$\tilde{F} \equiv \tilde{\rho} - \tilde{r}(\theta, t). \tag{B2e}$$

The unit normal vector on the core surface, $\tilde{\mathbf{n}}$, is outward from the ash outside the core, and $\mathbf{v}_s$ is the core surface velocity. The tildes signify dimensional properties. The use of the dimensionless properties,

$$\mathbf{x} = \frac{\tilde{\mathbf{x}}}{\tilde{R}_s}, u = \frac{c_A}{c_{Ab}}, r(\theta, t) = \frac{\tilde{r}(\theta, t)}{\tilde{R}_s}, Q = \frac{k\tilde{R}_s}{D_e}, \tau = \frac{b_1 k^2 c_{Ab}}{\rho_s \tilde{R}_s} t, \tag{B3}$$

where $\tilde{R}_s$ is the radius of the fictitious sphere which has the same volume as the particle and Q is the Thiele modulus for the unreacted core shrinking model, yields Eqs.(B2) in the dimensionless form

$$\nabla^2_{\tilde{x}} u = 0 \qquad \text{in the ash} \tag{B4a}$$

$$\frac{\partial u}{\partial n} = -Qu \qquad \text{at} \quad \rho = r(\theta, \tau) \tag{B4b}$$

$$u = 1 \qquad \text{at} \quad \rho = R(\theta) \tag{B4c}$$

$$-\frac{\partial r}{\partial \tau} = \sqrt{1 + (\frac{1}{r}\frac{\partial r}{\partial \theta})^2}\, u \quad \text{at} \quad \rho = r(\theta, \tau). \tag{B4d}$$

Aspect ratio and its derivative

Though there are various types of nonsphericity, we want to examine the effect of the spheroidal shape which is the most common nonsphericity encountered in practice. To represent the nonsphericity of spheroid, the eccentricity (e) and the aspect ratio (A_p) are used and their relationship for a spheroid is $A_p = (1-e^2)^{-1/2}$. The aspect ratio of the core and its time derivative are defined by

$$A_p = \frac{r(0,\tau)}{r(\frac{\pi}{2},\tau)}, \tag{B5}$$

$$\frac{dA_p}{d\tau} = \frac{1}{r^2(\frac{\pi}{2})}\left[\frac{\partial r}{\partial \tau}(0) r(\frac{\pi}{2}) - r(0)\frac{\partial r}{\partial \tau}(\frac{\pi}{2})\right]. \tag{B6}$$

The substitution of $\frac{\partial r}{\partial \theta} = 0$ at $\theta = 0, \frac{\pi}{2}$ and Eq.(B4d) in Eq.(B6) gives

$$\frac{dA_p}{d\tau} = \frac{1}{r^2(\frac{\pi}{2})}\left[r(0)u(\frac{\pi}{2}) - r(\frac{\pi}{2})u(0)\right], \tag{B7}$$

which are divided by $r(0) - r\,(\frac{\pi}{2})$ to yield

$$\frac{d\ln(A_p - 1)}{d\tau} r(\frac{\pi}{2}) = \frac{A_p u(\frac{\pi}{2}) - u(0)}{A_p - 1} (\equiv W'). \tag{B8}$$

The quantity W' shows the same asymptotic behaviors that were discussed in Chapter 2 for small and large Q.

Boundary integral method

The integral form of Laplace's equation derived in Chapter 2 reduces, with boundary conditions at the particle and core surfaces, Ω_1, Ω_2, to

$$-2\pi u_i = \int_{\Omega_1} u(\frac{\partial g}{\partial n} + Qg)\, dA + \int_{\Omega_2} \frac{\partial g}{\partial n} dA - \int_{\Omega_2} g \frac{\partial u}{\partial n} dA. \tag{B9}$$

Giving the singular point ξ to Ω_1 yields

$$\int_{\Omega_2} \frac{\partial g}{\partial n} dA = -4\pi \tag{B10}$$

while with the singular point ξ on Ω_2

$$\int_{\Omega_2} \frac{\partial g}{\partial n} dA = -2\pi \tag{B11}$$

by the Gauss divergence theorem. Then the integral equations to solve are

$$4\pi - 2\pi u_i = \int_{\Omega_1} u(\frac{\partial g}{\partial n} + Qg)\, dA - \int_{\Omega_2} g \frac{\partial u}{\partial n} dA \text{ with } \xi \text{ on } \Omega_1 \tag{B12}$$

$$0 = \int_{\Omega_1} u(\frac{\partial g}{\partial n} + Qg)\, dA - \int_{\Omega_2} g \frac{\partial u}{\partial n} dA \text{ with } \xi \text{ on } \Omega_2. \tag{B13}$$

For a spherical particle, u and $\frac{\partial u}{\partial n}$ are uniform all over the surfaces. The analytical solution for a sphere is derived by using constant u and $\frac{\partial u}{\partial n}$ in the above integral equations.

DISCUSSION

Before going into any calculations, we have to define the shapes of the whole particle and the unreacted core. In fact the core shape should be determined temporally by the kinematic boundary condition starting from the shape of the whole particle. Instead of going into such details, we just want to find the stability of the nonspherical core surface. It is, therefore, sufficient for the present to restrict the core shape to the same as that of the whole particle. The size of whole particle is normalized by the radius of the sphere of equal volume whereas the size of core is used as a parameter. The sizes of whole particle and core are represented as the radii of the spheres of equal volumes.

We calculated the core surface concentrations using the BI technique for the shapes e=0.6,0.8,0.9 and with r_s=0.3,0.5,0.7. Figure B1 describes the BI results of W' for the shape, e=0.6(A_p=1.25) and r_s=0.5, yielding essentially the same results as in Case I. The curves for e=0.8 and 0.9 are negligibly higher and the curve for r_s=0.7 is just a little higher than that for r_s=0.5. Roughly speaking, the quantity, W', is a function of Q only regardless of r_s and A_p. Figure B1 displays asymptotes of W',

$$W' \to 1 \qquad \text{for small } Q, \tag{B14a}$$

$$W' \to \frac{2}{Q} \qquad \text{for large } Q, \tag{B14b}$$

and so the rate of change of aspect ratio gives the asymptotic behaviors,

$$\frac{dA_p}{d\tau} \to \frac{A_p - 1}{r(\frac{\pi}{2}, \tau)} \qquad \text{for small } Q \tag{B15a}$$

$$\frac{dA_p}{d\tau} \to \frac{2(A_p - 1)}{Qr(\frac{\pi}{2}, \tau)} \qquad \text{for large } Q. \tag{B15b}$$

For the sphere of equal volume the shrinking rate of core is easily derived as

$$\frac{dr_s}{d\tau} = -\frac{1}{-r_s^2 Q + r_s Q + 1}. \tag{B16}$$

Integration of Eqs. (B15a) and (B15b) with the help of Eq.(B16) yields the inequalities,

$$A_p - 1 > (A_{p0} - 1)(\frac{1}{r_s}) \exp\left[\frac{Q}{2}(1 - r_s)^2\right] \text{ for small } Q \tag{B17a}$$

$$A_p - 1 > (A_{p0} - 1)(\frac{1}{r_s})^{2/Q} \exp[(1 - r_s)^2] \text{ for large } Q. \tag{B17b}$$

Equation (B17a) predicts the aspect ratio of the core becomes larger than 2 after 90% decrease of the core radius starting with an initial aspect ratio of 1.1.

Weisz and Goodwin (1963) performed an experiment on catalyst reactivation at various temperatures. The picture for high temperature shows a very sharp and spherical interface at high temperature. From their result the core shape can be considered to remain spherical at high temperature (i.e., diffusion control) till 50% decrease of radius starting from a spherical shape. This is consistent with the present theoretical result that the core shape remains unchanged essentially under the diffusion control. The present result predicts the rate of change of the core shape to be quite rapid with the small core size. Thus the core shape will be very nonspherical when the size of the core is very small. Weisz and Goodwin, however, show a picture only in which the core size is still big from the standpoint of the present analysis. A picture displayed by Wen and Wang (1970) shows a geometrical instability for a small core size, which is consistent with the result from the present analysis.

CONCLUSIONS

1. The boundary integral method is applied to the gas-solid reaction leaving ashes to find the concentration on the core surface. The quantity W' is a function of Q only regardless of r_s and A_p, and its behavior is almost the same as was seen in the shrinking particle except that W' is proportional to Q^{-1} rather than Q^{-2} under the diffusion control.
2. Under the diffusion control the core shape changes a little bit, but negligibly, so it remains almost spherical as long as the core size is not very small. The rate of change of aspect ratio is large under the reaction control.

NOTATION

Notation is the same as in Chapter 2 except the following list.

D_e	effective pore diffusion coefficient
Q	Damköhler number [Eq.(B3)]
r_s	dimensionless radius of spherical core
$r(\theta, t)$	dimensionless radial distance of core from particle center [Eq.(B3)]
W'	defined by Eq.(B8)

Greek letters

τ	dimensionless time variable defined by Eq.(B3)
Ω_1, Ω_2	surface boundaries of domain

REFERENCES

Do, D.D., 1982, On the Validity of the Shrinking Core Model in Noncatalytic Gas Solid Reaction, *Chem. Engng Sci.* **37**, 1477-1481.

Levenspiel, O., 1972, *Chemical Reaction Engineering*, Wiley, New York, pp. 357-400.

Weisz, P.B. and Goodwin, R.D., 1963, Combustion of Carbonaceous Deposits within Porous Catalyst Particles. I. Diffusion-Controlled Kinetics, *J.Cat.* **2**, 397-404.

Wen, C.Y. and Wang, S.C., 1970, Thermal and Diffusional Effects in Noncatalytic Solid Gas Reactions, *Ind. Eng. Chem.* **62**(8), 30-51.

Yagi, S. and Kunii, D., 1955, *Proc. 5th Int. Symp. on Combustion*, 231.

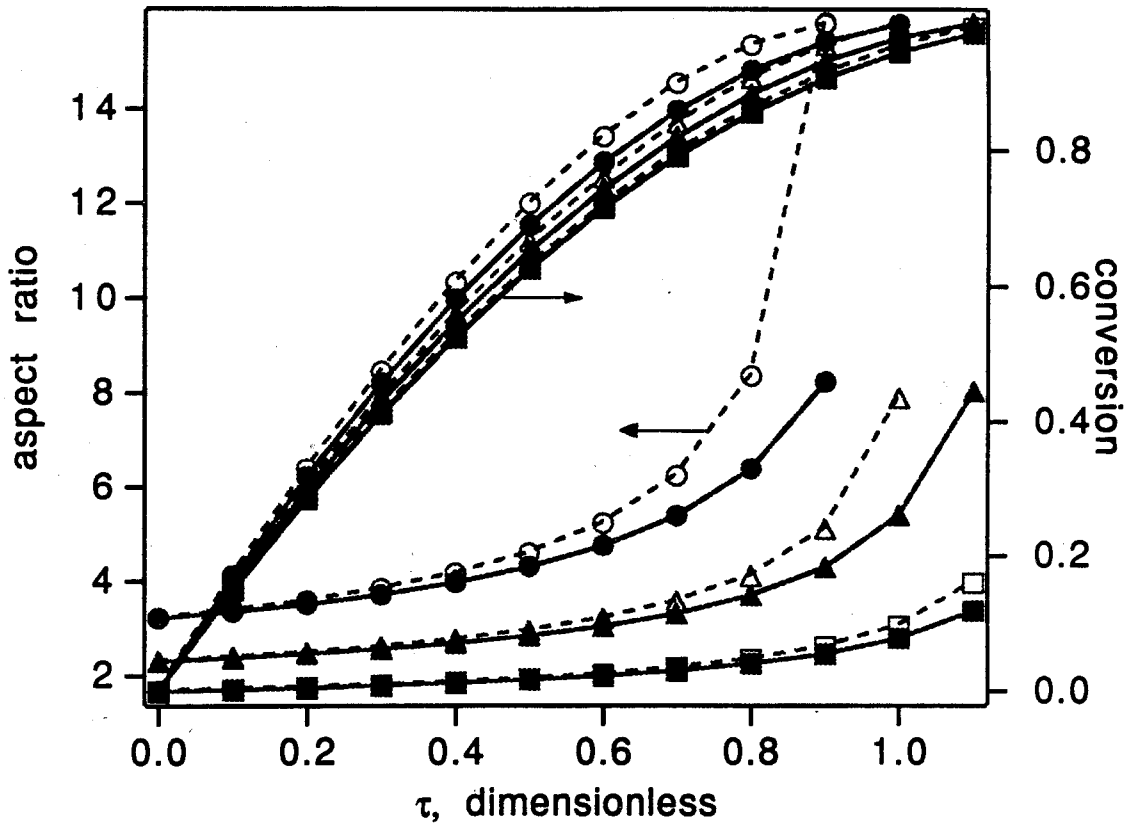

Figure A1. Aspect ratio and conversion vs. dimensionless time for prolate and oblate spheroids(□:$A_p(0) = 1.667$,△:$A_p(0) = 2.294$, ○:$A_p(0) = 3.2026$; solid lines : prolate spheroids, dashed lines : oblate spheroids).

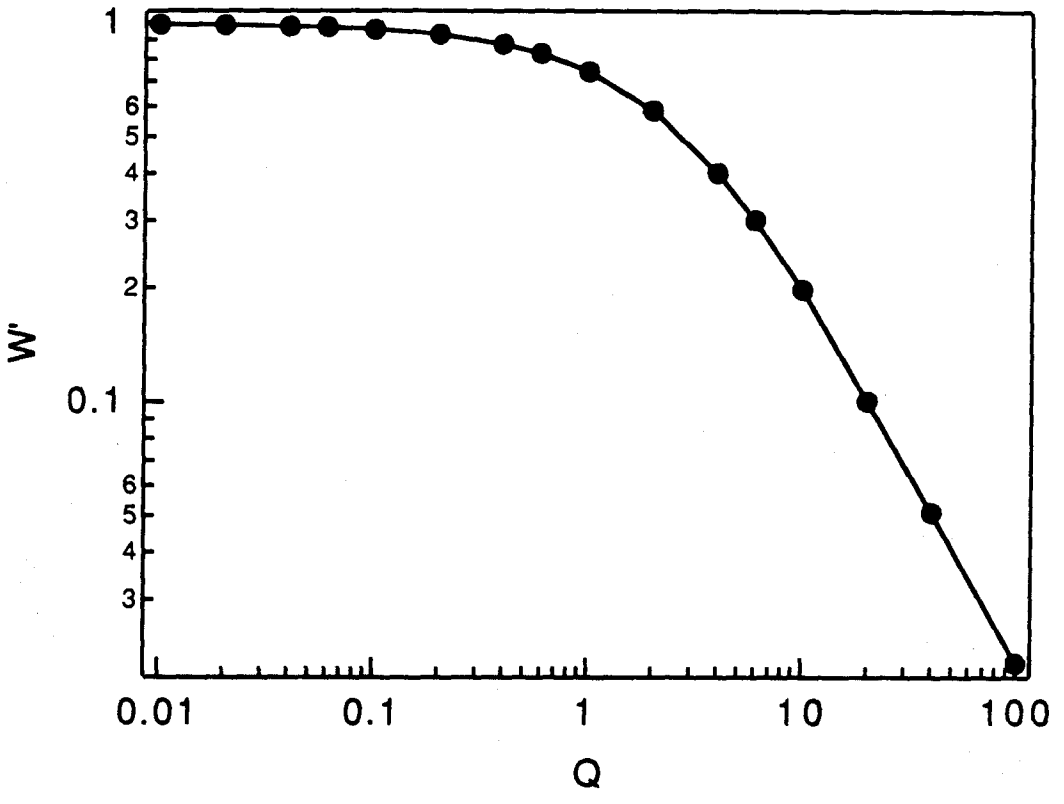

Figure B1. Rate of change of aspect rtaio of a reacting particle leaving ashes vs. Q ($\square$:$A_p(0) = 1.667$,$\triangle$:$A_p(0) = 2.294$, $\bigcirc$:$A_p(0) = 3.2026$; solid lines : prolate spheroids, dashed lines : oblate spheroids).